Doctoral Dissertation
Doctoral Program in Energy Engineering (30th Cycle)

Experimental and numerical investigation of a high boost and high injection pressure Diesel engine concept for heavy duty applications

Giulio Boccardo
* * * * * * * * * * * * * *

Supervisor
Prof. Federico Millo

Doctoral Examination Committee:

Dr. Carlo Beatrice, Referee, Istituto Motori - CNR
Prof. Carlo Nazareno Grimaldi, Referee, Università degli Studi di Perugia
Prof. Michael Bargende, Universität Stuttgart
Prof. Agostino Gambarotta, Università degli Studi di Parma
Prof. Jan Macek, Czech Technical University in Prague

Politecnico di Torino
June 5, 2018

I hereby declare that, the contents and organisation of this dissertation constitute my own original work and does not compromise in any way the rights of third parties, including those relating to the security of personal data.

…………………………………....

Giulio Boccardo

Turin, June 5, 2018

Summary

The upcoming European Stage V emissions regulation for Non-Road Heavy Duty Diesel Engines will force OEMs to adopt Diesel Particulate Filters, adding a further degree of complexity to the aftertreatment system, which in several cases already includes specific devices for NOx reduction. Since complex aftertreatment systems can rise packaging problems as well as reliability issues, a project in collaboration with Kohler, Politecnico di Torino, Ricardo and Denso, has been carried out to explore the feasibility of a Stage V compliant SCR-free architecture for a 90kW Non Road Diesel engine. To this scope a prototype engine based on the Kohler KDI3404, was equipped with a low-pressure Exhaust Gas Recirculation system, a two-stage turbocharger and a 3000 bar injection pressure-capable Fuel Injection System.

This thesis focuses on the experimental and numerical assessment of emissions and performances of this engine architecture over the Stage V certification procedure. It will be shown how the high-pressure Fuel Injection System is the key technology to meet the stringent requirements, demonstrating how increasing the injection pressure from 2000 to 3000 bar can dramatically improve the NOx-Soot and NOx-Particulate Number trade-off, together with engine efficiency, without adversely affecting the emission of nanoparticles. Moreover, the use of extremely high injection pressures in conjunction with after injection as a soot reduction technique, was found to be capable of achieving up to 50% smoke reduction with a more than acceptable engine efficiency degradation.

Thanks to a dedicated steady state and transient calibration, the engine was able to run a compliant NRSC and NRTC with more than 10% margin on NOx and a level of particulate matter and particulate number which can be easily managed by the DOC+DPF aftertreatment system. However, some components of the tested engine, such as the turbochargers, were found to be far from the optimal, thus resulting into relatively poor efficiency figures.

Therefore, a 1D-CFD model featuring predictive combustion and emissions models was developed in order to assess the full potentials of this architecture on a kind of “virtual test rig”, on which different components could be easily evaluated.

The model results proved that, with a better design of the exhaust and EGR line, and with a slightly higher performance turbocharger, consistent engine efficiency improvements could be obtained, making the SCR-free solution as a valuable alternative to the SCR architecture to meet the Stage V emissions regulations.

Acknowledgements

This thesis is the result of a two years-long project carried out in a close and fruitful collaboration between Politecnico di Torino, Kohler, Ricardo and Denso, which all deserve my special gratitude.

Foremost I would like to acknowledge Luigi Arnone and Stefano Manelli from Kohler which leaded and promoted the project, together with Cristian Capiluppi, Andrea Marinoni and Giuseppe Tutore for their invaluable support.

I owe heartfelt thanks to Simon Fagg and Paolo Gatti from Ricardo UK, for the work they have carried out in the preliminary design phase, for the support during the engine calibration procedure and for sharing their precious know-how.

My special thanks go to Naoki Arita, Michele Bastianelli and Dirk Queck from Denso, which supplied the Fuel Injection System and the engine control architecture, for their consistent contribution and support in the fine tuning of the system which made the project successful.

Last, but definitely not the least, I would also like to thank Shawn Harnish, Mike Bybee and Kevin Roggendorf from Gamma Technologies for their support in simulation activity and for hosting me in their offices in 2016.

Contents

1 INTRODUCTION 2

1.1 Non-Road Mobile Machines context 5
1.1.1 User Requirements 5
1.1.2 Legislation 7

1.2 Project Overview 12
1.3 Engine description 15
1.3.1 EGR 17
1.3.2 Turbocharging System 19
1.3.3 Fuel Injection System 20
1.3.4 Combustion System 21

2 FIRST EXPERIMENTAL PHASE 24

2.1 Experimental Setup 25
2.1.1 Steady-State Test Bench 26
2.1.2 Low-Pressure stage simulating device 27

2.2 Nozzles Selection 28
2.2.1 Protrusion Optimization 29
2.2.2 Nozzles comparisons 33

2.3 First calibration development 35

3 SECOND EXPERIMENTAL PHASE 38

3.1 Experimental Setup 39
3.1.1 Engine Layout 39
3.1.2 Facilities Description 39

3.2 Hardware assessment 41
3.2.1 Test Matrix 41
3.2.2 Particulate measurement correlation 42

3.2.3 Results..43

3.3 Steady state calibration development 50
3.4 Transient Calibration...54
3.4.1 EGR Linearization 54
3.4.2 Transient Control Calibration 60

3.5 Results on Certification Cycles..63

4 CONCLUSION AND OUTLOOK 68

4.1 Engine improvement potentials..69
4.1.1 Full – Load Model Validation 70
4.1.2 Exhaust and EGR Line pressure drop improvements....................75
4.1.3 Improved Turbochargers Efficiency...77

4.2 Conclusions...81

APPENDIX

A PARTICULATE MEASUREMENTS CORRELATIONS 84

A.1 Microsoot – Smokemeter correlation.. **84**
A.2 Particle Number - Mass correlation.. **86**
A.3 Particle Counter – SMPS.. **86**

B 1D – CFD Model...90

B.1 Predictive Combustion Model 91
B.1.1 Di-Pulse 91
B.1.2 Calibration Approach...91
B.1.3 Emissions Models...93

B.1.4 Injection Rates Map 94
B.1.5 Results 97
B.1.6 Emissions 98
B.1.7 Calibration Points Number Sensitivity 102

References...104

List of Abbreviations...108

List of Tables

Table 1.1 - Stage IV emission standards for NRMM Diesel Engines [8] 8
Table 1.2 - Stage V emission standards for NRMM Diesel Engines [8].................8
Table 1.3 - Non Road Steady Cycle (ISO 8178 -Type C1) [10] 9
Table 1.4 - Provisional High-Level targets on certification cycles 16
Table 1.5 - Engine Specifications 16
Table 1.6 - Full Load AFR and EGR Targets..17
Table 2.1 - Steady-State Test Bench dyno parameters 26
Table 2.2 - Nozzles portfolio 28
Table 2.3 - Ricardo preliminary calibration...29
Table 3.1 - EGR Sweeps measurement parameters...41
Table 3.2 - After Injection explorations measurement parameters........................42
Table 3.3 - NRTC compliance criterions...64

List of Figures

Figure 1.1 - Trends in emissions of air pollutants 3
Figure 1.2 - EU and USA NRMM NOx and PM Regulations 8
Figure 1.3 - Non Road Transient Cycle [AVL] 10
Figure 1.4 – WLTC and NRTC comparison......11
Figure 1.5 - NRSC and NRTC comparison 11
Figure 1.6 - Basic NTE zone [12]......11
Figure 1.7 - Stage V Compliant NRMM Engine Layout [RICARDO] 12
Figure 1.8 - Packaging comparison of SCR and SCR-free architectures 13
Figure 1.9 - Kohler KDI3404 Engine 15
Figure 1.10 - Full Load Performance......16
Figure 1.11 - 0D model responses to EGR circuit type and rated power 18
Figure 1.12 - EGR system overview......19
Figure 1.13 - Assessment of the DENSO 4th Gen. Ultra High Pressure FIS. 21
Figure 1.14 - CFD Equivance Ratio for TVCS and Conventional Bowl design ...23
Figure 1.15 - CFD Equivance Ratio for TVCS and Conventional Bowl design ...23
Figure 2.1 - 1st Phase Experimental Setup 25
Figure 2.2 - First Testing Phase Engine layout......26
Figure 2.3 - Low pressure stage simulating device 28
Figure 2.4 - Low Pressure stage simulating device schematic 27
Figure 2.5 - Nozzle Selection operating points......29
Figure 2.6 - Nozzle protrusion......30
Figure 2.7 - Protrusion comparison, Nozzle 7holes - 820cc......32
Figure 2.8 - Nozzles results comparison......34
Figure 2.9 - Example of steady state calibration 36
Figure 3.1 - Engine Layout in the Second Experimental Phase 40
Figure 3.2 - Operating point chosen for the hardware assessment 42
Figure 3.3 - Particulate measurement correlation......43
Figure 3.4 - 1400 rpm x 50% load - EGR sweeps 46
Figure 3.5 - 1400 rpm x 100% load – EGR Sweeps......46

Figure 3.6 - 2200 rpm x 75 % load – EGR Sweeps 47
Figure 3.7 - 2200 rpm x 50% load – EGR Sweeps 47
Figure 3.8 - Modes of particle size distributions vs injection pressure 48
Figure 3.9 - In cyl. pressure and HRR @ 2000 and 3000 bar injection pressure. .48
Figure 3.10 - 2200 rpm x 75% Load - After Injection exploration 49
Figure 3.11 - 2200 rpm x 50% Load - After Injection exploration 49
Figure 3.12 - Effect of after injection on in cylinder pressure and HRR. 50
Figure 3.13 - Steady State calibrations comparison 52
Figure 3.14 - Final Steady State calibration injection parameters 52
Figure 3.15 - Steady State calibration results on engine map 53
Figure 3.16 - EGR flow schematic 55
Figure 3.17 - EGR valve and Exhaust flap characterization 56
Figure 3.18 - Linearized positioning laws 58
Figure 3.19 - EGR linearization results assessment 59
Figure 3.20 - EGR Linearization Results assessment 60
Figure 3.21 - Load steps results 62
Figure 3.22 - NRSC breackdown 63
Figure 3.23 - NRTC Example 64
Figure 3.24 - NRTC compliance regressions 64
Figure 3.25 - NRTC NOx - Soot Tradeoff 65
Figure 3.26 - NRSC and NRTC Emission results 65
Figure 4.1 - Exp. in Cyl. pressure and burn rate of peak power operating point...69
Figure 4.2 - FL Model Validation 1/4 72
Figure 4.3 - FL Model Validation 2/4 73
Figure 4.4 - FL Model Validation 3/4 74
Figure 4.5 - FL Model Validation 4/4 75
Figure 4.6 - FL operating points on the turbocharger maps 77
Figure 4.7 - Turbocharger s efficiency comparison 78
Figure 4.8 - Engine Improvement Potentials 1/2 79
Figure 4.9 - Engine Improvement Potentials 2/2 80
Figure 4.10 - KDI3404 architectures efficiency comparison. 82

Figure A.1 - FSN - Soot Concentration correlation 85
Figure A.2 - Particulate measurement correlations 87
Figure A.3 - Particle Number - Mass Correlation 88
Figure A.4 - APC - SMPS Correlation 88
Figure B.1 - Multizone DIPulse Approach [46] 91
Figure B.2 - DIPulse Diffusion Combustion Rate Multiplier 92
Figure B.3 - Diffusion combustion simulation. 93
Figure B.4 - Available experimental injection rates 96
Figure B.5 - Injection profiles generation at constant rail pressure 96
Figure B.6 - Injection profiles generation at constant energizing time 97
Figure B.7 - Combustion parameters comparison 99
Figure B.8 - Engine Performance parameters comparison 99
Figure B.9 - Predicted vs Measured indicating results on Engine Map. 100
Figure B.10 - Predicted vs Measured indicating results on After Injection 100
Figure B.11 - Predicted vs Measured indi. results @1400 rpm x 100% load...... 101
Figure B.12 - Predicted vs Measured indi. Results @1400 rpm x 100% load. ... 101
Figure B.13 - NOx and Soot emissions comparison 102
Figure B.14 - Case Resolved Soot Emissions Comparison 102
Figure B.15 - Calibration Points Number Sensitivity 103

Chapter 1

Introduction

Part of the work described in this chapter has been previously published in:

- Gatti P, Fagg S, Cornwell R, Millo F, Boccardo G, Porcu D, et al. *Investigation of a "SCR-free" system to meet the Stage IV and beyond emissions limits*. Heavy-Duty, On- Off-highw. Engines 2016 11th Int. MTZ Conf., Ulm, Germany: MTZ; 2017, p. 274–91. doi:10.1007/978-3-658-19012-5_16

- Queck D, Herrmann OE, Bastianelli M, Naoki A, Manelli S, Capiluppi C, Fukuda A, Millo F, Boccardo G. *Next steps towards EGR-only concept for medium-duty industrial engine*. In: Liebl J, Beidl C, editors. Int. Mot. 2017 Mit Konf. Nfz-Motorentechnologie und Neue Kraftstoffe, Wiesbaden: Springer Fachmedien Wiesbaden; 2017, p. 555–72. doi:10.1007/978-3-658-17109-4_37.

Air pollution is a key environmental and social issue, with severe impact on health, vegetation, ecosystem and climate. Estimates of the health impacts attributable to exposure to air pollution indicate that $PM_{2.5}$ concentrations in 2014 were responsible for about 428 000 premature deaths in Europe, while 78000 are correlated to NO_2 and 14400 to O_3. Other than the social aspect it also has considerable economic impacts, cutting lives short, increasing medical costs and reducing productivity through working days lost across the economy [1].

Pollution is an issue that is being addressed globally. The developed countries started to enforce the earliest emission regulation in the second half of the 20th century, while others industrialized and industrializing countries are following in more recent times.

In Europe pollutant emissions were addressed by various international conventions, including the 1979 United Nations Economic Commission for Europe (UNECE) Convention on Long-range Transboundary Air Pollution (CLRTAP) and its various protocols, among which the 2012 amended Gothenburg Protocol is key in reducing emissions of selected pollutants across the pan-European region [1].

The Clean Air Policy Package for Europe, published by the European Commission in late 2013, aims to ensure full compliance with existing legislation by 2020 at the latest, and to further improve Europe's air quality, so that by 2030 the number of pollution-related premature deaths is reduced by half compared with 2005.

The emissions regulations succeeded to improve the air quality in Europe as shown in Figure 1.1, however a large portion of Europe is still exposed to pollutants concentrations exceeding the World Health Organization (WHO) Air Quality Guidelines, and challenges in emission reduction remain of primary importance [1].

The partial failure of the emission regulations is related to the inadequacy of the laboratory testing procedure, especially for Diesel equipped vehicles of the transport sector, which is one of the major contributors of pollutant emissions. This vehicles were found to produce four or five times higher emissions than the European standards in the real-world driving with respect to the certification procedure [2]. In order to oppose this phenomenon, emissions regulations in the power sector are now being tightened, especially for transport applications, adopting more aggressive cycles and real-world operation emission verification procedures.

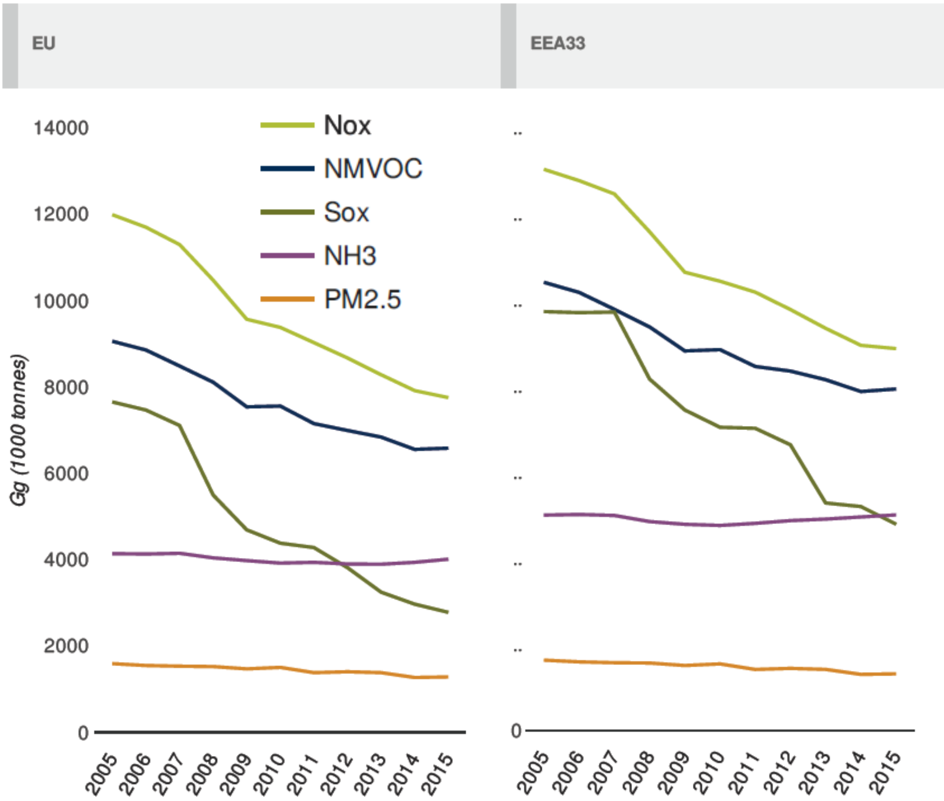

Figure 1.1 - Trends in emissions of air pollutants EU (left) and EEA-33 (right) [2]

In this context, Non Road Mobile Machineries (NRMM), which include any vehicle or operating machinery non directly devoted to the transportation of people or goods on the road, as better explained in the following Paragraph, play a role. NRMM are subjected to severe emissions regulations all around the world, which are being tightened with the target of improving Particulate Matter (PM) and NOx emissions. These pollutants are the most problematic in terms of harm to human health [2] and are the primary pollutants produced by Diesel engines, which is the dominating technology in this sector.

These new regulations are introducing new challenging issues in the design of such engines which must be addressed with the definition of new concepts and aftertreatment systems.

1.1 Non-Road Mobile Machines context

According to the definition reported in the European emission regulation "*non-road mobile machinery means any mobile machine, transportable equipment or vehicle with or without bodywork or wheels, not intended for the transport of passengers or goods on roads, and includes machinery installed on the chassis of vehicles intended for the transport of passengers or goods on roads"*[3]

A broader definition used in the United Kingdom states: "*Non-road mobile machinery is defined as any mobile machine, item of transportable industrial equipment, or vehicle - with or without bodywork - that is:*

- *not intended for carrying passengers or goods on the road*
- *installed with a combustion engine - either an internal spark ignition (SI) petrol engine, or a compression ignition diesel engine*

Examples of non-road mobile machinery include, but are not limited to:

- *garden equipment, such as hedge trimmers and hand-held chainsaws*
- *generators*
- *bulldozers*
- *pumps*
- *construction machinery*
- *industrial trucks*
- *fork lifts*
- *mobile cranes"*[4]

Within these definitions, the engine selected for the research project falls within the European Commission Non Road Diesel Engines original category of power rate between 75 and 130 kW, which has been extended in more recent regulations between 56 and 130 kW (EU Stage IV -10/2014). The applications of this kind of engines are extremely different varying between the truck-mounted forklift, with a duty cycle measured in minutes, and generators, with a duty cycles measured in days or months.
For this kind of power rate Diesel engines dominates the market thanks to its combination of durability, reliability, affordability and efficiency which drive the lowest Total Cost of Ownership (TCO) [5].

1.1.1 User Requirements

As mentioned in the previous Paragraph the field of application of the NRMM category is extremely various and the user requirements are extremely different.

In this paragraph the most important pillars of the design and operational requirements of these engines are analysed to better focus the motivations of this project.

- **Productivity**
  Those engines are normally installed on professional machines or in generators. As far as the professional machines are concerned, they can be loader, excavators, lifter or any type of agricultural machinery. Each of these applications has his own duty cycle that can be extremely different in terms of load and duration. The main goal for the engines equipped in these machinery is their ability to give productivity to the machine. For productivity is intended the amount of work which can be done in a given amount of time. This parameter is not regulated by a standard test and each manufacturer has its how procedure for its evaluation. Nevertheless, it has a strong dependency on the maximum performances, on the transient behaviour and on the load acceptability of the engine (depending on the application).

- **Total Cost of Ownership**
  Another parameter which is of crucial importance for this kind of machinery is Total Cost of Ownership (TCO). This parameter is the sum of the machine cost and of the operating cost, which includes the fluids consumption (Fuel + AdBlue if adopted) and the maintenance cost. The maintenance time, in which the machinery is not productive, is also considered as a cost, therefore the reliability is extremely important.
  For this reason, the introduction of new engine technologies is extremely challenging in this sector, since anything that does not bring immediate and significant improvement in the productivity does not worth the engineering effort to guarantee adequate reliability. Moreover, the fact that those machinery often operates in unfavourable environments must be considered in this regard.
  It is worth to highlight that higher is the size of the engine, higher is the relative weight of the fuel consumption over the TCO.

- **Packaging**
  Normally the design of the chassis of these machinery is well established, and the Original Equipment Manufacturers (OEMs) are not prone to modify the engine bay to accommodate more bulky engines, or to integrate wider air ducts or wider heat exchangers, or to accommodate new tanks for additional fluids.

- **Safety and Fuel availability**
  Those machineries normally operate in unfavourable environment, very dusty and dirty, often under extreme temperatures, and are subjected to hard vibrations. For this reason, engine which operates with low

flammability and low degree of explosiveness fuels are normally favoured, clearing the way to the success of Diesel technology in this field.

That said, since Diesel fuel is always present in construction area or, from a broader viewpoint, in the heavy duty field, machinery operating with Diesel are favourable also from the logistic point of view of having only one type of fuel.

1.1.2 Legislation

Historically the United States (US) regulations have been slightly tighter than the European Union (EU) counterparts in terms of NOx and PM emissions, as reported in Figure 1.2. Nowadays EU has overtaken US in setting the emission standards for this category of engines releasing the Stage V regulation which will be active in 2020.

This new regulation furtherly pushed the limit for particulate matter mass down to 0.015 g/kWh and firstly introduced the limit on particle number to $1x10^{12}$ #/kWh (details on the difference between Stage IV and Stage V regulation can be find in Table 1.1 and Table 1.2). Moreover, it would increase compliance and enforcement by strengthening rules on market surveillance by adopting portable emission measurement systems (PEMS) to monitor Particulate Matter, HC and NOx over normal duty cycles [6].

According to [7] this translates for OEMs in the mandatory use of Diesel Particulate Filters (DPF) since no practical way is available to reach this level of particles emissions with any in-cylinder emission control strategy.

The introduction of the DPF is particularly critical for NRMM, since it is an aftertreatment device that affects the engine performance (and therefore the productivity of the machinery) due to engine backpressure increase and due to the strategies that must be put in place for its regeneration. It is extremely critical especially for the application which have an extremely short duty cycle as the truck-mounted forklifts. These machines are used to load and unload the truck they travel along with, and they are operated for a very short time not giving the DOC (Diesel Oxidation Catalyst) and the DPF the possibility to reach the temperature needed to activate the regeneration process. The only possibility for the DPF regeneration is a stand still strategy manually activated by the user, in which the machinery is left offline to complete a cycle of warm-up and DPF regeneration before being able to operate again. This kind of regeneration strategy that can last for several tenths of minutes, strongly affects the productivity of the machine.

Moreover, DPF can bring several packaging problems especially if the engine is already equipped with other complex aftertreatment system for NOx.

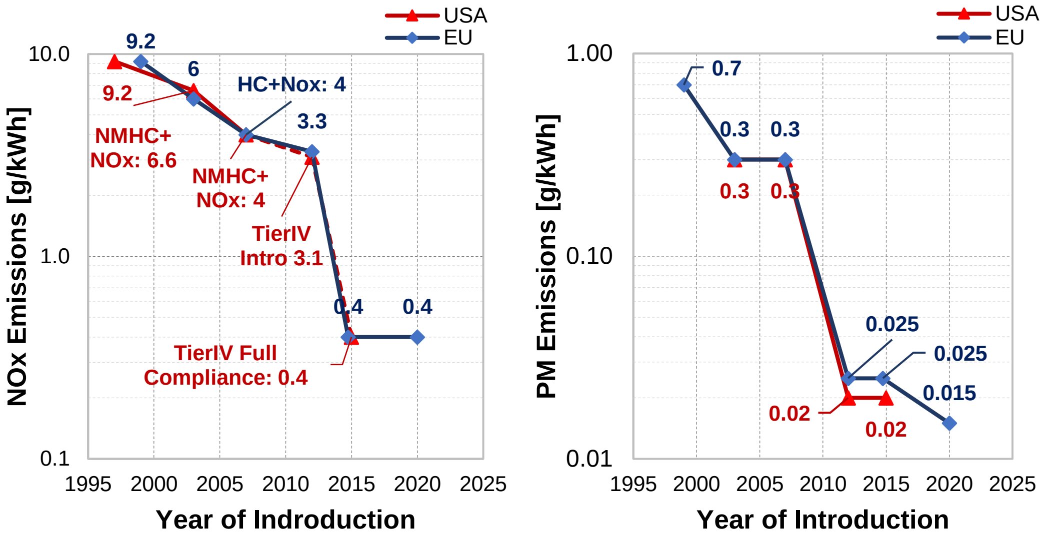

Figure 1.2 - EU and USA NRMM NOx and PM Regulations
(56 < Peak Power < 130 kW) [8][9]

Table 1.1 - Stage IV emission standards for NRMM Diesel Engines [8]

Cat.	**Net Power** *kW*	**Date**	**CO**	**HC**	**NOx**	**PM**
			g/kWh			
Q	130 ≤ P ≤ 560	2014.01	3.5	0.19	0.4	0.025
R	56 ≤ P < 130	2014.10	5.0	0.19	0.4	0.025

Table 1.2 - Stage V emission standards for NRMM Diesel Engines [8]

Category	**Ign.**	**Net Power** *kW*	**Date**	**CO**	**HC**	**NOx**	**PM**	**PN** *1/kWh*
				g/kWh				
NRE-v/c-1	CI	P < 8	2019	8.00	7.50[a,c]		0.40[b]	-
NRE-v/c-2	CI	8 ≤ P < 19	2019	6.60	7.50[a,c]		0.40	-
NRE-v/c-3	CI	19 ≤ P < 37	2019	5.00	4.70[a,c]		0.015	1×10^{12}
NRE-v/c-4	CI	37 ≤ P < 56	2019	5.00	4.70[a,c]		0.015	1×10^{12}
NRE-v/c-5	All	56 ≤ P < 130	2020	5.00	0.19[c]	0.40	0.015	1×10^{12}
NRE-v/c-6	All	130 ≤ P ≤ 560	2019	3.50	0.19[c]	0.40	0.015	1×10^{12}
NRE-v/c-7	All	P > 560	2019	3.50	0.19[d]	3.50	0.045	-

[a] HC+NOx
[b] 0.60 for hand-startable, air-cooled direct injection engines
[c] A = 1.10 for gas engines
[d] A = 6.00 for gas engines

Type Approval Tests:

The type approval test requires the measurement of the engine emissions along two cycles: the Non Road Steady Cycle (NRSC) and Non Road Transient Cycle (NRTC).

NRSC

The NRSC is a sequence of several steady state modes with different weighting factors as schematically reported in Table 1.3. This test is reported within the international standard for exhaust emission measurement ISO 8178 with the identification "Type C1".

Table 1.3 - Non Road Steady Cycle (ISO 8178 -Type C1) [10]

Mode number	**1**	**2**	**3**	**4**	**5**	**6**	**7**	**8**	**9**	**10**	**11**
Torque, %	100	75	50	25	10	100	75	50	25	10	0
Speed	Rated speed					Intermediate speed					Low idle
Type C1	0.15	0.15	0.15	-	0.10	0.10	0.10	0.10	-	-	0.15

Referring to Table 1.3 "rated speed" identifies the speed at which the manufacturer declares the maximum power, and "intermediate speed" the speed corresponding to the maximum torque. In the last row the relative weighting factors of each operating point are reported.

NRTC

The NRTC test is a transient driving cycle for mobile nonroad engines developed by the US Environment Protection Agency (EPA) in cooperation with the authorities in the European Union (EU). The test is used internationally for emission certification/type approval of nonroad engines [11].

The cycle was developed by means of a statistical analysis of the Real-World cycles of different machineries and tries to represent each NRMM application as Figure 1.3 by AVL shows.

The cycle is an engine dynamometer transient driving schedule with a total duration of 1238 seconds, normalized over the maximum torque and the maximum speed. It is run twice, with a cold and a hot start, with a 20-minute soak period between the tests. The cold start weighting factor is 10% in the EU and 5% in the US [11], making the cold start definitely not a concern for this kind of engines, thanks to the relatively low weighting factor and to the extremely aggressiveness of the cycle which makes the aftertreatment to warm up quite soon. The cycle, in fact, covers almost all the engine map with very frequent operation near the full load. Moreover, it is extremely transient demanding with frequent loadsteps from very low loads to full load in less than two seconds. To give a practical evidence of the aggressiveness of this cycle a comparison with the load profile of a medium-size passenger car diesel engine over the Worldwide Harmonized Light Vehicles Test Cycle (WLTC) is reported in Figure 1.4. Finally, the comparison of the NRTC and NRSC (assuming speed of maximum torque equal to 50%) over the normalized engine map is reported in Figure 1.5.

NTE

From US Tier IV, NRMM engines must comply also to the Not-To-Exceed Standard (NTE), which is a further instrument to guarantee that Heavy Duty Engines emissions are controlled over the full range of speed and load combinations commonly experienced in use. It does not involve a specific testing procedure and can include any steady or transient operation within the NTE control area.

The basic definitions of NTE area are the following [12]:

- All engine speeds 15% above the ESC (European Stationary Cycle) speeds [13].
- All engine load points greater than or equal to 30% or more of the maximum torque value produced by the engine.
- All speed and load points where the power produced by the engine is higher than 30% of the maximum power.

Engines which are certified with regulations requiring NOx and PM below 2.5 g/kWh or 0.07 g/kWh respectively, can apply a factor of 1.5 on the emissions regulated value when operating in this area.

All the operating conditions which are not covered by those test procedures are not regulated.

Comparing Figure 1.5 and Figure 1.6, it results clear that the non-regulated zone and NTE zone applies only at low speed high load, which is the only region of the engine map not covered by the more stringent NRSC and NRTC.

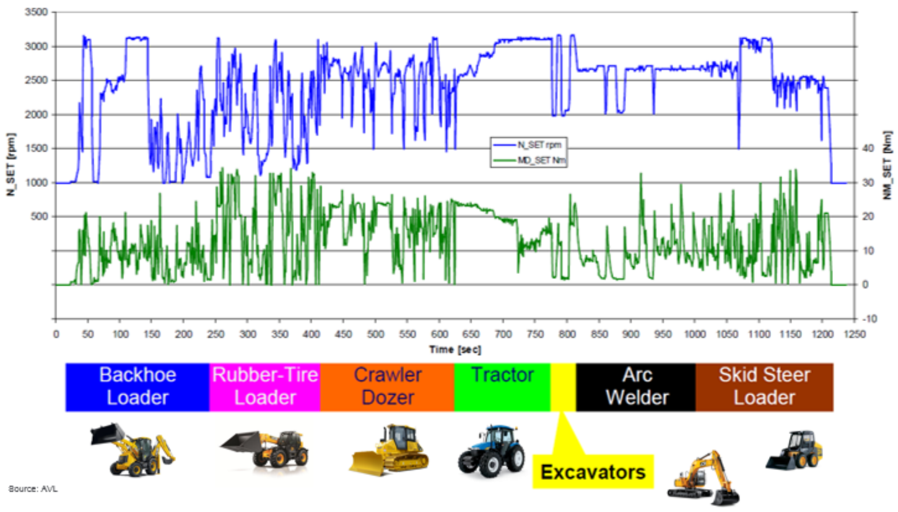

Figure 1.3 - Non Road Transient Cycle [AVL]

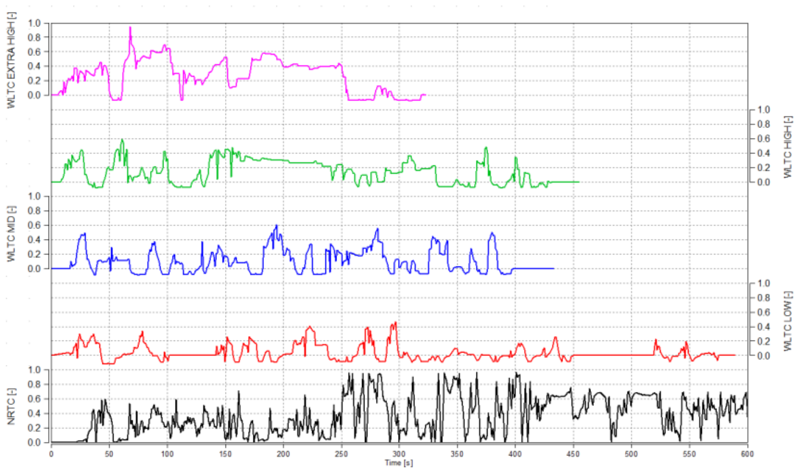

Figure 1.4 – WLTC and NRTC comparison

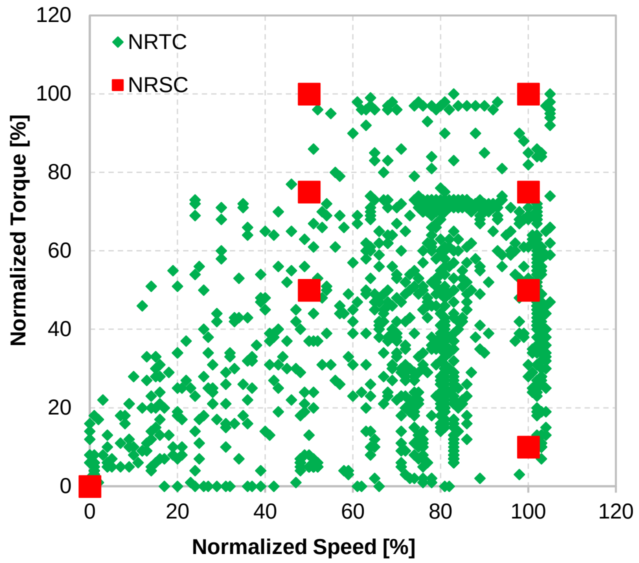

Figure 1.5 - NRSC and NRTC comparison

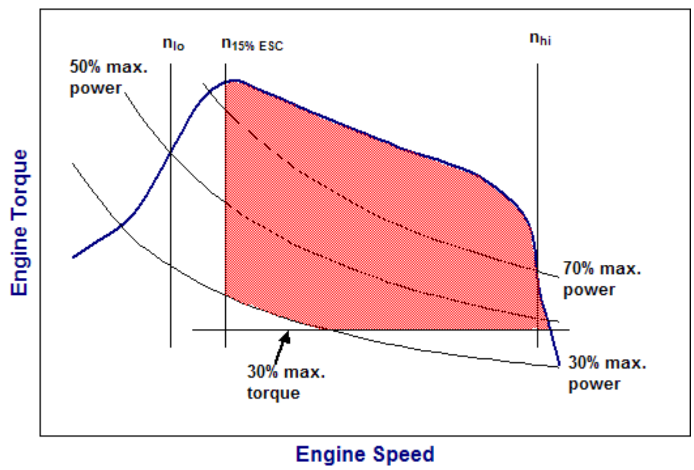

Figure 1.6 - Basic NTE zone [12]

1.2 Project Overview

As previously explained, the European Commission is introducing with the Stage V regulation the limit on particle number, forcing the engine manufacturers to introduce DPF in their aftertreatment systems, since no practical way is available to meet the limit of $1x10^{12}$ #/kWh with any in-cylinder technique [7].
On the other hand, NOx limit has been kept constant from Stage IV, and several layouts are feasible to meet the limit of 0.4 g/kWh.
Ricardo investigated three main engine layouts, to meet the NRMM Stage V for engine power rate between 56 and 130 kW regulation, which are summarized in Figure 1.7.

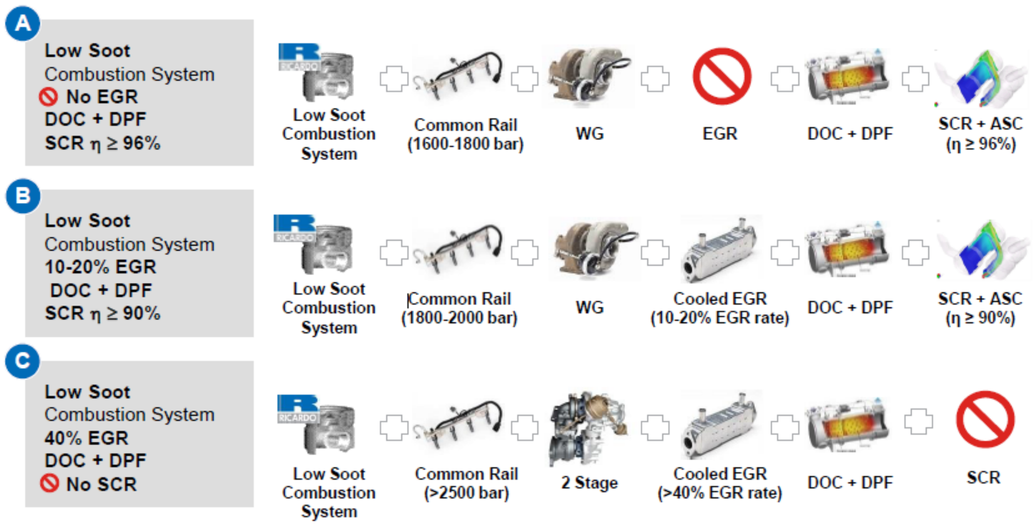

Figure 1.7 - Stage V Compliant NRMM Engine Layout [14]

- **Solution A** features quite standard engine layout, completely avoiding the use of Exhaust Gas Recirculation (EGR) and demanding all the NOx reduction to a high efficiency Selective Catalytic Reduction (SCR) combined with an Ammonia Slip Catalyst (ASC). For this kind of layout, a standard single stage turbocharging system and low to medium injection pressure Common Rail (CR) Fuel Injection System (FIS) is enough.
- **Solution B** relaxes the efficiency requirement of NOx catalyst, introducing the use of low rate of Cooled EGR to partially reduce the in cylinder NOx formation. This will require higher boost pressure to keep Air-to-Fuel Ratio (AFR) and smoke under control, and increased injection pressure to deal with the increased charge density and slower combustion due to the EGR dilution effect.
- **Solution C** avoids completely the use of any aftertreatment for NOx, demanding all the NOx reduction to extremely high rate of cooled EGR. In order to pursue this solution a high performance boosting system, such as an intercooled two stages turbocharger, must be used in order

to guarantee adequate AFR with such amount of EGR. The extremely high charge density will require an extremely high-pressure FIS to guarantee good mixing and acceptable combustion duration.

In the emissions power band between 55 and 100 kW, which represents almost the 30% of the market, Kohler have developed the KDI3404, a 3.4 liters, 4 cylinders Diesel engine compliant with Stage IV and Tier IVf regulation, sold in different power configurations between 75 and 100 kW. All the applications feature SCR catalyst for NOx. The introduction of the DPF with the upcoming Stage V pushed Kohler to start a project in collaboration with Politecnico di Torino, Denso and Ricardo, to explore the possibility to meet Stage V emission regulation exploiting the last-proposed solution.

SCR-free architectures could offer some advantages for this kind of application since SCR systems typically present several drawbacks, such as significant packaging issues especially when combined with a DPF, need for an infrastructure for a second liquid and additional sensors and actuators, at the risk of reducing the robustness and increasing the cost.

As a further support of the packaging concerns, in Figure 1.8 the design of the current production engine (Stage IV with SCR) and the design of the Stage V SCR-free layout is compared. It is worth to remind that a Stage V SCR layout would anyway require DOC and DPF.

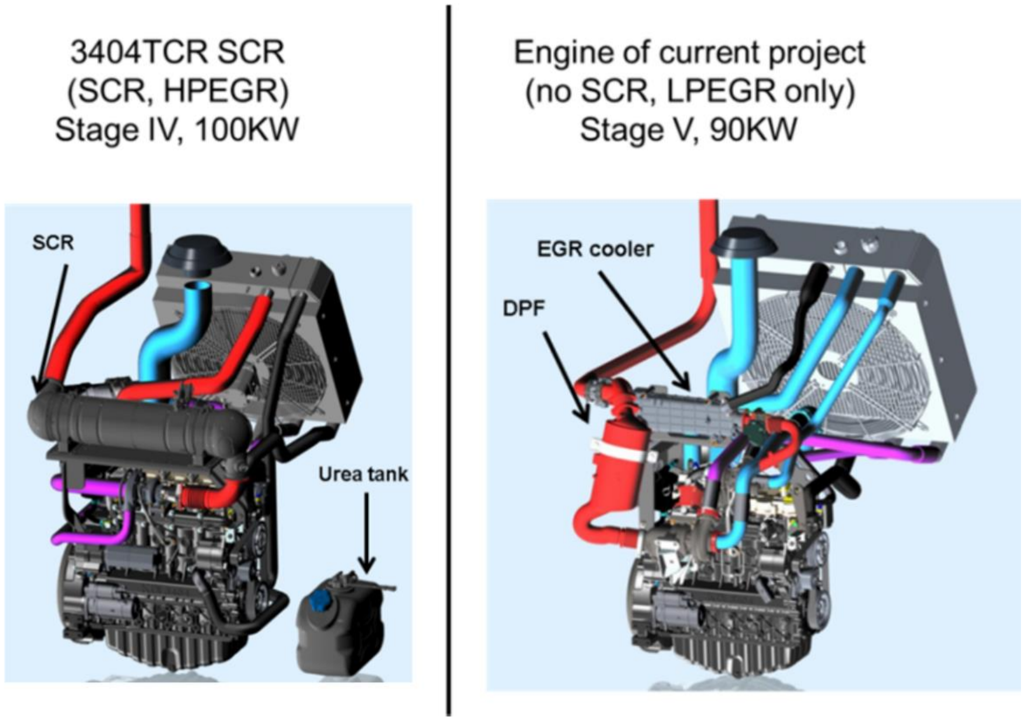

Figure 1.8 – Packaging comparison of SCR and SCR-free architectures [15]

Few examples of similar architectures are reported in literature.

In [16] the use of extremely high injection pressure in combination with cooled EGR rate above 40 % was needed to achieve the engine out level prescribed in Tier

4f with a lambda of 1.5 in a 30 kW/l engine, requiring a boost pressure of 5 bar (absolute).

In [17], a 6 cylinders, 6 liters, MAN Heavy Duty Diesel Engine was modified with a 2500 bar FIS to try to meet the Stage IV limits without SCR. Without an ad-hoc optimization of the calibration and of the combustion system, this engine was able to reach 0.6 g/kWh of NOx with acceptable transient performance at the price of high smoke emissions.

The project was developed in three phases:

- **Preliminary Phase:** in this phase which was Ricardo and Kohler main responsibility, the main tasks were the following:
  - AFR and EGR targets definitions to meet the legislative limits.
  - Combustion system definition: combustion chamber, swirl ratio and injector nozzles portfolio to be experimentally tested.
  - Turbochargers matching.
  - EGR cooler sizing and airpath definition.

- **First Experimental Phase:** in this phase which has been carried out in the steady-state test bench of the Energy Department of Politecnico di Torino (DENERG), the engine was tested with a provisional design in order to carry out the Nozzle Selection, to experimentally confirm the AFR and EGR targets, and so the boosting requirements, and to develop a first steady state calibration. This part of the project is widely discussed in Chapter 2.

- **Second Experimental Phase:** this last phase, which is extensively described in Chapter 3, was carried out with the final engine setup in the transient test bench of DENERG. The main task was the development of a steady state and transient calibration able to meet the Stage V Emissions standards.

1.3 Engine description

The engine chosen for the project was a modified version of the normal production KDI3404TCR shown in Figure 1.9.

Figure 1.9 - Kohler KDI3404 Engine

This engine is on the market in different power rates since 2014 and it is compliant with the EU Stage IV standard featuring High Pressure EGR, 2000 bar Denso Common Rail FIS and a single stage turbocharger controlled by a mechanical wastegate.

The engine was modified for the purposes of the project by replacing the single stage turbocharger with a two stages unit, the HP EGR line was replaced by a LP pressure pathway, the combustion system (cylinder head + combustion chamber) was developed ad hoc, and the 2000 bar common rail FIS was replaced with a 4th Generation Denso Common Rail capable of 3000 bar injection pressure.

The high level targets are reported in Table 1.4 for what concerns emissions, and in Figure 1.10 in which the performance of the normal production Stage IV are plotted with the target for this project. A modest power derating was accepted due to the early stage of development of the engine technology.

In Table 1.5 the main engine specifications are summarized.

Table 1.4 - Provisional High-Level targets on certification cycles [14]

		NOx [g/kWh]	HC [g/kWh]	CO [g/kWh]	PM [g/kWh]	PN [#/kWh]
Legislated Limit	EU Stage V	0.4	0.19	5	0.015	$1*10^{12}$
Provisional Engineering Targets	Tailpipe Emissions	< 0.34	0.15	1.5	0.012	$8*10^{11}$
	Aftertreatment Conversion Efficiency	-	DOC >90%	DOC >90%	DOC >90% DPF >99%	DPF>99%
	Engine Out Emissions	< 0.34	< 1.5	< 15	<1.2	$<8*10^{13}$

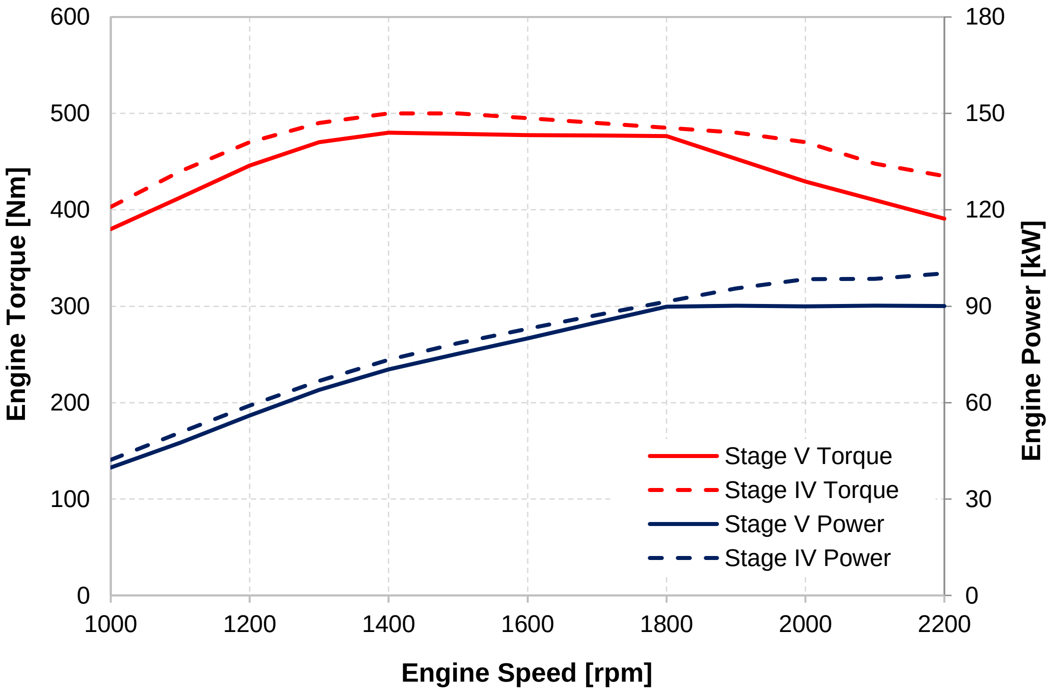

Figure 1.10 - Full Load Performance

Table 1.5 – Stage V Engine Specifications

Engine Type	Diesel / 4 Cylinders In Line / Cast Iron Crankcase
Valvetrain	4 Valves / Pushrod - Rocker with hydraulic tappets
Bore	96 mm
Stroke	116 mm
CR	16
Displacement	3.4 liters
Turbocharger	2 Stages (Intercooler + Aftercooler)
EGR	Cooled Low Pressure
Fuel System	Denso HP6 Pump / G4S Injectors / 3000 bar Injection Pressure
Aftertreatment	DOC + DPF
Performance	480 Nm @ 1400 rpm / 90kW @ 2200 rpm

To define the engine layout and properly size each component Ricardo performed a keypoint analysis of both NRSC and NRTC to define the target values for EGR rate and AFR. This was obtained ahead of any detailed 1D or 3D Computational Fluid Dynamics (CFD) simulation activity, using a well-established 0D modelling approach, which uses empirical NOx and soot/smoke/PM relationships to rapidly explore the design space with minimal computational effort.

The outputs of this methodology are the AFR and EGR target over the full load operating conditions, summarized in Table 1.6.

Table 1.6 - Full Load AFR and EGR Targets [14]

Speed	rpm	1000	1200	1400	1600	1800	2200
Torque	Nm	380	446	480	478	451	391
AFR	-	17.5	17.5	17.7	18.1	18.6	19
EGR	%	10	20	40	38	38	42

Of particular note is the very high EGR rate at full load, coupled with the need of maintaining acceptable minimum AFR. It is clear that this combination of targets place very strong demands on the air/EGR [18][19][20] and combustion systems.

In the following Paragraphs a detailed description of the engine components selected to meet these ambitious targets is presented.

1.3.1 EGR

The ability to recirculate EGR is the key factor for this kind of engine layout. Without the correct amount of EGR, the only way to control NOx emission is to retard the injection timing to reduce the combustion temperature with big penalty in fuel consumption. The ability to recirculate EGR is defined from one side by the EGR system and its ability to exploit the pressure difference between exhaust and intake pressure to drive the exhaust gases, and on the possibility to increase this pressure difference when needed.

On the other hand, the EGR rate is limited by the necessity of keeping acceptable AFR to control soot emissions, therefore the EGR tolerance increase as the boost pressure increase, making the charging system a paramount component.

As widely reported in literature, EGR reduces NOx mainly by lowering the combustion temperature, therefore the EGR temperature is of crucial importance to fully exploit the EGR rate making the sizing of the EGR cooler another key aspect of the design. Mainly three layouts are available for EGR circuits: high pressure (HP-EGR), low pressure (LP-EGR) and the combination of the two or dual loop (DL-EGR).

In the HP architecture, a fraction of the exhaust gases is diverted from the exhaust manifold upstream of the turbine, to the intake manifold downstream of the intercooler forcing the gases through an EGR cooler. The system is controlled by an EGR valve placed downstream of the cooler for obvious thermal concerns.

In the LP architecture instead, the exhaust gas is sampled downstream of the aftertreatment and recirculated upstream of the compressor after being cooled in an

EGR cooler. The system is controlled by an EGR valve that regulates the flow and a flap that can be placed alternatively in the intake line or in the exhaust line to increase the pressure differential to flow the EGR. Numerical analysis have shown that the exhaust positioning of this valve is more effective from the efficiency point of view [19].

The HP and LP architectures can also be combined obtaining what is usually called a hybrid or dual loop system.

Although the HP circuits have been the most widespread up to now, the LP architecture offers the opportunity to achieve higher EGR rate while maintaining low intake temperatures and with perfect mixing. Moreover, the introduction of DPF and the consequent clean EGR being recirculated, solves the concerns about compressor wheel damaging and cooler fouling. However LP EGR often shows poor transient performance and requires more sophisticated control [21].

Ricardo carried out an investigation of the sensitivity of key EGR hardware attributes to rated power using their 0D modelling approach which confirmed the selection of LP-EGR as the preferred route to going forward. The results of this analysis are reported in Figure 1.11, which indicates the response of various engine parameters as rated power is varied between 80 and 100 kW (23.5-29.4 kW/l, 12.8-16.0 bar BMEP) if LP or HP-EGR is used. With LP-EGR, generally, the thermal load on compressors, interstage cooler, EGR cooler, and intake manifold boost pressure are all reduced compared to the HP-EGR case. Additionally the target power of 90 kW is confirmed as being sensibly achievable within the engine structural Peak Firing Pressure (PFP – Maximum in cylinder pressure) limit, which was initially set to 170 bar for this application, even though the hardware can withstand up to 180 bar.

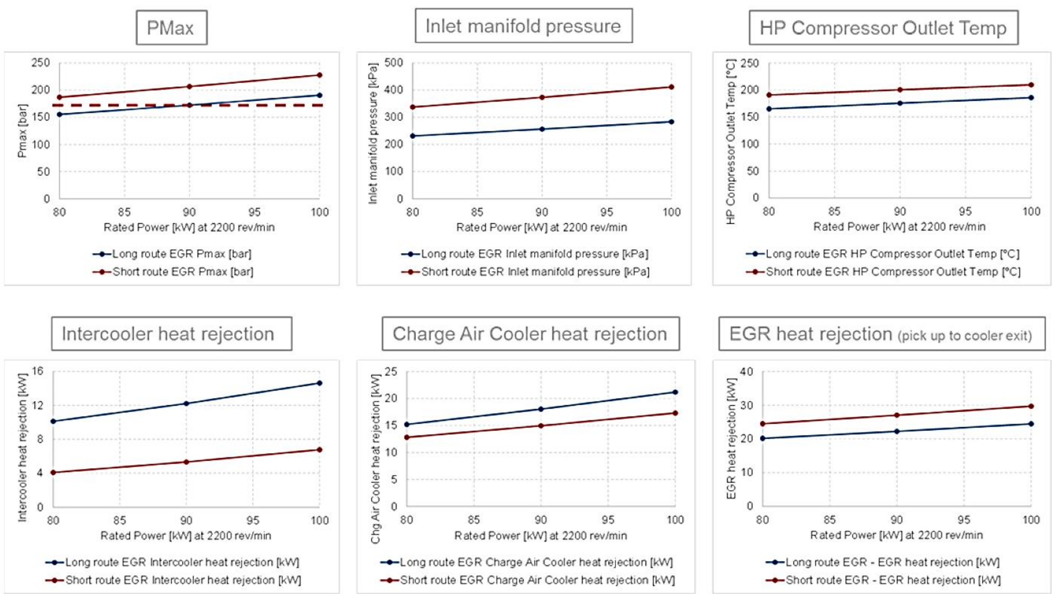

Figure 1.11 - 0D model responses to EGR circuit type and rated power [14]

The final LP-EGR system, which has been used in the Second Phase of testing (Chapter 3) and developed in collaboration with Denso especially as the control is concerned, recirculates the exhaust gases in the intake line downstream of the air filter, sampling downstream of the DPF. It features two valves: one placed downstream of the EGR Cooler (V2 in Figure 1.12), that regulates the flow of the bypass, and another placed in the exhaust line downstream of the bypass junction (V1 in Figure 1.12). This one is used to generate backpressure to force EGR recirculation when the pressure drop between exhaust and intake lines is not enough to obtain the desired flow.

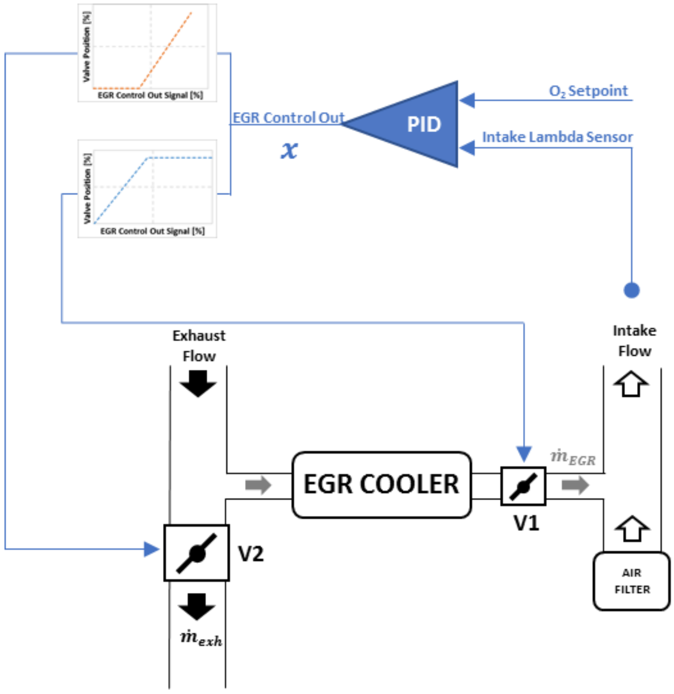

Figure 1.12 - EGR system overview [22]

The control works with a set-point of O_2 concentration in the intake line, which is measured by a lambda sensor placed downstream of the high pressure compressor and upstream of the aftercooler in order to avoid water condensation on the sensor. It outputs a non-dimensional variable (range 0 – 100) which is translated by two functions in the position of the two valves. More information on the EGR control are given in Paragraph 3.4.

1.3.2 Turbocharging System

As explained before, the turbocharging system is a key component for this application. The higher is the charge density, the higher is the EGR that can be mixed while keeping adequate AFR, thus controlling NOx with more efficiency-oriented injection timing. In order to maximize this effect, an intercooled and aftercooled two stages system was selected. A single stage turbocharger, would not have been enough, due to amount of EGR to be recirculated which would have caused an extremely high thermal load on the compressor. A two stages system instead splits the pressure ratio requirement on two stages and reduce the thermal load by means of an intercooler [20]. The final turbocharging architecture used two fixed geometry stages: the low pressure stage has higher flow than the high pressure one and it is not controlled, while the high pressure is controlled by means of a mechanical WasteGate (WG).

1.3.3 Fuel Injection System

The fuel injection system is the enabler technology of this engine layout. Increasing the charge density for the abovementioned reasons, causes lower fuel jet penetration and less air utilization leading to high smoke and poor EGR tolerance. Increasing injection pressure could be a countermeasure to this phenomenon, providing further opportunities to improve fuel consumption thanks to the reduced injection and combustion duration [16]. Increasing the injection pressure up to 3000 bar has been proved to be very effective in improving NOx/Soot and NOx/BSFC tradeoff as shown in [16][23][24][25], where reductions in soot emissions between 40 and 70% at constant NO_x level were observed. In [18] smoke emission benefits were found only up to 2500 bar, but efficiency improvements were found up to 3000 bar. It is worth mentioning that increasing the injection pressure could be a viable option also for more common engine layout, if coupled with a reduced injector nozzles hydraulic flow thus improving fuel atomization and the NO_x-Soot tradeoff consequently [24].

For this project Denso provided their 4th Generation Common Rail (CR) system rated for 2500 bar, enabling rail pressure up to 3000 bar for development purpose. The fuel injection system includes a HP6 high pressure pump featuring two pumping elements and G4S injectors operating without static leakage.

As known from previous investigations carried out by Denso on a 10 liters engine, since the system is operating without static leakage the drive power for the fuel pump is significantly reduced leading at same injection pressure to 1% less Indicated Mean Effective Pressure (IMEP) with the same engine load (Figure 1.13). When increasing the injection pressure to 3000 bar the friction is still lower than for the conventional system at 1800 bar and, as combined effect with the reduced combustion duration, the Brake Specific Fuel Consumption (BSFC) is neutral to the increase of injection pressure, providing 1 to 1.5% benefit. Moreover, in the steady state point shown in Figure 1.13 the soot is reduced by 70% thanks to increased Rail pressure. This result was measured at a still high NOx level of 2 g/kWh. Similar results are reported in [24], but the BSFC improvement was reported as more than 5% when increasing the injection pressure from 2000 to 3000 bar at a constant NOx level of 2.2 g/kWh. On the other hand, BSFC is reported to be quite insensitive to the reduction of engine out NOx from 2 g/kWh down to 0.8 g/kWh.

As far as the nozzle definition is concerned, it was one of the main task of the first testing phase, which is extensively described in Paragraph 2.2.

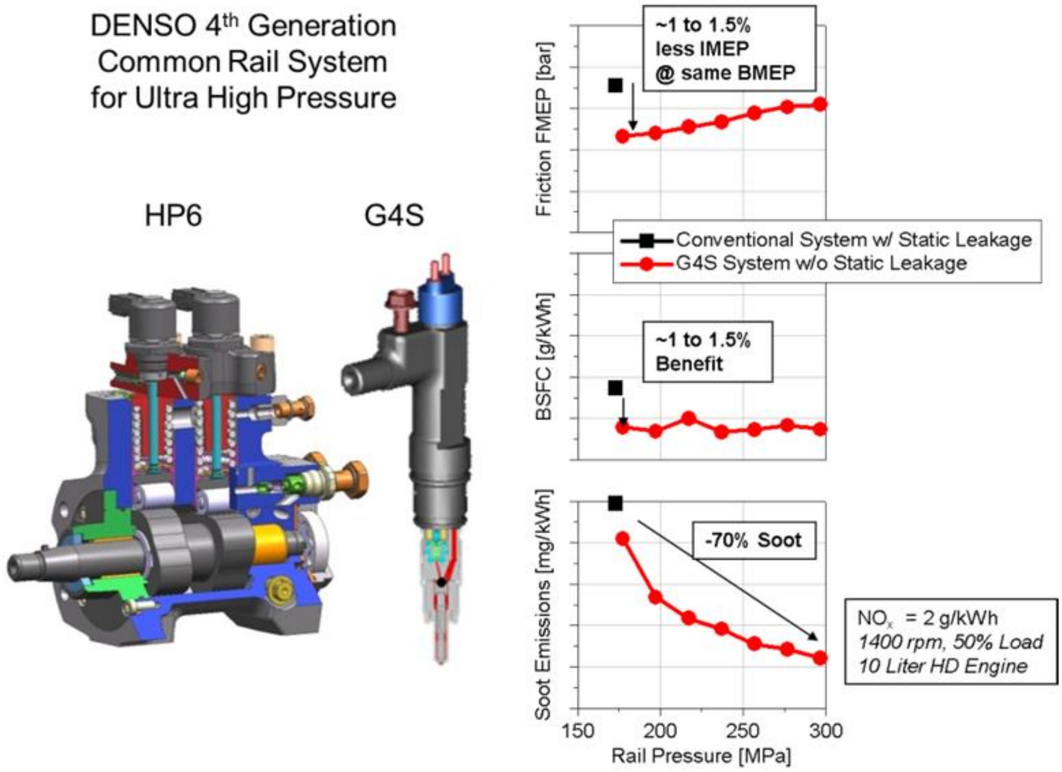

Figure 1.13 – Assessment of the DENSO 4th Gen. Ultra High Pressure FIS [15]

1.3.4 Combustion System

The opportunity of using a FIS with much higher injection pressure availability provides two alternative possible combustion strategies to meet the programme targets, i.e.:

A. Significant shortening of injection period
   Motivation: best efficiency
   Likely characteristics: high spray momentum due to large nozzle holes, tendency to optimise with a wider piston bowl
B. Significant reduction in nozzle hole size (same period - smaller holes)
   Motivation: best soot
   Likely characteristics: lower spray momentum, tendency to optimise with a narrower piston bowl

CFD simulations carried out by Ricardo identified that the combination of Twin Vortex Combustion System (TVCS) style bowl [26]–[31] together with 8 hole injector nozzle produced a favourable mixing regime as reported in Figure 1.14 and Figure 1.15. Those Figures report a matrix comparison of a conventional bowl and a TVCS bowl and two nozzles: a 8 holes with higher flow rate (930cc/min) and a 7 holes with lower flow (730 cc/min) at 75% load, rated speed and 2250 bar injection pressure.

TVCS bowl showed improved fuel mixing compared to the conventional wider design as it is evident in Figure 1.14 in which the large pocket of rich mixture present in the conventional bowl cannot be found in the TVCS design.

In Figure 1.14 and in Figure 1.15, it can be observed that the TVCS-style piston bowl shows a marked transformation of fuel/air cloud into an upward moving plume later in the injection/combustion process, keeping rich mixture well away from the cooler cylinder walls (with consequent benefits in combustion progress without quenching and soot-in-oil).

Secondly the 8-hole nozzle shows a markedly beneficial merging/dissolution of the individual spray plumes with corresponding rapid dispersion of rich regions.

As far as the swirl is concerned, the retention of the swirl level of 2.0 Rs used in the base engine was decided. In fact, although in general a higher swirl level might be expected to give an improvement in terms of mixing, other CFD analysis showed that as the swirl increases, the interaction with the piston bowl decreases thus making the TVCS lip ineffective.

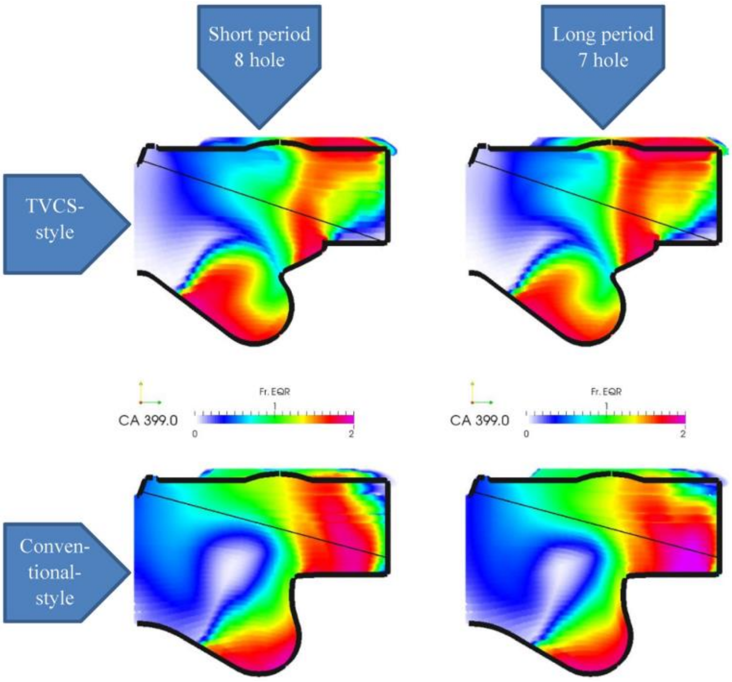

Figure 1.14 – CFD Equivance Ratio for TVCS and Conventional Bowl design for two injection nozzles at rated speed, 75% of Load, 2250bar Injection pressure - Side View [14]

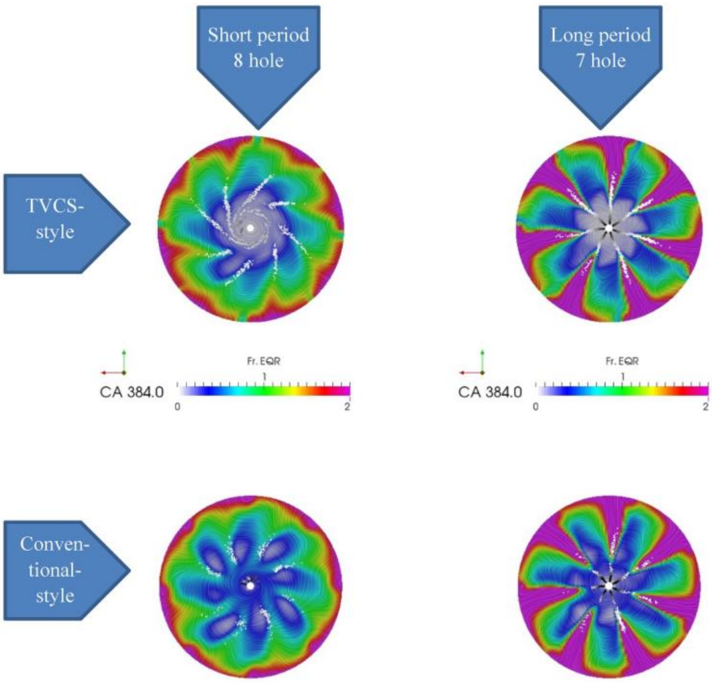

Figure 1.15 - CFD Equivance Ratio for TVCS and Conventional Bowl design for two injection nozzles at rated speed, 75% of Load, 2250bar injection pressure - Top view [14]

Chapter 2

First Experimental Phase

Part of the work described in this chapter has been previously published in:

- Gatti P, Fagg S, Cornwell R, Millo F, Boccardo G, Porcu D, et al. *Investigation of a "SCR-free" system to meet the Stage IV and beyond emissions limits*. Heavy-Duty, On- Off-highw. Engines 2016 11th Int. MTZ Conf., Ulm, Germany: MTZ; 2017, p. 274–91. doi:10.1007/978-3-658-19012-5_16

In this chapter the first experimental phase of the project is described. This phase was mainly devoted to the nozzle selection, the definition of the boosting requirements and the development of a preliminary steady state calibration. These activities were carried out in the steady state test bench of DENERG. The engine configuration tested in this phase was at the very early stage of development: the turbocharging system was the single stage version of the current production Stage IV, and a simulating low-pressure stage device was used instead. The low pressure EGR pathway was built according to the charging system, recirculating downstream of the DPF to the inlet of the physical high-pressure turbocharger. The FIS was instead already the Denso IV Generation Common Rail, capable of 3000 bar injection pressure.

2.1 Experimental Setup

Figure 2.1 - 1st Phase Experimental Setup

The engine used in this phase was a normal production Kohler 3404, equipped with the new combustion chamber and the new 3000 bar FIS. The turbocharger was the normal production model since the boost requirement for the two-stage system had to be defined here, exploiting to the low pressure simulating device described in Paragraph 2.1.2.

The aftertreatment of the normal production engine was replaced by a closed coupled DOC+DPF, and the high pressure EGR line was closed and replaced by Low-pressure-like pathway to recirculate exhaust gas between downstream of the DPF and upstream of the “physical” turbocharger. The EGR line featured a cooler flowed by engine coolant, made by two coupled normal production EGR cooler. The system was operated by two valves: one placed downstream of the EGR cooler operated by the Engine Control Unit (ECU), and another placed in the exhaust line, downstream of the junction remotely operated by the test bench operator. This valve was needed to generate enough backpressure to force EGR recirculation. The backpressure had to be higher than the pressure provided by the auxiliary low-pressure system and to some extent acted to keep into account the pressure drop of the low-pressure stage turbine. The biggest concern of this layout at the time of installation, was that the DPF had to be stressed by very high pressure (up to 3 bar in peak power point), however it did not show any problem within all the tests campaign. A schematic of the engine layout is reported in Figure 2.2.

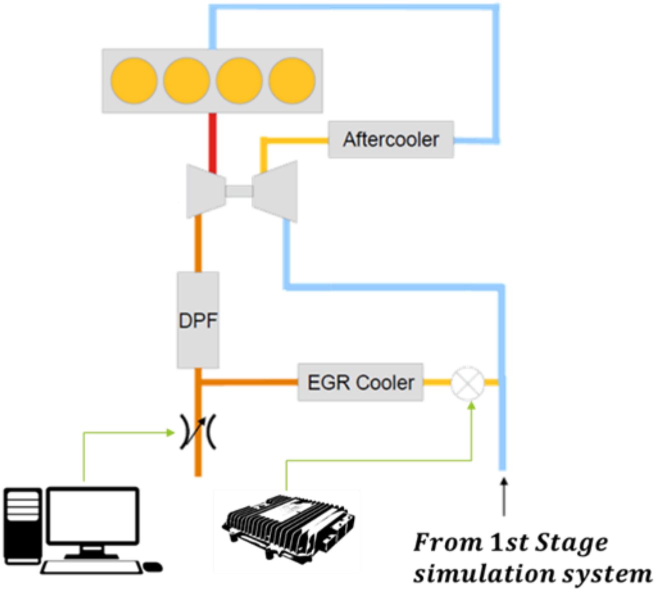

Figure 2.2 - First Testing Phase Engine layout

2.1.1 Steady-State Test Bench

The Steady state test bench of DENERG in which the engine was mounted, is equipped with a Borghi e Saveri FE 260 eddy current dyno with the characteristics reported in Table 2.1.

Table 2.1 - Steady-State Test Bench dyno parameters

	Max Power	Max Speed	Max Torque	Max Torque Speed	Moment of Inertia
BORGHI & SAVERI FE260S	kW	RPM	Nm	RPM	Kg/m2
	191	12000	610	1200	0.176

In this test bench air temperature and humidity are not controlled, however the combustive air was drawn from the compressed air net of the lab and delivered to the engine by the Low-Pressure stage simulating device presented in the following paragraph. The compressed air is oil-free and dehumidified with a quite good temperature stability. The engine cooling was guaranteed by a water to water heat exchanger in which the water drawn by the water main was modulated by a PI controlled valve to target 90°C at the engine outlet. Similarly, the Aftercooler (see Figure 2.2) between “physical” high pressure compressor and intake manifold was an air to water regulated heat exchanger to target a pre-defined intake manifold temperature.

The test bench was equipped with the following measurement devices:

- AVL Fuel balance 733S to measure the fuel consumption coupled with a fuel conditioning system to keep fuel temperature at 37°C at the inlet of the high-pressure pump.
- AVL 415s Smokemeter to measure the Filter Smoke Numer (FSN) and, indirectly, the Soot concentration, upstream the aftertreatment.
- Double line AVL AMAi60 to measure independently THC, CO, CO_2, NOx, O_2. One line of the AMAi60 was placed to sample engine out and the other one to sample at the intake manifold to trace EGR.
- Two in-cylinder high frequency piezoelectric Kistler 6056A pressure transducer and a high frequency current clamp to measure the solenoid injector current, recorded with a homemade, National Instrument-based, indicating system (PowerPan).

2.1.2 Low-Pressure stage simulating device

As already explained, a two-stage turbocharging system was not available in this preliminary phase in which the boosting requirement had to be still defined. For this reason, an auxiliary compressed air delivering system had to be developed to feed the "physical" turbocharger representing the high-pressure stage.

This system exploits the compressed air net of the lab which is delivered and dried by an oil-free compressor at 8 bar. The device, presented in Figure 2.4 and in Figure 2.3, has a first pressure reduction unit to bring the pressure down to 5 bar for safety reason, a filter and a second manually adjustable reduction unit to reduce the pressure between 1 and 3 bar. The third reduction unit is controlled by a PID controller to regulate the pressure in the downstream reservoir to a value remotely set by the user. Between the reservoir and the engine, an ON/OFF valve remotely operated is placed to connect and disconnect the system from the engine.

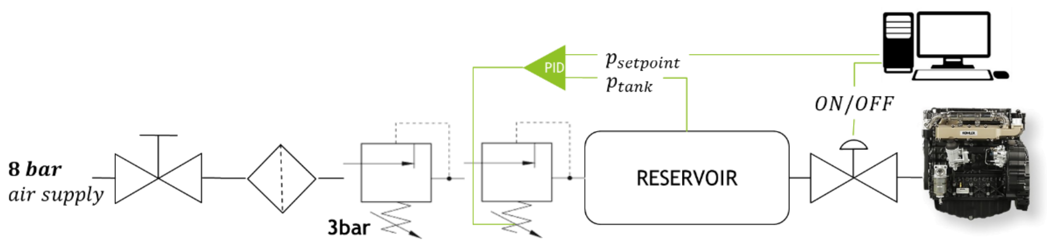

Figure 2.3 - Low Pressure stage simulating device schematic

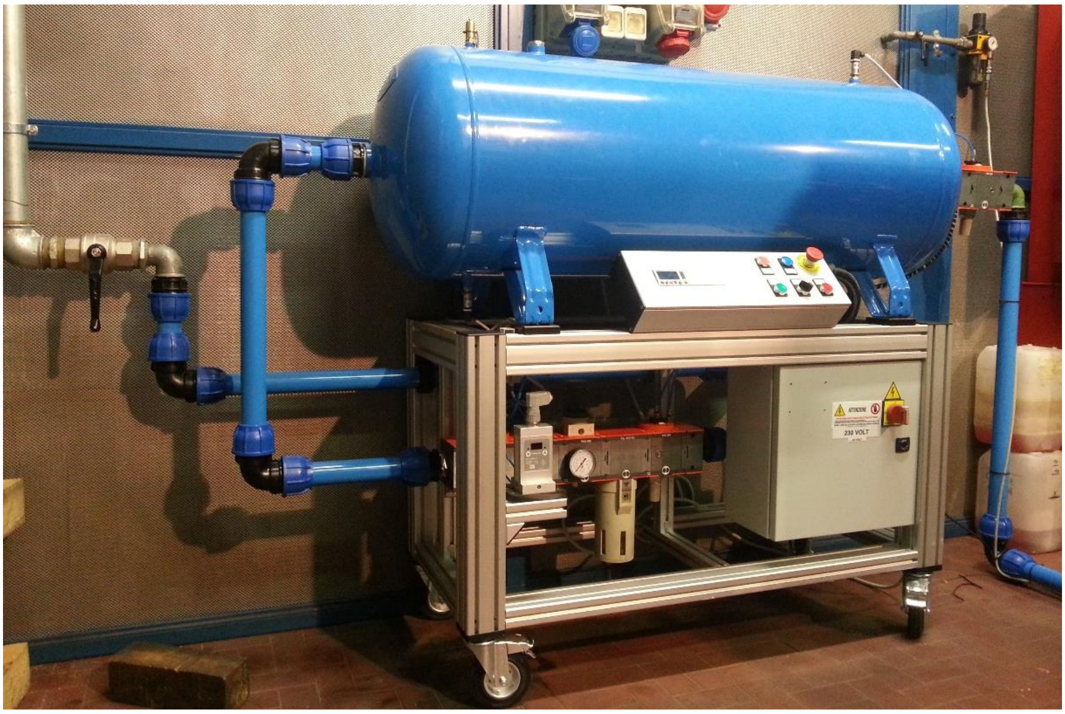

Figure 2.4 - Low pressure stage simulating device

2.2 Nozzle Selection

The main task of Phase 1 was the selection of the Injectors Nozzle within a wide nozzles portfolio, to identify the solution which has the best tradeoff between emissions and efficiency.

This activity was carried out in four operating points of the NRSC: 50% and 100% load at intermediate speed and rated speed as shown in Figure 2.5.

The nozzle portfolio is reported in Table 2.2, while the emission and efficiency targets in these four operating points are reported in

Table 2.3 together with a preliminary calibration defined by Ricardo.

Table 2.2 - Nozzle portfolio

ID	**Number of Holes**	**HoleDiameter [mm]**	**Flow** (atDP=100bar) **[cc/min]**	**Comment**
1	8	0.135	930	Shortest injection period
2	7	0.135	820	Centre specification
3	6	0.138	730	Longest injection period
4	9	0.127	930	Short injection period – reduced hole diameter
5	7	0.127	730	Long injection period – reduced hole diameter
6	10	0.121	930	Short injection period –further reduced hole diameter
7	8	0.119	730	Long injection period –further reduced hole diameter
8	6	0.138	730	Long injection period narrower cone angle

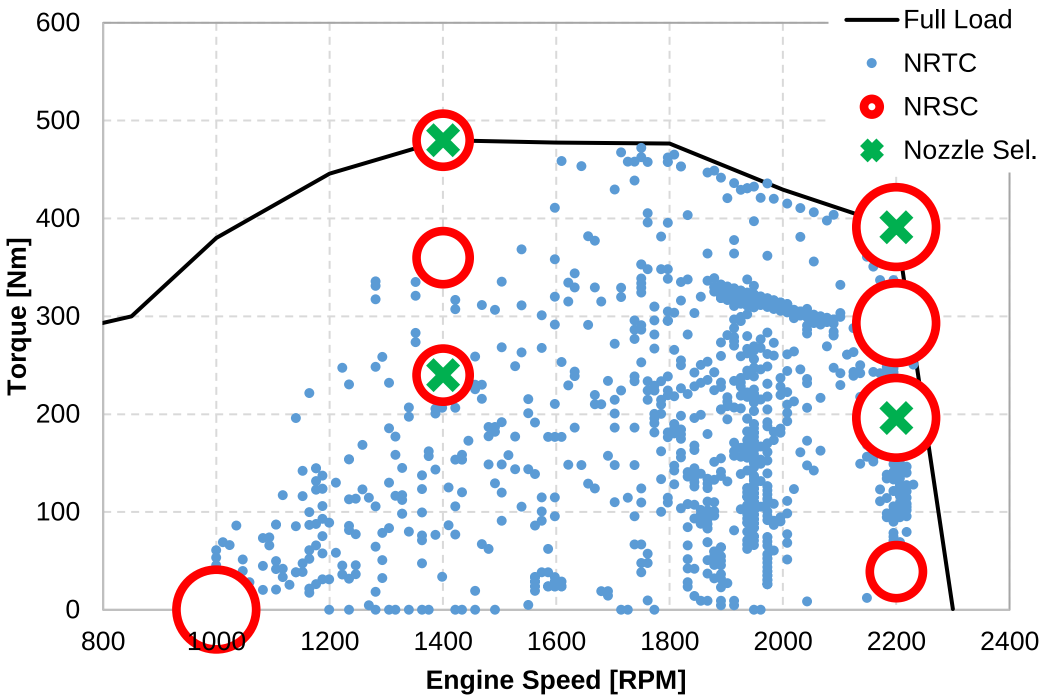

Figure 2.5 - Nozzle Selection operating points (dimension of NRSC points marker is representative of the weighting factor)

Table 2.3 - Preliminary calibration and emission targets

			Intermediate Speed		Rated Speed	
Operating Point	**Speed**	RPM	1400	1400	2200	2200
	Load	%	50	100	50	100
	Torque	Nm	240	480	196	391
	BMEP	bar	9	18	7	14.5
Calibration	**AFR**	-	19.7	17.7	21	19
	EGR	%	49	40	50	42
	SOI	°CAbTDCf	2	4	3	5
	P Rail	bar	2000	2500	3000	3000
	Boost	bar (abs)	2.4	3.2	2.4	3.3
Target	**NOx**	g/kWh	0.25	0.33	0.29	0.35
	FSN	-	0.37	0.62	0.26	0.44
	BSFC	g/kWh	240	217	279	243

2.2.1 Protrusion Optimization

To fairly compare one nozzle to another, the nozzle protrusion must be optimized to find the best spray-combustion chamber interaction. The protrusion of the nozzle was varied by changing the copper washer between the injector body and the injector seat in the cylinder head as showed in Figure 2.6

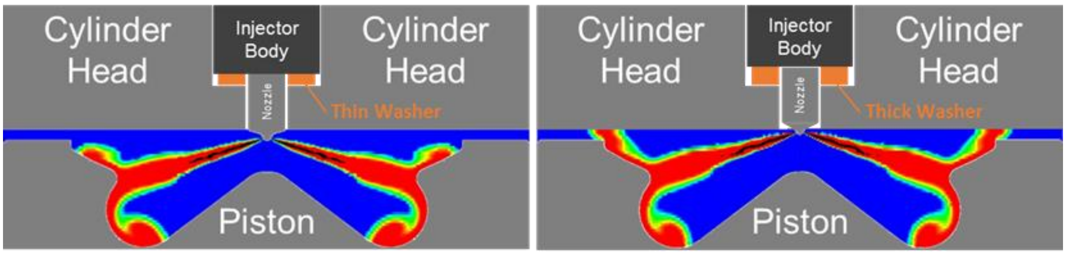

Figure 2.6 – Nozzle protrusion

The minimum washer thickness available was 0.5 mm, which defined the minimum resolution of the protrusion optimization. Hereafter the nozzle protrusion is identified by the thickness of the copper washer and it is worth to highlight for the sake of clarity, that thicker is the washer, less protruded is the nozzle in the combustion chamber.

Since the protrusion of the nozzle affects the spray interaction with the combustion chamber and the air-utilization consequently, it affects predominantly the smoke emissions and secondly NOx and efficiency. Therefore, the protrusion effect was evaluated measuring angle at the Start of Injection (SOI) sweeps at same calibration for different protrusions in the four different operating points. The calibration chosen initially was close to the “first attempt” calibration developed via simulation by Ricardo and reported in Table 2.3. However, since a proper engine calibration was carried out in parallel with the nozzle selection, the latter protrusions comparisons were made with a different calibration which used more retarded injection timings, higher boost and higher injection pressure, in order to mitigate soot emissions. More about this topic in Paragraph 2.3.

An example of the nozzle protrusion optimization is reported in Figure 2.7 where the results of the SOI Sweeps are reported in terms of NOx and FSN in the four selected operating conditions for the 820cc - 7 holes nozzle (ID 2 in Table 2.2). The solid markers refer to points measured with a calibration close to Ricardo initial estimations, while the empty markers refer to a calibration closer to the emission targets, therefore they should not be compared together.

Since the test bench did not have a closed loop pedal control to keep a fixed level of load and the manual adjustment of the pedal after each SOI variation would have required a lot of time and could have affected the results due to fast DPF loading in some very sooty conditions, those results were measured at a fixed injected quantity.

The other calibration parameters were kept constant except the EGR that was set on the first point to meet the target NOx emission of

Table 2.3. Unfortunately, due to unavoidable inaccuracies in the setting of EGR, due to the manual procedure, some discrepancy in the specific NOx emission can be found in some cases. A discrepancy on NOx emission, strictly speaking, makes the comparison unfair, however the differences are very limited, and the results were anyway judged valid.

A summary of the results is reported in the bottom part of Figure 2.7 to clarify that for this injector the best results are obtained with the 2 mm washer. This kind of study was carried out for all the tested injectors which were then compared with their best protrusion.

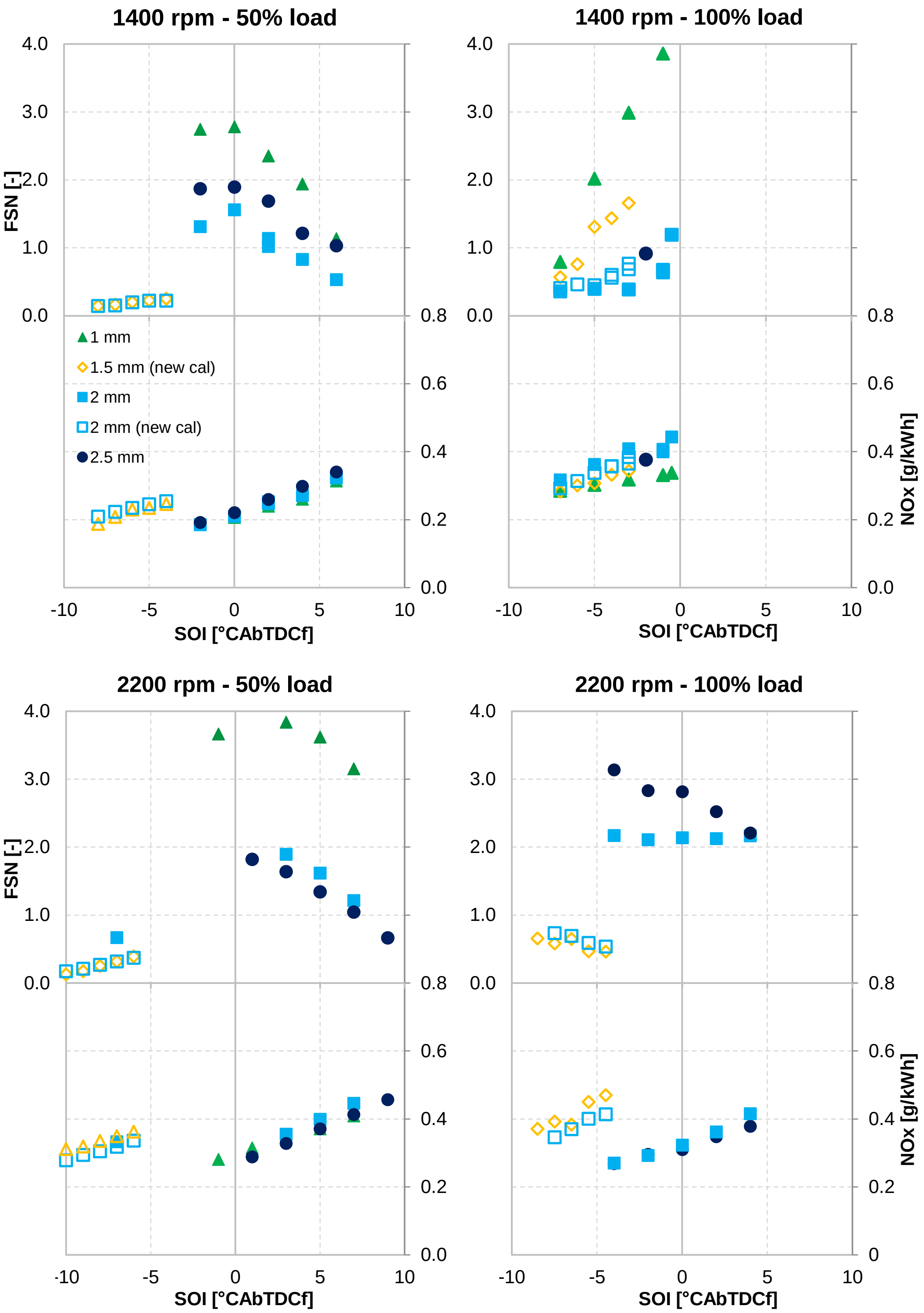

	1400 x 50%	1400 x 100%	2200 x 50%	2200 x 100%
1 mm	✗✗	✗✗	✗✗	
1.5 mm	✓	✗	✓	✓
2 mm	✓	✓	✓	✓
2.5 mm	✗	✓	✓	✗

Figure 2.7 - Protrusion comparison, Nozzle 7holes - 820cc

2.2.2 Nozzle comparisons

The nozzles have been compared each others with the best protrusion found with the procedure explained in the previous Paragraph. To compare the nozzles results, EGR sweeps with same calibration were measured. The results are the NOx-Soot and NOx-BSFC tradeoff reported in Figure 2.8, in which are compared the two nozzles which showed the best performances within the nozzles portfolio. They are the 7 holes 730 cc/min (ID5) and the 7 holes 820 cc/min (ID2) with 1.5 mm washer and 2 mm washer respectively. The final selection process focused on these two configurations.

As shown in Figure 2.8 at 1400 rpm the two nozzles are behaving almost in the same way, both in terms of efficiency and emissions and it was possible to achieve and overtake the emissions targets (black cross) in both the operating conditions with some margin on efficiency. On this last statemen it is worth to remember that this hardware does not includes the low-pressure turbocharger which can possibly add some backpressure and worsen the fuel consumption.

Looking at the results at 2200 rpm, it results clear that the 820 cc/min presents some advantages in terms of fuel consumption both at 50% and 100% load, keeping almost the same results of the 730 cc/min in terms of NOx-FSN tradeoff and settling the score.

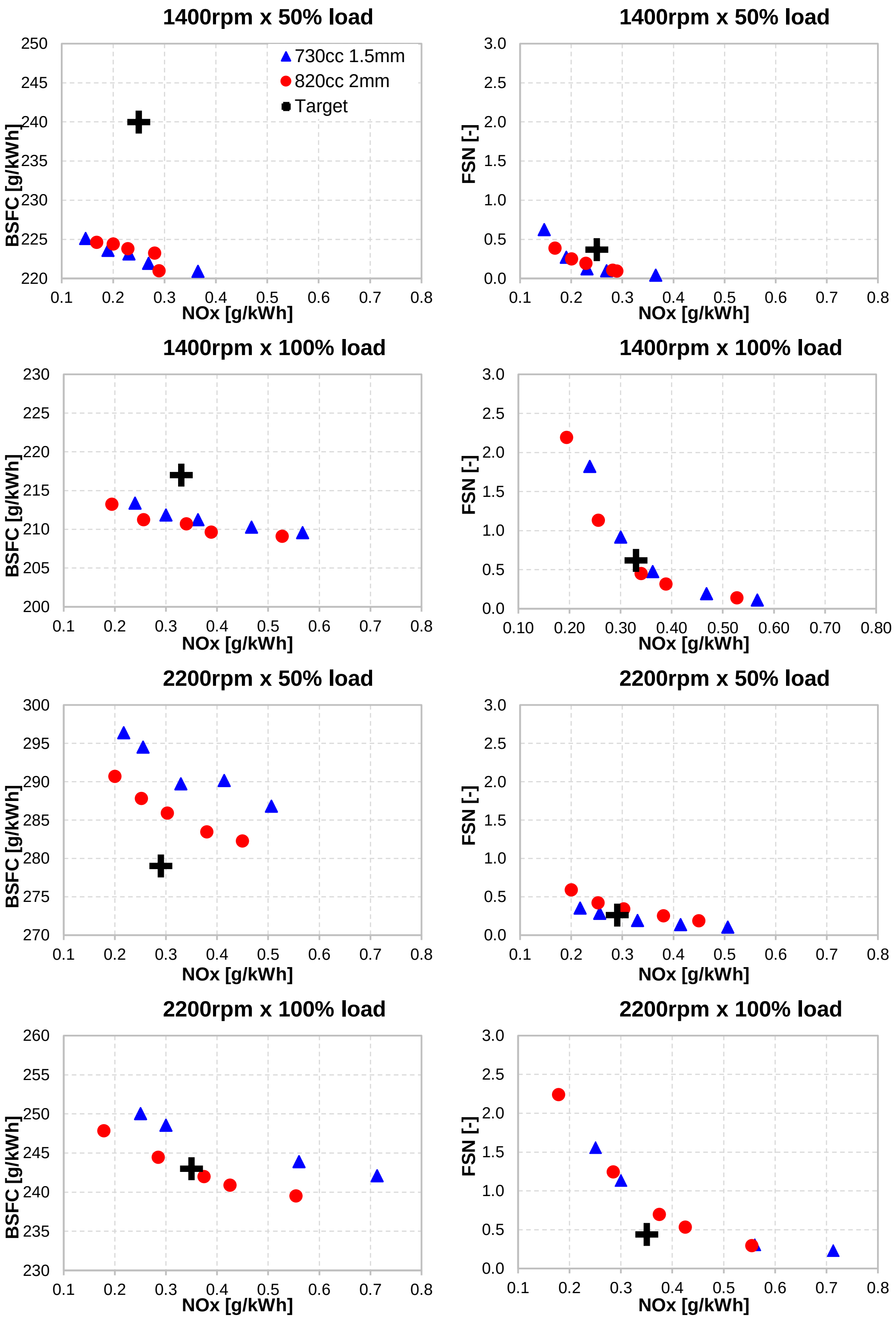

		1400 x 50%	1400 x 100%	2200 x 50%	2200 x 100%
730 cc – 7 holes	EMISSIONS	=	=	✓	=
	EFFICIENCY	=	=	✗	✗
820 cc – 7 holes	EMISSIONS	=	=	✗	=
	EFFICIENCY	=	=	✓	✓

Figure 2.8 - Nozzle results comparison

2.3 First calibration development

As a collateral activity a preliminary steady state calibration was developed starting from the Ricardo indications in

Table 2.3. As already explained, in this test bench there wasn't any automation for what concern load control or measurement procedure, or ECU programming, therefore this activity had to be carried out manually with an extremely time-consuming trial and error approach. For this reason the calibration could not be fully optimized. Nevertheless, some precious information have been obtained and were used as guidelines in the second phase.

Due to the simplification in the calibration and since noise was not a concern, a single main injection pattern was mainly adopted. Moreover, the pilot injection was found to increase the smoke tendency to unacceptable values with such low AFR, making it ineffective in reducing NOx. However, it was used at low loads where the engine was running with higher AFR. On the other hand, after injection was proved to be very effective in reducing Smoke without NOx penalty, especially at high speed, as will be widely discussed in the next Chapter.

As from the first experimental results it was clear that the engine required a much more retarded injection timing than what Ricardo estimated to meet the NOx with acceptable smoke values.

In Figure 2.9 some results obtained at Peak Power operating conditions with different calibration close to the NOx target are reported. In Calibration Set #1 a boost pressure of 3.4 bar and a timing of -6 °CAbTDC required around 40% of EGR to reach the target NOx producing very high smoke emissions. In Set #2 a 4 mm^3 after injection was introduced reducing the smoke by 30%. Doubling the after quantity has further reduced the smoke bringing it down to 60% of the single main value, as shown by Set #3.

In Point 4 the boost pressure was increased up to 3.65 bar, which translated in an increase of AFR that reduced FSN down to 0.76. In Set #5 and #6 an optimization of the after injection quantity was carried out with the results of a slight reduction of soot. In Point #7 a further retarded timing of -7 °CA was tried in order to pursue the FSN target, which caused only a modest reduction of FSN and a consistent deterioration of the BSFC.

Even though the targets could not be accomplished in all the operating conditions, the results obtained in this first experimental phase encouraged to build the engine with the final layout, and to proceed to the second experimental phase described in the following Chapter.

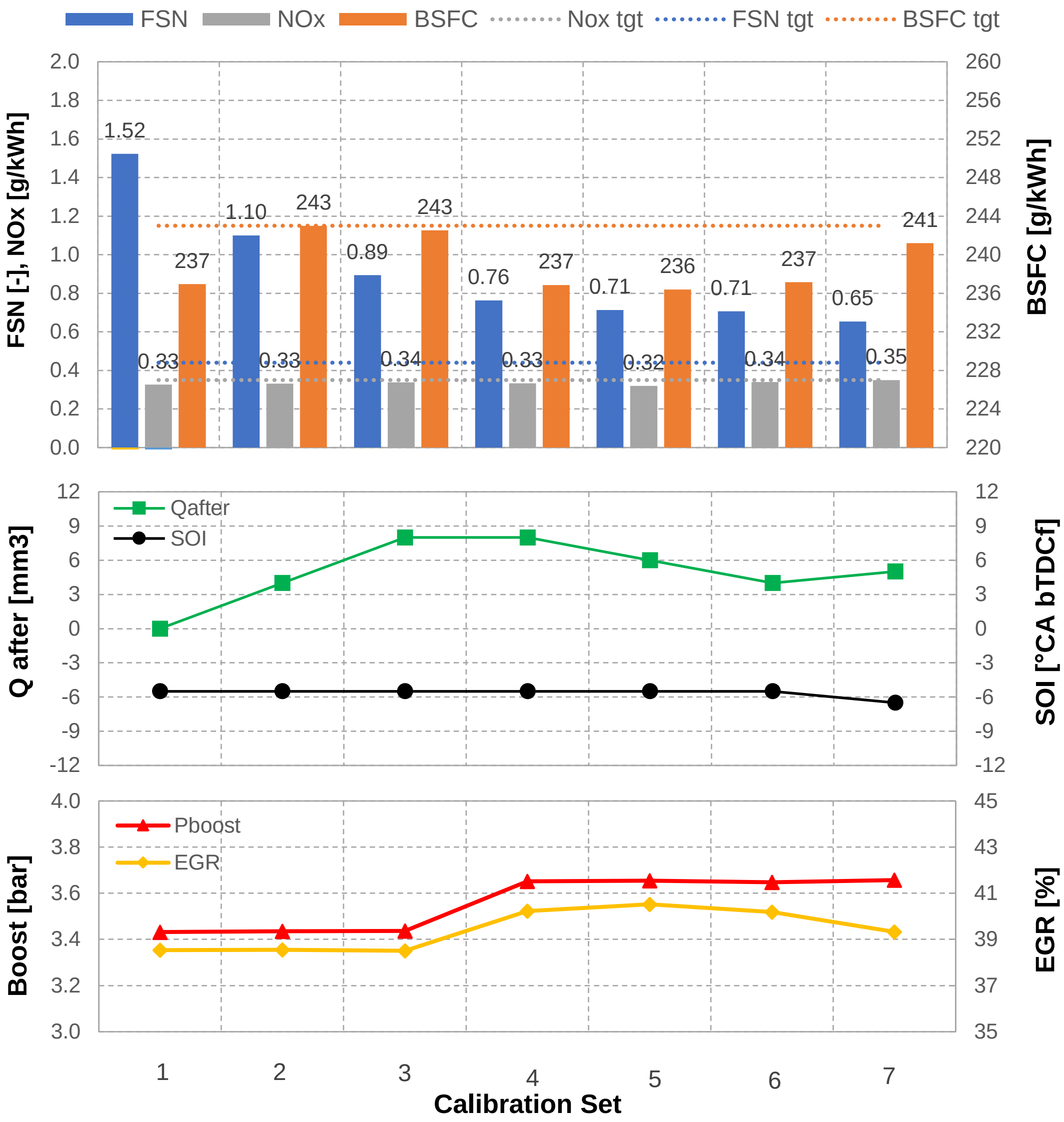

Figure 2.9 - Example of steady state calibration at Peak Power operating condition

Chapter 3

Second Experimental Phase

Part of the work described in this chapter has been previously published in:

- Gatti P, Fagg S, Cornwell R, Millo F, Boccardo G, Porcu D, et al. *Investigation of a "SCR-free" system to meet the Stage IV and beyond emissions limits*. Heavy-Duty, On- Off-highw. Engines 2016 11th Int. MTZ Conf., Ulm, Germany: MTZ; 2017, p. 274–91. doi:10.1007/978-3-658-19012-5_16

- Queck D, Herrmann OE, Bastianelli M, Naoki A, Manelli S, Capiluppi C, Fukuda A, Millo F, Boccardo G. *Next steps towards EGR-only concept for medium-duty industrial engine*. In: Liebl J, Beidl C, editors. Int. Mot. 2017 Mit Konf. Nfz-Motorentechnologie und Neue Kraftstoffe, Wiesbaden: Springer Fachmedien Wiesbaden; 2017, p. 555–72. doi:10.1007/978-3-658-17109-4_37

- Boccardo G, Millo F, Piano A, Arnone L, Manelli S, Capiluppi C. *A Fully Physical Correlation for Low Pressure EGR Control Linearization*. SAE Tech Pap 2017;2017–Septe. doi:10.4271/2017-24-0011.

In the second phase, a new KDI3404 equipped with a two stages turbocharger and a proper low pressure EGR line was mounted in the dynamic test bench of DENERG.
During this phase, the engine was calibrated in steady state and under transient operation to evaluate its performance on the certification cycles. At the end of the project a hardware assessment was carried out to evaluate the engine performance in terms of emissions and efficiency, with a special focus on the extremely high fuel injection pressure. However, this last part is here presented before the calibration and certification section, since it is functional to the description and motivation of some steady state calibration choices.

3.1 Experimental Setup

3.1.1 Engine Layout

As previously pointed out, the engine was tested in its final configuration, means with the two-stage turbocharger and with a proper designed low pressure EGR line.

As far as the turbocharger is concerned, the low pressure unit was a non-controlled fixed geometry, while the high pressure was controlled via a mechanical WG. The WG preload was defined by the first operating limit reached increasing the load, which was the maximum exhaust manifold pressure of 5.2 bar. The WG preload was set in the peak power point (maximum mass flow rate) in order to meet the operational limit in all the engine map.

Intercooler and aftercooler were simulated using two air-to-water heat exchangers operating with the water of the water main. The water flow rate to the two heat exchangers was regulated independently with a feedback loop run by the test bench automation, targeting a cooler gas temperature outlet of 60°C to prevent condensation.

The EGR line which will be discussed in detail later in the text, keeps the same architecture of the First Experimental Phase of the project, but it is now placed downstream of the low pressure turbocharger, still sampling downstream of the DPF. The valves are now both operated by the ECU.

A diagram of the engine layout is reported in Figure 3.1.

3.1.2 Facilities Description

The engine was tested in a highly dynamic test bench with controlled cabin temperature (25°C), intake air temperature (25°C) and intake air humidity (50% RH).

The fuel consumption was measured via an AVL KMA4000 fuel flow meter.

The facilities include a two lines AVL AMAi60 emission analyser to measure NO, NOx, HC, CO, CO_2 and O_2 concentrations independently, plus a third line only for CO_2. It was used to measure emission concentrations Engine Out (EO), Tailpipe (TP) and the third line sampled in the intake manifold to trace EGR with the CO_2 method.

As far as the soot is concerned, an AVL 415S G002 SmokeMeter (SM) and an AVL MicroSoot Sensor (MSS) were used to measure FSN and Soot concentration at engine out.

Finally, an AVL Particle Counter (APC) was used to measure the Particle Number (PN) concentration in the exhaust gas. As the MSS, this instrument has a built-in conditioning unit which uses a two stages dilutor. For both instruments the Dilution Ratio (DR) was set to correctly exploit the measuring range of the devices according to the soot emission level, resulting in a DR of 5 for the MSS and of 15000 for the APC.

In order to evaluate the impact of the extremely high injection pressure on particle size distribution, a TSI 3080 Scanning Mobility Particle Sizer (SMPS) was used. This instrument was set to work with a 0.071 cm inlet impactor, a 1.5 l/m aerosol flow and a 15 l/m sheath flow covering a particle diameter range from 6 to 229 nm as reported in [32]. The sampling system includes a two stage Dekati DI-2000 dilutor and a heated sampling probe at 150°C.

As for the gaseous emissions, all those instruments can be configured to sample tailpipe for certification purposes, however the results presented hereafter refer always to engine out concentrations.

The engine was also equipped with 2 in-cylinder high frequency Kistler 6056A piezoelectric pressure transducers and a high frequency current clamp to measure the solenoid injector current, which were recorded by an AVL IndiCom system.

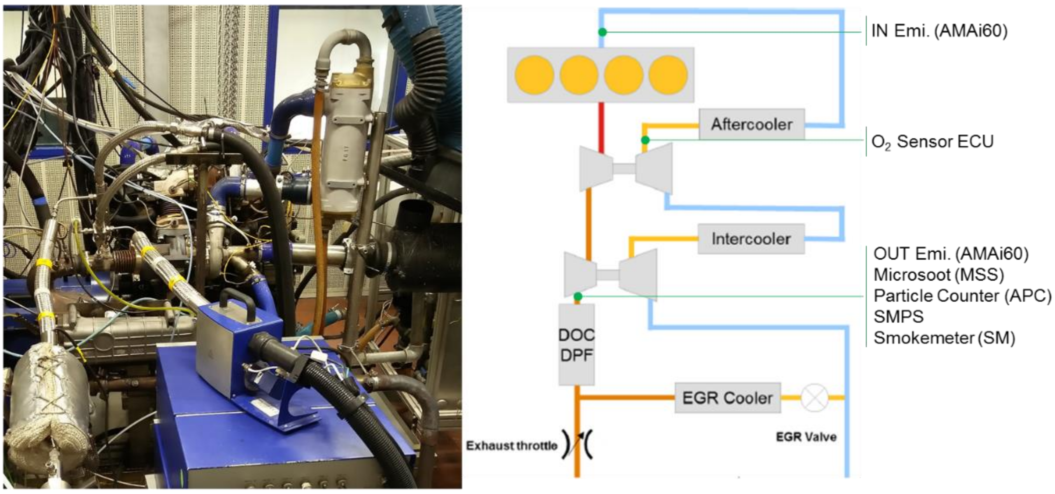

Figure 3.1 - Engine Layout in the Second Experimental Phase

3.2 Hardware assessment

In order to assess the potential of this engine configuration and especially of the extremely high injection pressure and its impact on the NOx-Soot tradeoff and efficiency, some ad hoc tests were carried out.

Moreover, as mentioned in Paragraph 2.3, the after injection was found to be very beneficial with such high injection pressure to reduce smoke emissions and its effect was therefore deeply evaluated.

After injection can improve soot emission since it enhances mixing, increases the burned gas temperature and splits the fuel in shorter injections improving the mixture formation due to jet replenishment. This strategy is particularly valuable and effective with this engine, since it can be implemented without penalty on NO_x and the three action mechanisms are boosted by the extremely high injection pressure, which should also limit the drawback in BSFC thanks to the short pulses. However its effectiveness is not universal and it is very sensitive to the engine and operating conditions [33].

3.2.1 Test Matrix

To assess the injection pressure effect, several EGR sweeps were performed at different rail pressure and in different engine operating points, selected within the certification cycles as shown in Table 3.1.

Table 3.1 - EGR Sweeps measurement parameters

Speed *[rpm]*	**Load** *[%]*	**Torque** *[Nm]*	**SOI Main** *[°CA bTDCf]*	**Rail Pressure** *[bar]*	**EGR** *[%]* – (SMPS meas.)
1400	50	240	-4.4	2000 → 3000	19 → 43 – (40)
1400	100	480	-7.1	2000 → 3000	14 → 32 – (30)
2200	50	196	0	2000 → 3000	34 → 44 – (40)
2200	75	293	0	2000 → 3000	29 → 37 – (34)

For all these operating points the SOI was kept constant and a sweep of EGR was performed at 5 different rail pressure levels from 2000 to 3000 bar with a step of 250 bar. For a fixed level of EGR, chosen near the centre of the tradeoff, the particle distribution was measured for the 5 rail pressure levels. SOI values were selected from the steady state calibration, although at the highest engine speed (2200 rpm), it has to be advanced substantially to allow a proper combustion process, with the lowest injection pressure.

As far as the after injection is concerned, the analysis was carried out measuring a matrix of after injection quantity and Dwell Time (DT) between main and after at maximum rail pressure for two operating points. The parameters are summarized in Table 3.2.

Table 3.2 - After Injection explorations measurement parameters

Speed *[rpm]*	**Load** *[%]*	**Torque** *[Nm]*	**SOI Main** *[°CA bTDCf]*	**Rail P.** *[bar]*	**EGR** *[%]*	**After Q.** *[mm^3]*	**Dwell Time** *[µs]*
2200	50	196	0	3000	44	2.5 → 10	500 → 1000
2200	75	293	0	3000	38	2.5 → 10	500 → 1100

For these tests the particle size distribution was measured for the lowest smoke calibration found and compared with the same calibration without after injection.

The choice of the keypoints can be visualized in

Figure 3.2 where they are plotted together with the full load curve and the operating points of the certification cycles NRSC and NRTC.

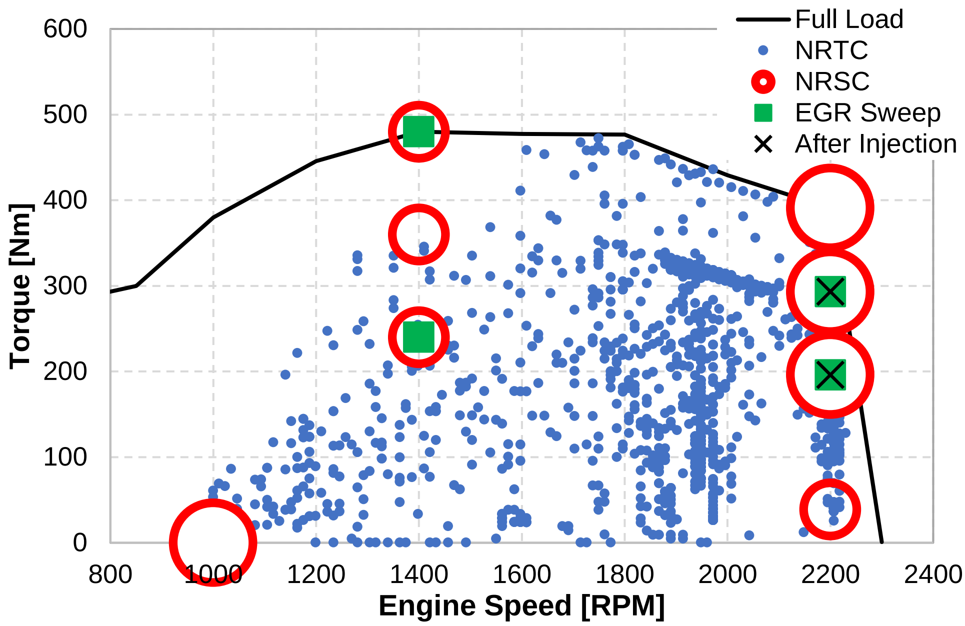

Figure 3.2 - Operating point chosen for the hardware assessment (dimension of NRSC points marker is representative of the weighting factor)

3.2.2 Particulate measurement correlation

Before presenting the results of the hardware assessment and of the certification cycles, an abstract of Appendix A is reported in this paragraph to evaluate the consistency of the particle-related measurements.

In Figure 3.3a the correlation between the soot concentration measured by the Smokemeter, calculated by the FSN with the AVL correlation, and the equivalent measurement of the Microsoot Sensor is reported. The two measurement devices have completely different measurement principles, however a very good linear correlation is found. As shown in Appendix A the MSS measurement can be corrected in different ways to achieve a better correlation with the smoke measurement. However since the results hereafter presented are always reported as one to one comparison between identical results set, no corrections were applied.

In Figure 3.3b the correlation between the measurement of the APC and the total count of the SMPS is reported in the four operating points of the EGR sweeps at different Rail Pressure. The two instruments have different counting efficiencies and different sampling lines, therefore a not univocal correlation is expected, as widely explained in Appendix A. However, as Figure 3.3b shows, a linear correlation is found per each operating condition, in which a quite stable particle distribution is expected.

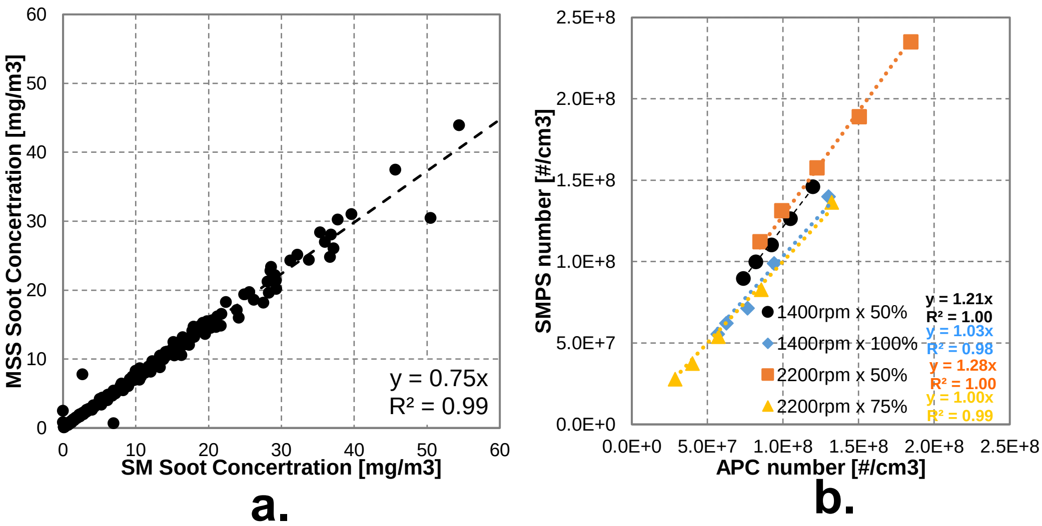

Figure 3.3 - Particulate measurement correlation
a: MSS / SM
b: SMPS / APC

3.2.3 Results

- **EGR SWEEPS**

In Figure 3.4 the Soot/NO_x (measured by the MSS), BSFC/NO_x, PN/NO_x tradeoff and the average of 5 measurements of particle size distribution for the central point of the tradeoff at constant EGR, are reported at different rail pressure for the operating point 1400 rpm x 50% load. For this operating point, increasing the rail pressure improves almost proportionally the NO_x/Soot tradeoff reducing soot from 50 mg/kWh to 35 mg/kWh at 0.2 g/kWh of NO_x. The BSFC/NO_x tradeoff does not show a unique trend: in fact it improves increasing the rail pressure up to 2500 bar, while 2500 bar and 2750 bar shows similar results, and BSFC drastically worsens further increasing the injection pressure to 3000 bar. It is worth to remark that those EGR sweeps were measured at constant SOI and therefore, increasing the rail pressure, the angle at 50% of Mass of Fuel Burnt (MFB50) advances, increasing efficiency and NO_x emission. Globally moving from 2000 to 3000 bar results in a MFB50 advance of about 2°CA. However, in this operating point, for injection pressures higher than 2750 bar, the thermodynamic benefits of the increased injection pressure are exceeded by the additional friction required by the FIS and by the increased in cylinder pressure. To give an estimation, in this operating condition, increasing the injection pressure from 2000 to 3000 bar costs 0.15 bar of FMEP. By the Chen-Flynn relation the increased in-cylinder peak pressure was evaluated to be responsible of around 0.05 bar (35% of the total friction increase).

SMPS measurements do not show any sensible difference in the shape of the particle distribution, as confirmed by the trend of the modes of the particle distribution with the rail pressure presented in Figure 3.8, which for this operating point is constant and close to 45 nm. However, a reduction of the particle number in almost all diameters domain is observed, becoming negligible only for particles smaller than 10 nm. Similar results are obtained for the 1400 rpm x 100% load (Figure 3.5), even though the particle size distribution moves slightly towards smaller particles, with the mode decreasing from 65 nm at 2000 bar to 50 nm at 3000 bar. A less clear effect on emissions is found in this operating condition but the effect on BSFC is even more evident than for the previous case, levelling to 3 g/kwh for injection pressure higher than 2750bar. This means that the beneficial thermodynamic effect of the increased injection pressure is way overcompensating the increase in friction due to the high pressure FIS and of the peak firing pressure.

The results for the operating point 2200 rpm x 75% load are reported in Figure 3.6. In this operating point increasing the rail pressure up to 3000 bar is much more effective: the Soot/NO_x tradeoff improves by 75% decreasing soot emissions from 115 mg/kWh to 30 mg/kWh at 0.5 g/kWh of NO_x. BSFC improves almost proportionally increasing the injection pressure up to 2750 bar and remains constant for further increase of the injection pressure up to 3000 bar. As for 1400 rpm x 50% and 100% load, SMPS measurements show a reduction of the particle number in the particle size range higher than 12nm, and, as confirmed by the PN/NO_x trade-off, the 3000 bar injection pressure is very effective in reducing the total particles emission which is almost halved. As for the 1400 rpm x 100% load, the distribution mode decreases by around 15 nm increasing the injection pressure up to 3000 bar. Those results are confirmed by the measurements at 2200 rpm x 50% load reported in Figure 3.7.

In Figure 3.9 the comparison of the in-cylinder pressure trace and of the Heat Release Rate (HRR) for 1400 and 2200 rpm 50% load operating conditions are presented for the central point of the tradeoff (SMPS points) for the case at 2000 and 3000 bar injection pressure.

It results immediately clear how much the 3000 bar combustion is faster than 2000 bar in both cases. This translates into the dramatic increase in efficiency of around 5 g/kWh of BSFC observed at 2200 rpm, which is instead only 1.5 g/kWh at 1400 rpm. Looking at the difference in the Indicated Specific Fuel Consumption (ISFC), however, near the same benefits can be observed (4.3 g/kWh at 1400rpm and 5.8 g/kWh at 2200 rpm) confirming that the different behaviour has to be addressed to the different organic losses related to the injection pressure increase.

- **AFTER INJECTION**

As far as the after injection is concerned, in Figure 3.10 the results of the study in the operating point 2200 rpm x 75% load are reported. The effect of the after injection was assessed varying the DT from 500 (the minimum allowed by the FIS) to 1000 µs and the injected quantity was increased from 2.5 to 10 mm^3. The optimum, in which an FSN of 0.6 was recorded, is found with an injected quantity of 5 mm^3 and the minimum allowed DT. An FSN of 0.9 was measured without after injection corresponding to a smoke reduction of more than 30%. SMPS measurements show a consistent decrease of particles above 20 nm and a moderate increase for particles smaller than this diameter. This is probably due to the particulate oxidation which is promoted by the after injection, leading to the fragmentation of bigger agglomerates and thus increasing the number of smaller particles which cannot be completely oxidized [34].
Similar results are obtained at 2200 rpm x 50% load where the benefit of the after injection is even higher, decreasing the FSN from 1.2 to 0.6 with 500 µs of DT and 7.5 mm3 (Figure 3.11). The decreasing effectiveness of the after injection with the load is known in literature, however in this case seems this should not be completely addressed to the nonlinear growth in soot quantity with fuel mass per injection [33], since at 75% load operating condition the total smoke emission without after injection is lower than at 50% load. However it should be taken into account that in this case the two operating points have different SOI, different boost pressure and different EGR rate, which of course affect smoke emissions. On the other hand the fact that the highest soot reduction was found with the minimum dwell time suggests that the prevailing mechanisms are the enhanced mixing and increased temperature which may be intensified by the faster combustion at 3000 bar injection pressure [33]. Another explanation can be found in a very recent work by Lind et al. [35]: by means of optical techniques it was evaluated that closely-coupled post-injections are effective in reducing soot, not only by shortening the main injection duration, but also by the extremely effective oxidation action of the entrainment wave of the previous injection on the soot produced by the after, thus resulting in a soot-free injection that brings the total soot emission at the level of an equivalent lower load.
Thanks also to the very fast combustion of the after injection at 3000 bar, which takes less than 10 °CA at 50% load as shown in Figure 3.12, in which the effect of after injection on cylinder pressure trace and Heat Release Rate (HRR) is reported, the decrease in engine efficiency is limited to 1.8 g/kWh for the 75% load and 0.5 g/kWh for the 50% load operating points.

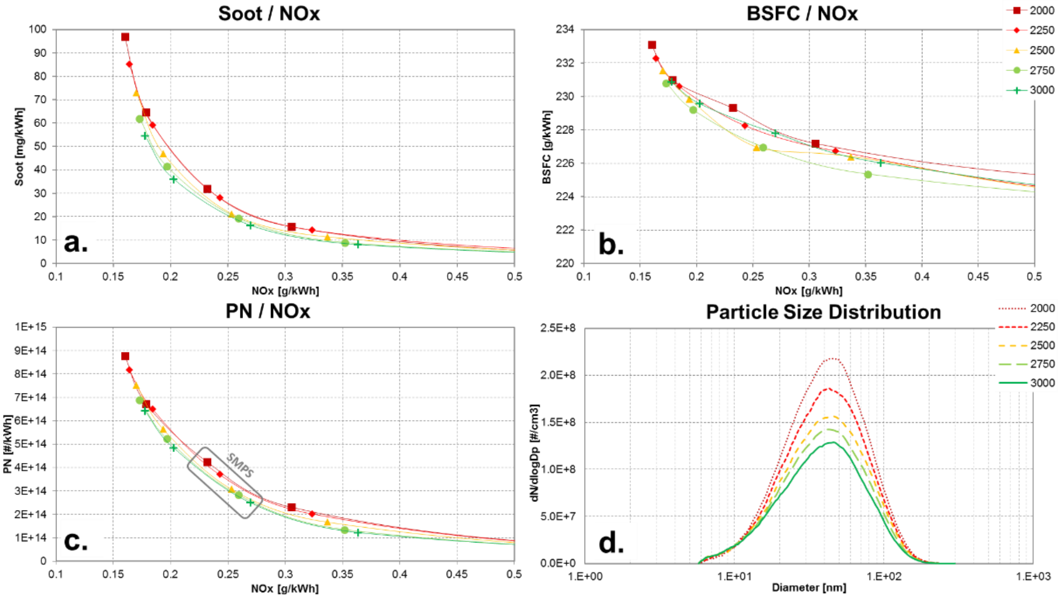

Figure 3.4 – 1400 rpm x 50% load - EGR sweeps

a. **Soot (MSS) / NO_x tradeoff at different rail pressures**
b. **BSFC / NO_x tradeoff at different rail pressures**
c. **PN / NO_x tradeoff at different rail pressures**
d. **Particle size distribution at 40% EGR for different rail pressures**

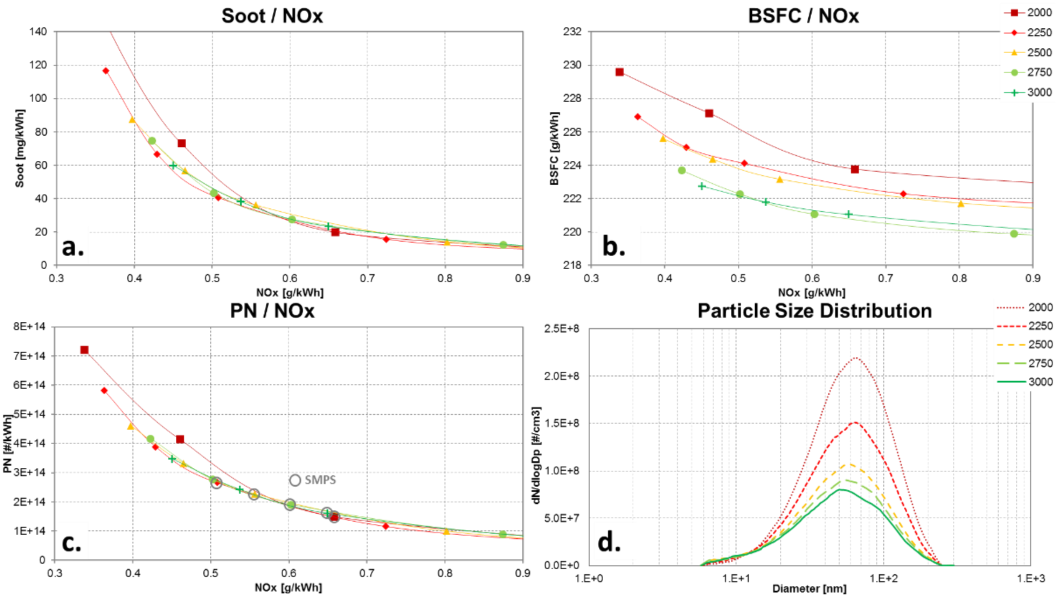

Figure 3.5 - 1400 rpm x 100% load – EGR Sweeps

a. **Soot (MSS) / NOx tradeoff at different rail pressures**
b. **BSFC / NOx tradeoff at different rail pressures**
c. **PN / NOx tradeoff at different rail pressures**
d. **Particle size distribution at 30% EGR for different rail pressures**

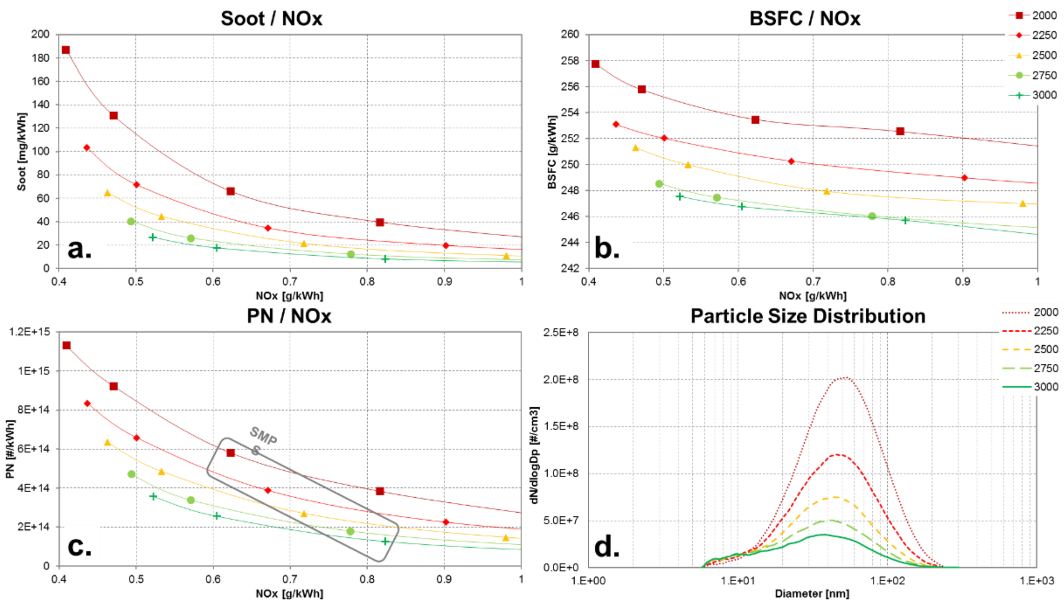

Figure 3.6 - 2200 rpm x 75 % load – EGR Sweeps

a. Soot (MSS) / NOx tradeoff at different rail pressures
b. BSFC / NOx tradeoff at different rail pressures
c. PN / NOx tradeoff at different rail pressures
d. Particle size distribution at 34% EGR for different rail pressures

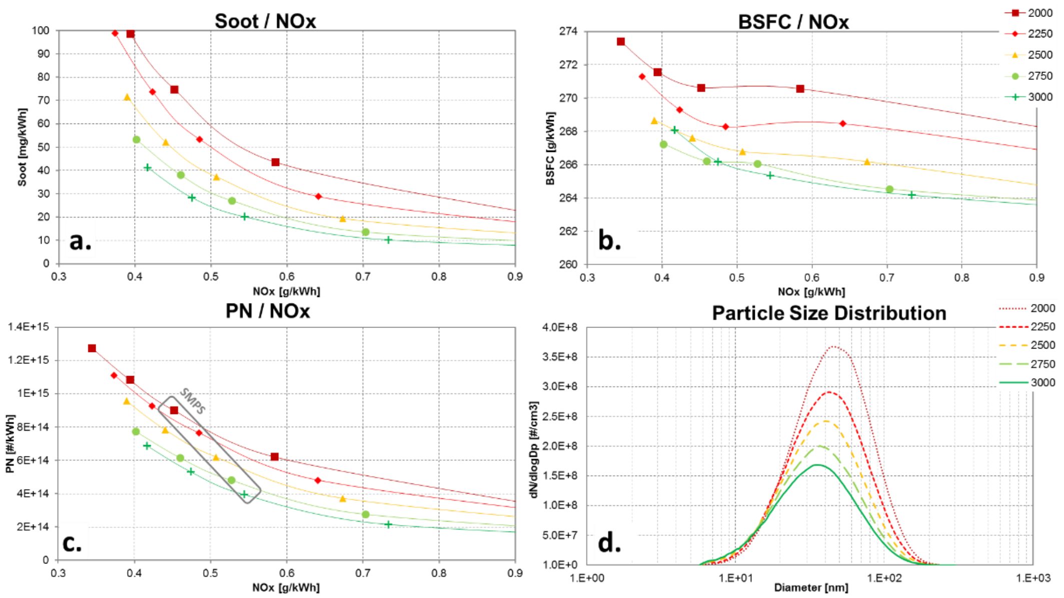

Figure 3.7 - 2200 rpm x 50% load – EGR Sweeps

a. Soot (MSS) / NOx tradeoff at different rail pressures
b. BSFC / NOx tradeoff at different rail pressures
c. PN / NOx tradeoff at different rail pressures
d. Particle size distribution at 40% EGR for different rail pressures

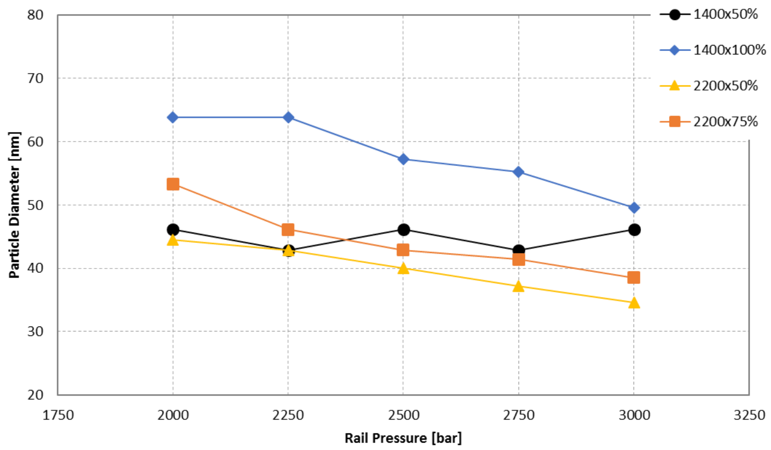

Figure 3.8 - Modes of particle size distributions vs injection pressure

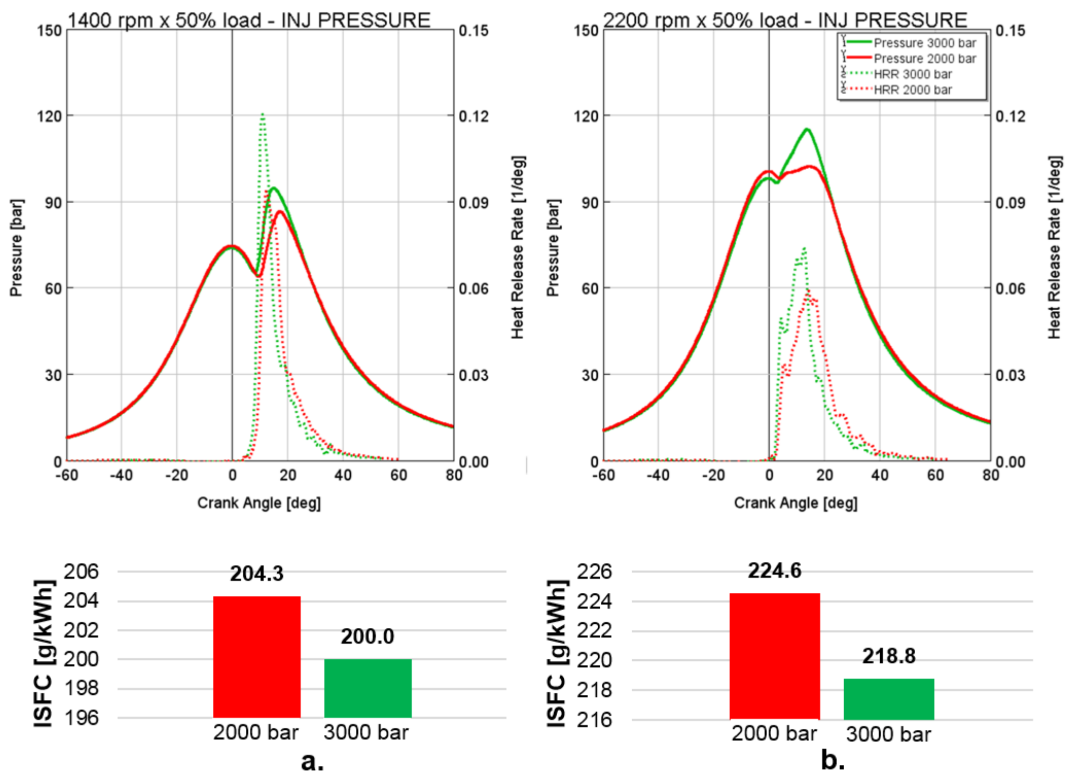

Figure 3.9 - In cyl. pressure and HRR @ 2000 and 3000 bar injection pressure.

a. **1400 rpm 50% load – 40% EGR (SMPS point)**
b. **2200 rpm 50% load – 40% EGR (SMPS point)**

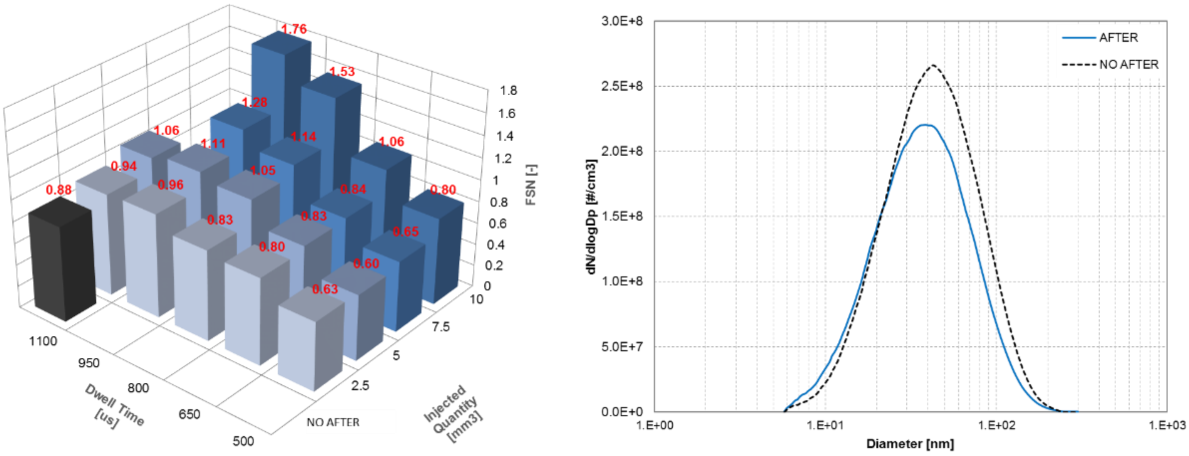

a. b.

Figure 3.10 - 2200 rpm x 75% Load - After Injection exploration @ 3000 bar inj. pressure, 37% EGR

a. FSN in the exploration domain

b. Particle distribution without after and with lowest smoke calibration (DT: 500µs / Quantity: 5mm^3)

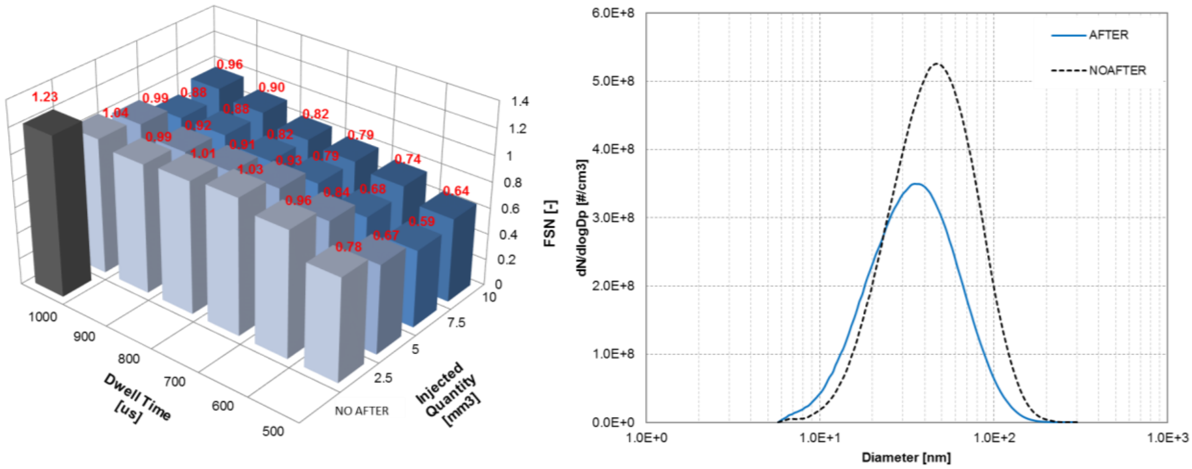

a. b.

Figure 3.11 - 2200 rpm x 50% Load - After Injection exploration @ 3000 bar inj. pressure, 44% EGR

a. FSN in the exploration domain

b. Particle distribution without after and with lower smoke calibration (DT: 500µs / Quantity: 7.5mm^3)

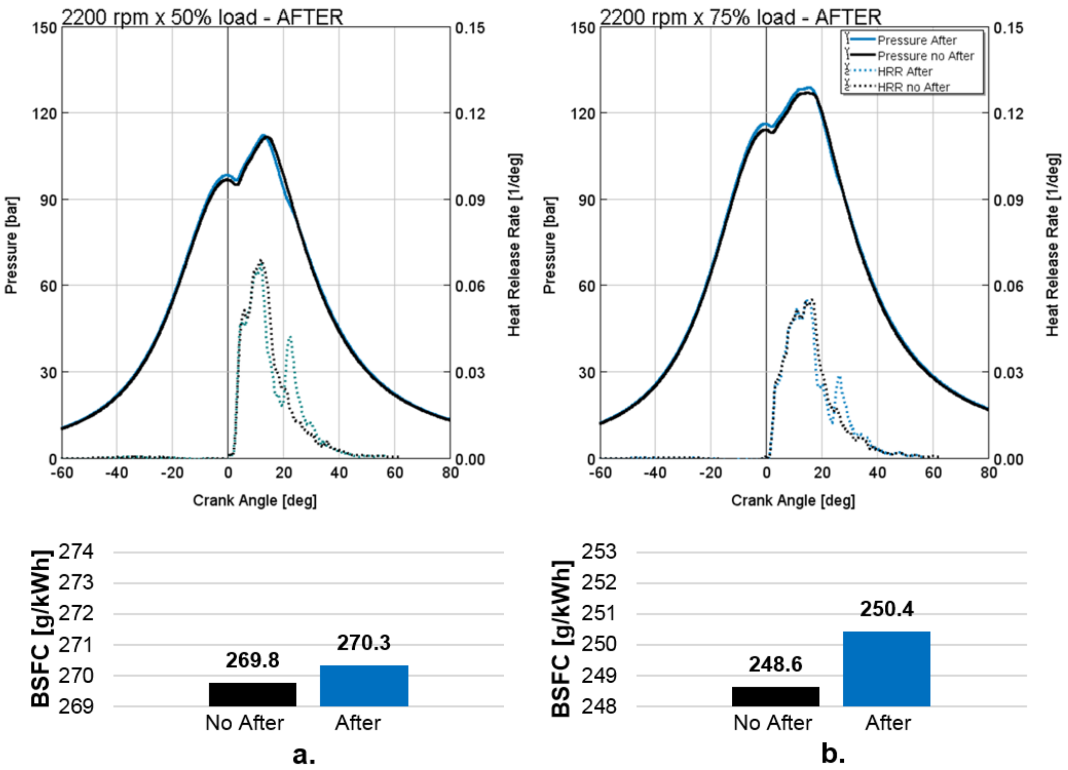

Figure 3.12 – Effect of after injection on in cylinder pressure and HRR.

a. **2200 rpm 50% load – 44% EGR – After DT: 500 us, Q: 7.5 mm^3 – 3000 bar**
b. **2200 rpm 75% load – 37% EGR – After DT: 500 us, Q: 5.0 mm^3 – 3000 bar**

3.3 Steady state calibration development

The calibration activity started with the verification of the preliminary calibration developed in the first phase. That calibration, however, was developed with the hypothesis of having an adequate level of boost which could guarantee adequate AFR, given the amount of EGR needed to meet NOx emissions at the chosen SOI. Unfortunately, the boosting system was not able to provide the required boost pressure and a recalibration was needed to meet the NOx emissions with acceptable smoke.

An example is presented in Figure 3.13, where a comparison of different calibration steps along Phase 1 and Phase 2 is reported. The initial Ricardo requirements and calibration suggestions (Table 2.3) are reported in black, in green the best calibration found in the first phase, in blue the calibration shown in the tradeoff of Figure 2.8, in yellow the first iteration with the final hardware and in red the delivered calibration. It results immediately clear how much the boost pressure in the second phase was lower than in the first phase (up to 0.5 bar). This translated in much lower AFR which caused very high soot emission and required a more retarded timing (especially at peak torque).

A wider picture is given by the contour plots presented in Figure 3.15. It results clear that the calibration is completely NOx-oriented as shown by the NOx emission which is lower than 0.4 g/kWh in the whole engine map except for the NTE zone and the non-regulated zone. The AFR decreases with the load due to increased EGR in order to keep low NOx in the certification area and scarce boost pressure. As BSFC shows, the engine efficiency decrease moving towards rated power point. This is due to increased soot tendency in that area which requested higher AFR ratio to keep acceptable smoke and very retarded combustion to keep NOx below 0.4 g/kWh. At rated speed the turbocharging performance was limited by the exhaust backpressure which was higher than 5 bar and close to the mechanical limit of the component. This suggests that a more appropriate turbocharging system would have permitted much better efficiency in the whole engine map, but especially in the rated power zone.

As far as the injection parameters are concerned in Figure 3.14 the contour plots of the injection pressure and of the injection pattern used are reported. The injection pressure in progressively increased up to 3000 bar as load and speed increase, and a wide operation area at maximum injection pressure is adopted according to the results of Paragraph 3.2 which proved the benefits of high injection pressure from medium to high load.

Concerning the injection pattern, four solutions were adopted:

- a **Pre + Main** was used at low load. In this area very high rate of EGR had to be recirculated since, due to high oxygen concentration, it was less effective in reducing NOx, and retarded timings could not be adopted due to HC concerns. A close Pilot (or Pre) was used to reduce premixed combustion of the main injection (main responsible of NOx) and to control HC by reducing the quenching tendency thanks to the increased in cylinder temperature. It also ensured smooth operation [36][37][38]. This pattern was used also in the non-regulated zone where EGR was not used.

- **Pilot + Pre + Main** was used in low idle area to furtherly reduce NOx, since the weight of idle in the certification cycles is significant.

- **Single Main** was used in the central area of the map where high rate of EGR were adopted and the Pre was found to be inconvenient from an efficiency point of view and due to smoke increase tendency [36][37][38].

- **Main + After** was used at high speed to mitigate soot according to the results of Paragraph 3.2, where further SOI delay was unfeasible or not convenient from an efficiency point of view.

- A small area of **Pre + Main + After** operation was used at high speed as a result of the merging of **Pre + Main** at low load and **Main + After** at medium to high load.

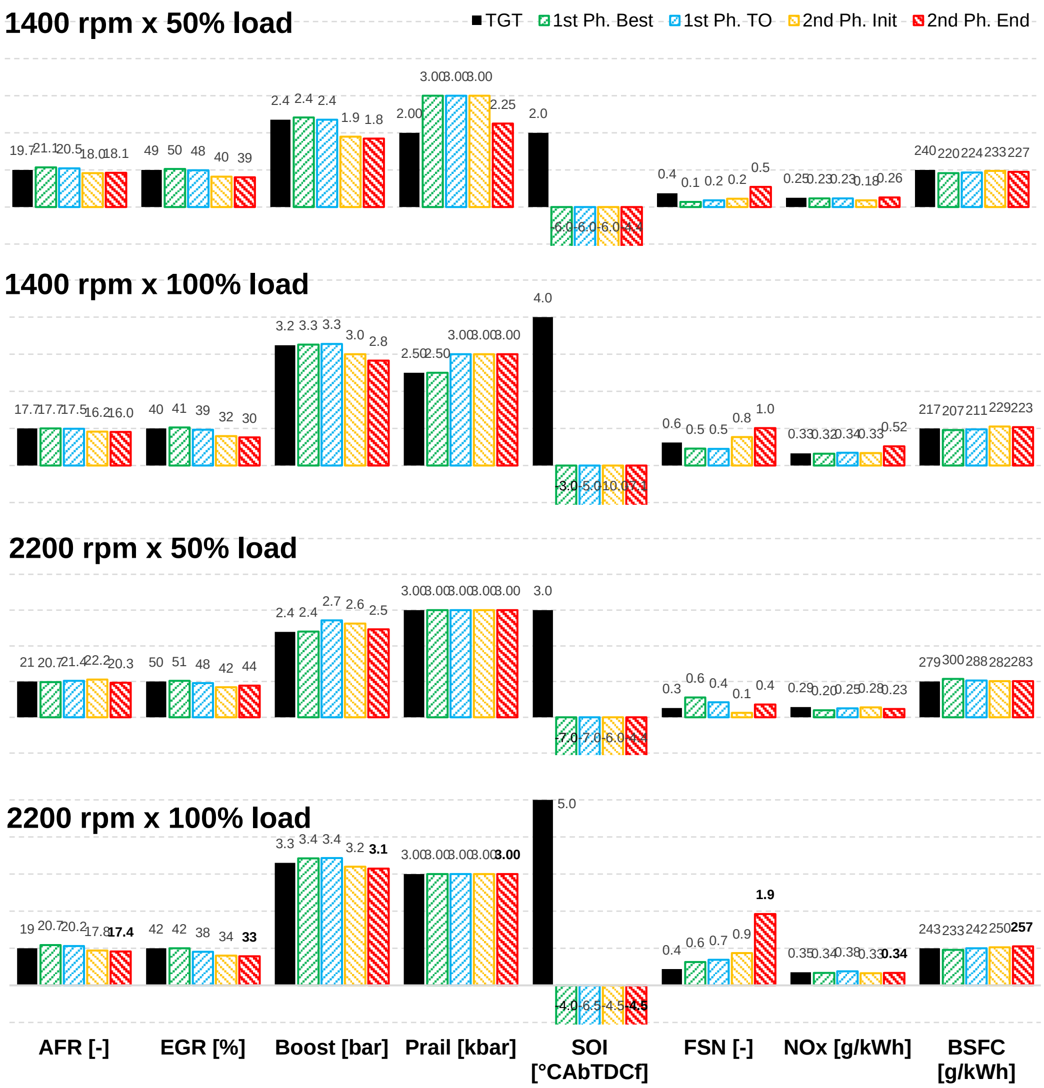

Figure 3.13 - Steady State calibrations comparison

TGT:	**Initial calibration and targets (Table 2.3)**
1st Ph. Best:	**Best calibration in the first phase**
1st Ph. TO:	**Calibration of the tradeoff in Figure 2.8**
2nd Ph. Init:	**Initial Calibration of the Second Phase**
2nd Ph. End:	**Delivered Calibration**

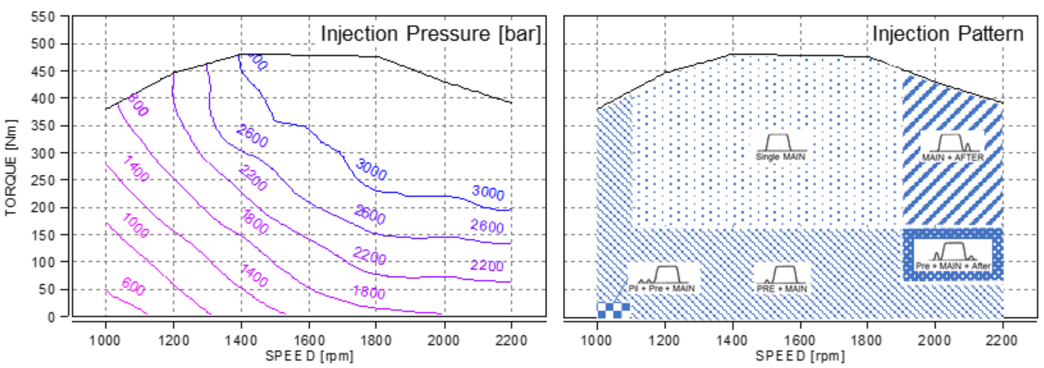

Figure 3.14 - Final Steady State calibration injection parameters

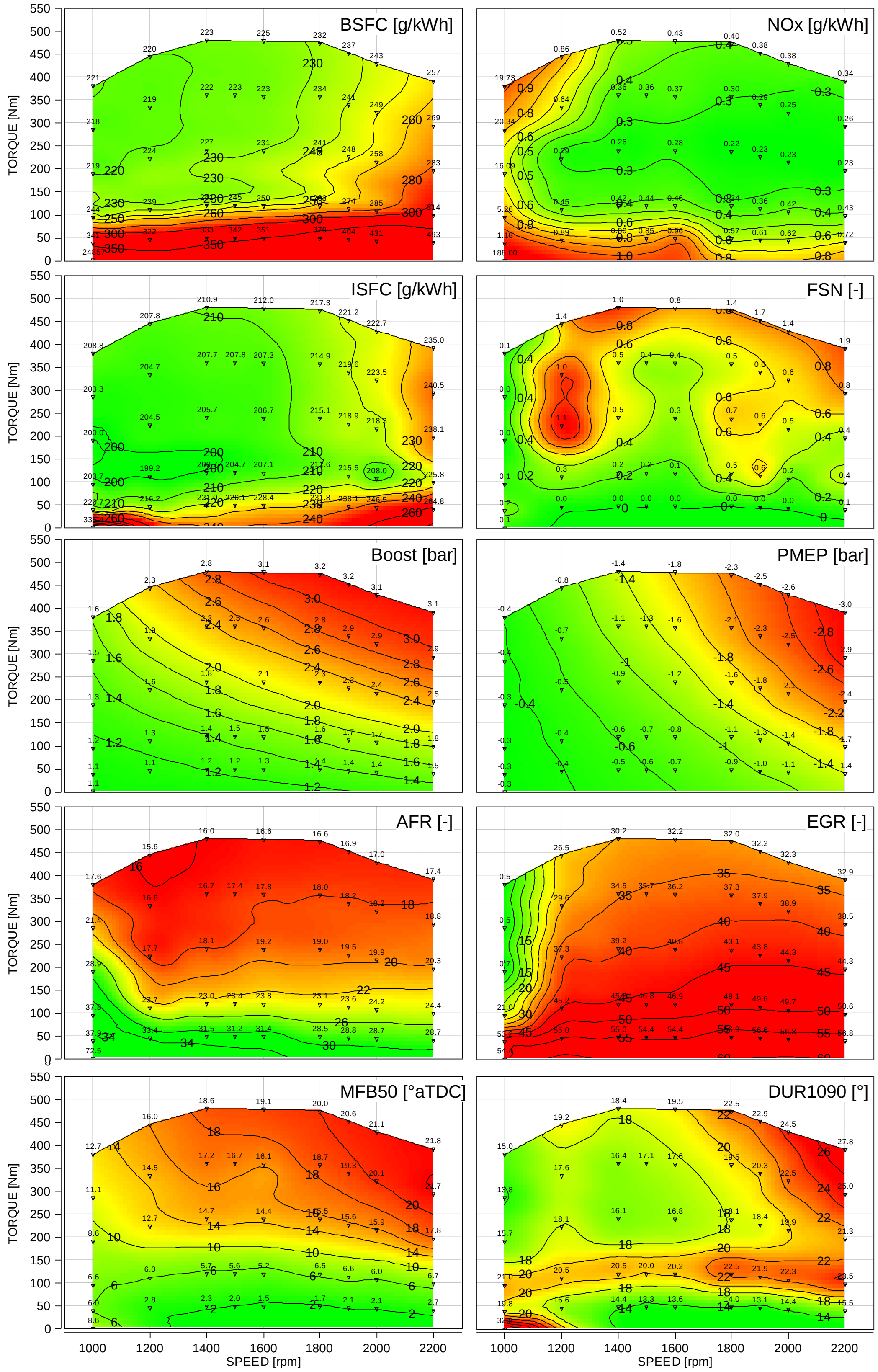

Figure 3.15 - Steady State calibration results on engine map

3.4 Transient Calibration

The transient calibration was functional to the NRTC operation and focused mainly in the calibration of the smoke limitation strategy and on the management of the EGR during transient.

3.4.1 EGR Linearization

The first task was the linearization of the EGR control.

As already explained in Paragraph 1.3.1 the EGR is operated by two valves: an exhaust flap and an EGR valve.

The control is in closed loop with the O_2 concentration measured by a lambda sensor placed downstream of the high-pressure compressor. The control outputs a non-dimensional variable (range 0 – 100) which is translated by two functions in the position of the two valves.

In order to enhance the stability of the control and reduce the fuel consumption penalty, the valves positioning laws have been optimized in order to obtain a linear response of the control with the EGR rate and to minimize the backpressure increase needed to recirculate EGR.

Exhaust Line CFD Characterization

The first step was the flow characterization of the two valves, which was carried out exploiting the 1D-CFD model described in Appendix B, defining the correlation between valve position versus effective flow area. In order to do that about 20 engine operating points were experimentally measured at different valves positions. The engine model was setup to reproduce the experimental data by concentrating all the pressure losses between the measurement points (reported in Figure 3.16 as the coloured dots) in the orifices which represent the valves, and calibrating their diameters in order to replicate the experimental pressure drop, with the same EGR rate.

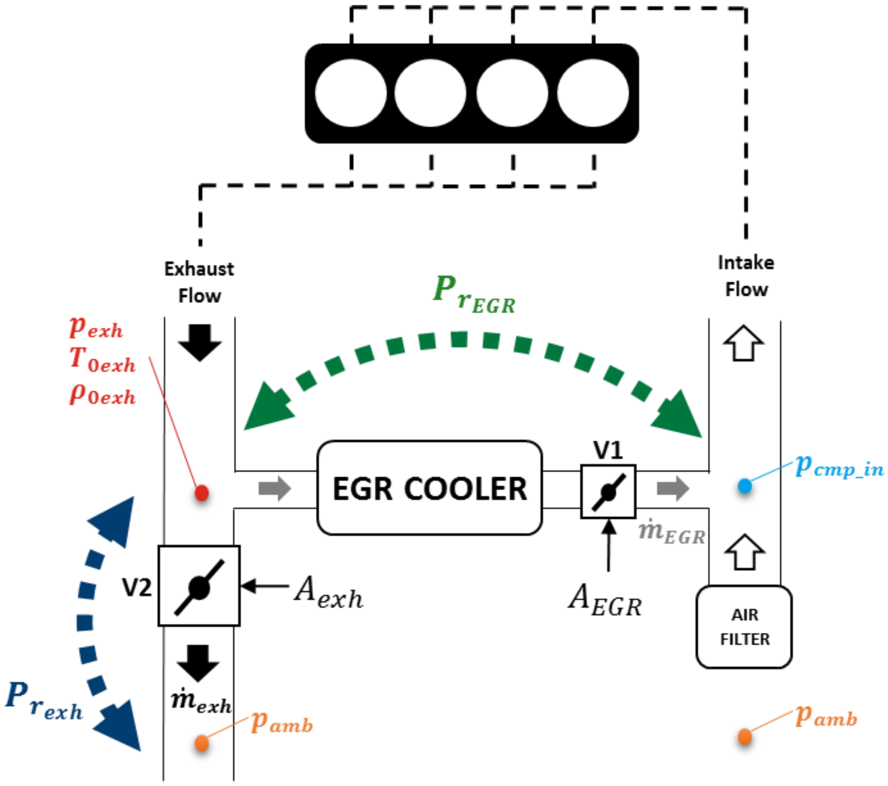

Figure 3.16 - EGR flow schematic [22]

It was important to group all the source of pressure drop of the exhaust line (Exhaust Flap + muffler + piping) in the Exhaust Flap and all the pressure drop of the EGR bypass (EGR Valve + EGR cooler + piping) in the EGR Valve, otherwise it would not have been possible to justify the following simplifications.

Correlating the resulting equivalent diameters with the corresponding experimental valve positions from the ECU, it was possible to obtain a physical correlation between the valve position and the effective flow area, reported in Figure 3.17.

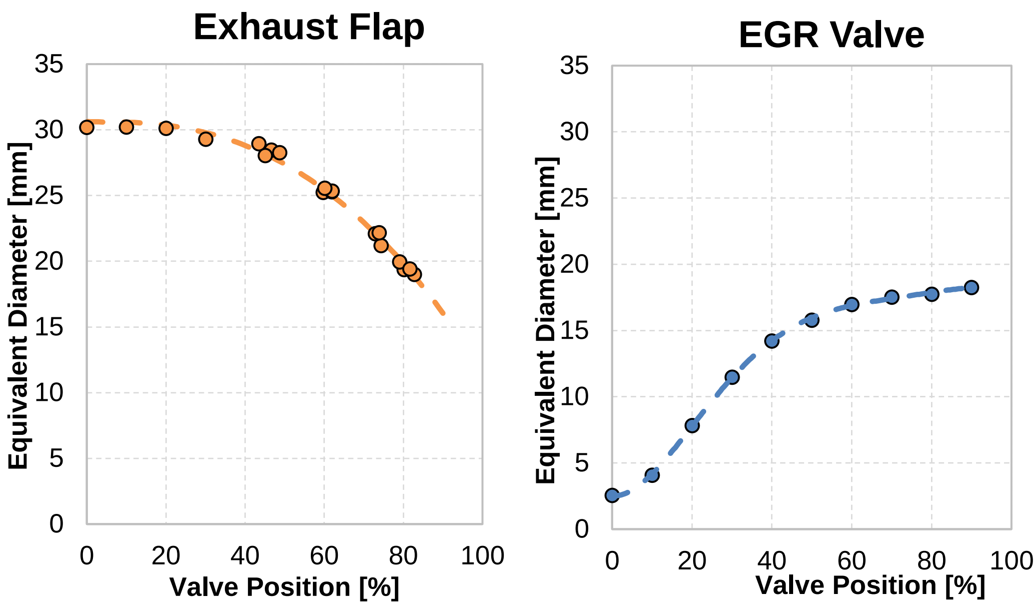

Figure 3.17 - EGR valve and Exhaust flap characterization [22]

It is worth mentioning that the valve characterization does not strictly require the use of a 1D model, but the same laws presented in Figure 3.17 can be determined also analytically using the equations reported in the next Paragraph. However, this work was part of a wider project aiming to develop a "virtual test rig" to evaluate hardware modifications and different engine calibrations, making this approach preferable to be consistent with the results and not overlapping the characterization error with the unavoidable model inaccuracies. Moreover, the model can rely on a wide and consolidated library of fluid properties which guarantees a very accurate determination of the specific heat in the wide range of temperatures and gas compositions of the operating conditions measured for the valve characterization, thus possibly leading to more accurate results. Additionally, a calibrated 1D-CFD model gives the user the flexibility to change components of the exhaust line and EGR pathway and, knowing their flow characteristics, generate linearized valves positioning laws without the needs of new experimental data. This could be very beneficial if different architectures have to be compared and/or a system optimization has to be carried out.

Physical Correlation.

The mass flow through a valve can be calculated by means of the following formula:

$$\dot{m} = A_{eff}\rho_{is}U_{is} \tag{3.1}$$

$$\rho_{is} = \rho_0 P_r^{1/\gamma} \tag{3.2}$$

$$U_{is} = \sqrt{RT_0}\left(\frac{2\gamma}{\gamma-1}\left[1 - P_r^{\frac{\gamma-1}{\gamma}}\right]\right)^{\frac{1}{2}} \tag{3.3}$$

Where

$\dot{m}$ = mass flow rate

A_{eff} = effective flow area

ρ_{is} = density at the throat
ρ_0= upstream stagnation density
U_{is} = isentropic velocity at the throat
P_r = absolute pressure ratio (static outlet pressure/total inlet pressure)
R = gas constant
T_0 = upstream stagnation temperature
γ = specific heat ratio (1.4 for air at 300 K)

Therefore the EGR mass flow rate and the exhaust mass flow rate will be:

$$\dot{m_{EGR}} = A_{EGR}\rho_{0_{exh}} f\left(P_{r_{EGR}}, T_{0_{exh}}\right) \tag{3.4}$$
$$\dot{m_{exh}} = A_{exh}\rho_{0_{exh}} f\left(P_{r_{exh}}, T_{0_{exh}}\right) \tag{3.5}$$

Where (referring to Figure 3.16)

$$P_{r_{EGR}} = \frac{p_{exh}}{p_{cmp\_in}} \tag{3.6}$$
$$P_{r_{exh}} = \frac{p_{exh}}{p_{amb}} \tag{3.7}$$

Assuming $p_{cmp\_in} \approx p_{amb}$ (negligible pressure drop on the air filter), the two mass flow rates differ only for the effective areas. The error introduced by this simplification can be estimated comparing the experimental $P_{r_{EGR}}$ and $P_{r_{exh}}$ resulting in a deviation of 13% on average.
The EGR percentage is defined as

$$EGR = 100 \cdot \frac{\dot{m_{EGR}}}{\dot{m_{EGR}}+\dot{m_{air}}} = 100 \cdot \frac{\dot{m_{EGR}}}{\dot{m_{EGR}}+\dot{m_{exh}}-\dot{m_{fuel}}} \tag{3.8}$$

Assuming $\dot{m_{fuel}}$ negligible respect $\dot{m_{EGR}} + \dot{m_{exh}}$ (error lower than 5% with AFR higher than 20), the (3.8) becomes:

$$EGR \cong 100 \cdot \frac{\dot{m_{EGR}}}{\dot{m_{EGR}}+\dot{m_{exh}}} \tag{3.9}$$

Which substituting (3.4) and (3.5) becomes:

$$EGR \cong 100 \cdot \frac{A_{EGR}}{A_{exh}+A_{EGR}} \tag{3.10}$$

Control Linearization

Since the goal is to obtain a linear control, the EGR must follow the following relationship:

$$EGR = k \cdot x \tag{3.11}$$

Where x is the EGR control output.

Assuming that the maximum EGR rate to be recirculated is 70%, when the control output is 100, *k* is determined equal to 0.7. The value of 70% was chosen in order to fully exploit the EGR control output range while keeping some margin on the maximum EGR rate effectively recirculated (around 60%).

The equation (3.10) becomes:

$$100 \cdot \frac{A_{EGR}}{A_{exh}+A_{EGR}} = 0.7 \cdot x \tag{3.12}$$

The solution, reported in Figure 3.18a, is determined by choosing, between all the possible combinations of the two areas that satisfy the equation, the one that has the maximum A_{exh}, meaning the lowest backpressure and minimum BSFC increase.

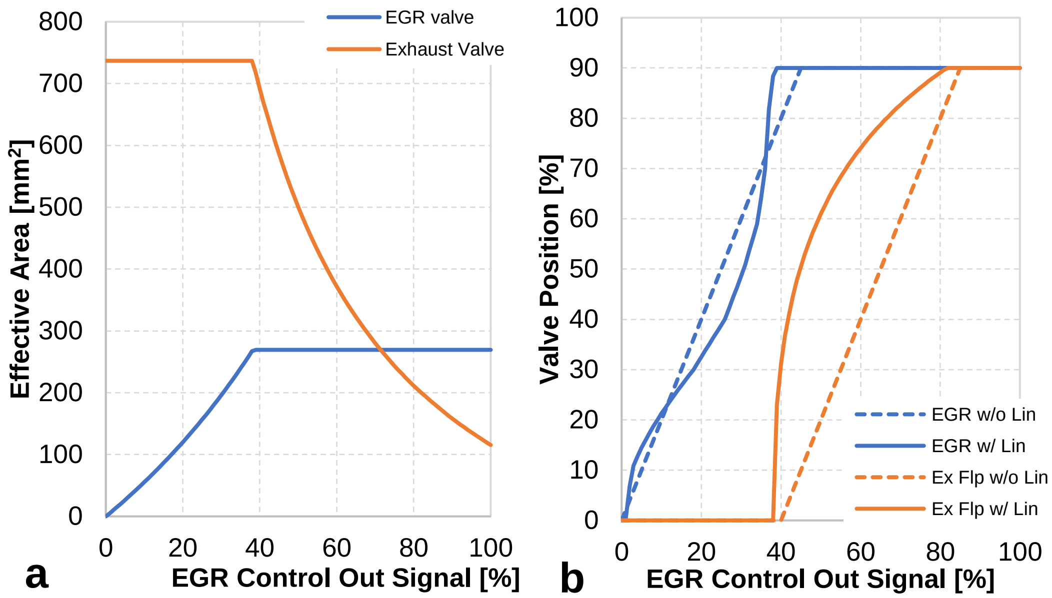

Figure 3.18 - Linearized positioning laws [22]
a. Equivalent areas positioning laws
b. Equivalent diameter positioning laws

Converting the resulting areas back into the corresponding non-dimensional position of the valves, the positioning laws plotted in Figure 3.18b are obtained, in which are reported in dashed lines the positioning laws referring to the original simplified approach and in solid lines the new positioning laws output from the linearization process. The blue curves refer to the EGR valve, while the orange ones to the Exhaust valve.

Results

This approach was assessed with two sets of experimental data, one measured in the early stage of the project in different operating conditions spread in the engine map for a total of 127 operating points, while the second is the dataset referring to the hardware assessment and steady state calibration final evaluation of Paragraph 3.2 and 3.3. The dataset without the linearization of the valves was measured during the steady state calibration of the engine, with different EGR rates, boost levels, rail pressures and injection patterns, using the original simplified position laws of the valves reported in dashed lines in Figure 3.18b.

Comparing the abovementioned experimental measurements, by plotting the EGR control output variables versus EGR rate, the effectiveness of the proposed approach can be demonstrated, as Figure 3.19 shows.

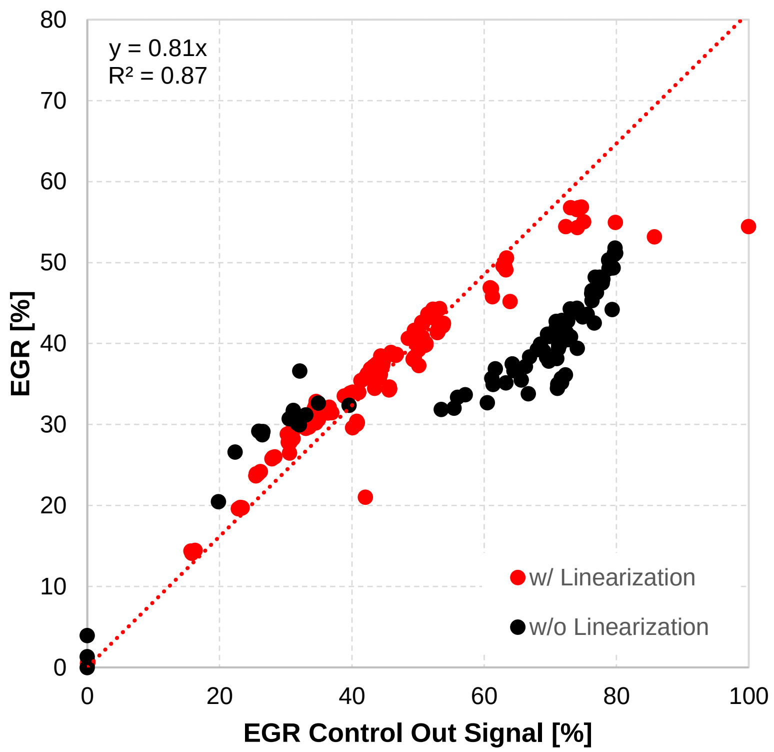

Figure 3.19 - EGR linearization results assessment [22]

Looking at the results of Figure 3.19 it seems that above 80% of the EGR control signal the EGR rate does not increase anymore. It is worth to be clarified that while the EGR Valve above 90% is already fully open (the command is in degree), the exhaust flap keeps closing until 100%, therefore, to avoid the risk of excessive backpressure, the flap was limited to operate from 0 to 90%. This limit was set in the operating point with the maximum EGR request to guarantee the correct EGR rate.

It is worth to point out that this method was not directly applicable in this case since the control is O_2 based and not EGR based. In fact the linearization is valid only at a fixed operating point (almost constant mass flow breathed by the engine) where the intake O_2 concentration is inversely proportional to the EGR rate, as shown in Figure 3.20 in which the O_2 concentration measured by the lambda sensor is plotted against the EGR control variable in four operating points. However, as will be shown later, the closed loop control is coupled by a strong feed-forward logic and the PI controller (for which the linearization is important) enters in action mainly at the end of a transient, to fill the gap left by the feed forward logic. In this condition the control linearization is valid.

As a future work could be interesting to evaluate an EGR based control logic which could potentially require less calibration effort.

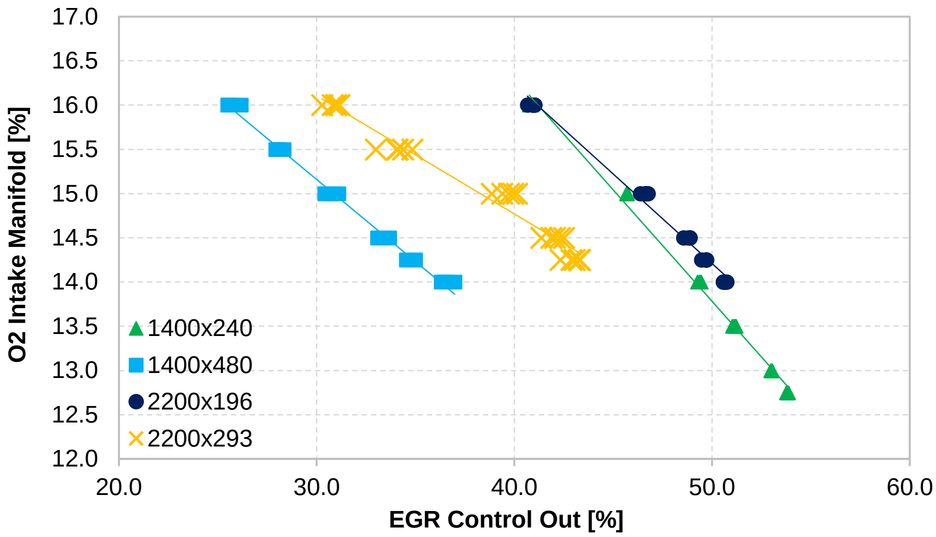

Figure 3.20 - EGR Linearization Results assessment

3.4.2 Transient Control Calibration

The transient engine control logic was developed by DENSO and required the calibration of EGR control strategy, a transient detection logic and a smoke limitation strategy.

As far as the EGR is concerned, this operates, with a Proportional-Integral (PI) loop control based on the signal of an O_2 sensor placed downstream of the high-pressure compressor as mentioned in the previous Paragraph. This control is composed by a feedback part and a feed forward part, which is substantially made by a "precontrol" map, in which the control output values in steady state conditions are stored (Fuel Injected Quantity vs Engine Speed). The feedback part was calibrated by filling the maps of proportional and integral part coefficients versus engine speed and injected quantity.

The transient detection logic was used to smoothly switch between steady-state control map to transient-optimized calibrations. It detects transient operation by checking the difference between actual boost pressure (measured by a pressure sensor in the intake manifold) and the value mapped in steady state conditions (engine speed vs injected quantity map). The boost deviation and its gradient define a parameter called "Transient Factor" ranging between 0 and 1. It was used to choose the values of the target O_2 and precontrol values of the EGR control logic in a range between the mapped steady state and fully transient value. It was also used to smoothly ramp out and back in the feedback part. The transient O_2 target and precontrol maps works exactly as the steady state ones and were in fact calibrated as an offset copy. The offset values were calibrated to obtain the target NRTC NOx emissions results.

Concerning the smoke limitation strategy, it was mainly based on a map of minimum lambda function of engine speed and boost pressure. It is worth to point out that the engine was not equipped by an air flow meter and the air flow (needed to evaluate the maximum injected quantity from the mapped lambda) was estimated by a flow model based on mapped volumetric efficiency. The smoke map was calibrated along constant speed loadsteps, with the target to optimize NOx and Time To Torque (TTT) and the constrain of limiting MSS soot to a maximum value of around 60 mg/m^3 corresponding to an FSN of 3 as shown in Figure A.2 (Appendix A).

The results of the abovementioned loadsteps are reported in Figure 3.21. In those tests the engine was set to follow a step of load at constant speed from 10% pedal to Full Load in 1 second in a range between 1000 and 2200 rpm with steps of 200 rpm.

The 1000 rpm case was outside of the emissions-regulated area, except for idle and very low load and the engine was left to work without EGR as soon as the load increase, as shown by the intake O_2% trace (orange) and NOx trace (green).

At 1200 rpm the EGR starts to be modulated during transient even though most of the 1200 rpm range stands in the NTE zone and the NOx requirements are less stringent.

The perfect example of the adopted transient strategy is at 1400 rpm (peak torque speed): as soon as the pedal step up, the injected quantity increases up to the smoke limitation map value (black dashed line). Consequently, the O_2 intake manifold drops, since the exhaust gas becomes suddenly much poorer of oxygen (lower AFR) and the smoke emissions (gray line), limited by the smoke map, starts to increase. In the meantime, the transient detection logic detects the transient operation and switches the EGR control to use the transient maps allowing the engine to breath more clean air and let the smoke limit strategy to inject more fuel to increase the torque. Once the boost pressure (red line) approaches the peak torque value, the transient detection strategy starts to reduce the transient factor thus switching back smoothly to the steady state maps and the O_2% at the intake manifold becomes to decrease again with the NOx.

Increasing the engine speed, the turbocharger performances improve and the boost pressure build-up is faster, making the transient less critical in terms of soot and NOx emission.

Even though the engine layout was not optimized and the capacity between the exhaust flap and intake runner is big (around 30 liters), TTT of the engine was lower than two seconds in every case, promising to be greatly improved with a more engineered airpath design.

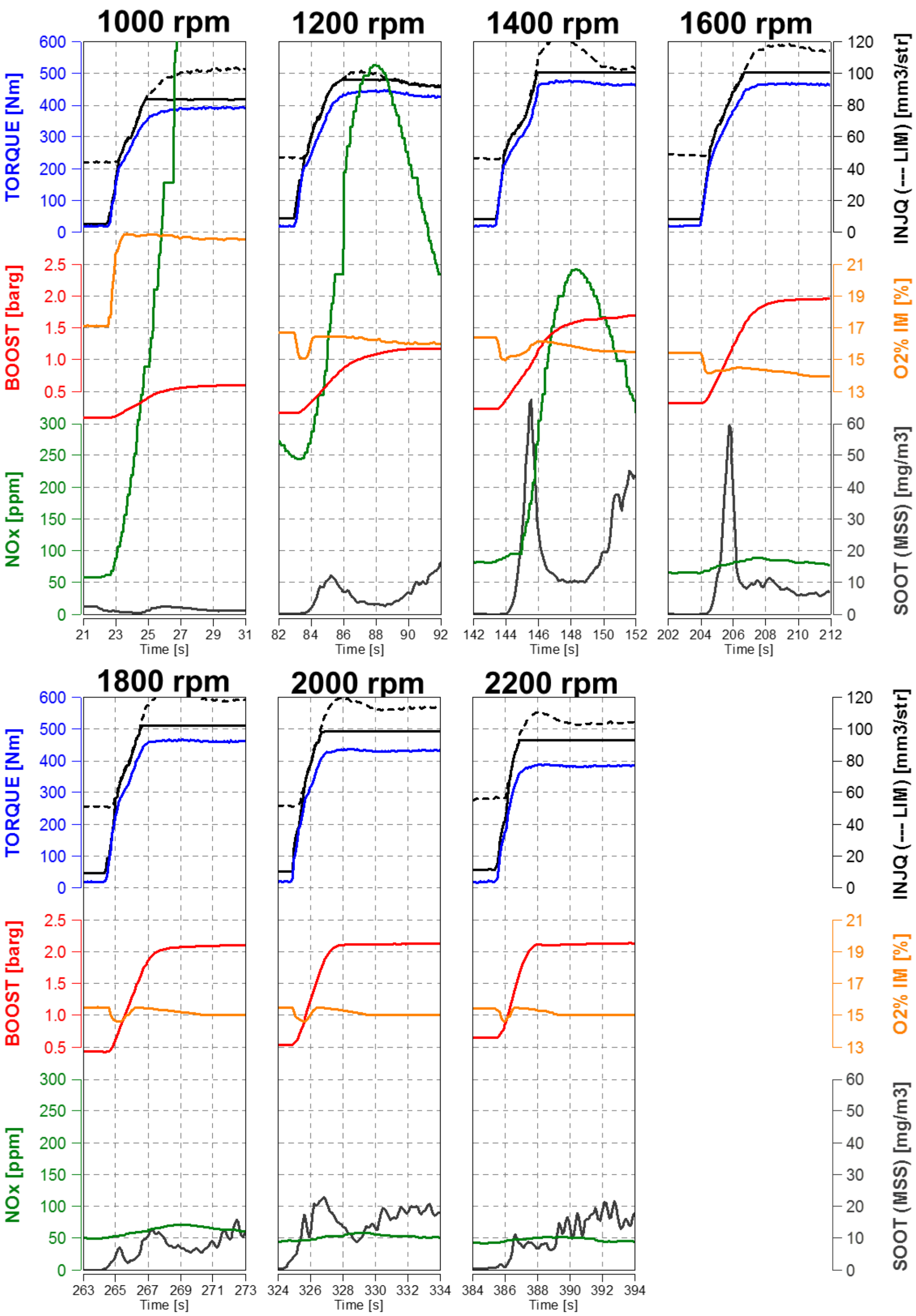

Figure 3.21 – Load steps results

3.5 Results on Certification Cycles

In this Paragraph the results on the two certification cycles are analysed.

As far as the NRSC is concerned, in Figure 3.22 the breakdown of the test in terms of BSFC, NOx and MSS Soot in all the points of the cycle is reported. The emissions reported in g/h, are weighted by the relative weighting factor of each operating point. It is worth to remark that the final emission value for this test has to be calculated by:

$$E_x\left[\frac{g}{kWh}\right] = \frac{\sum_1^n e_{x_i} w_i}{\sum_1^n P_i} \tag{3.13}$$

Where:

- E_x: is the final specific emission x in g/kWh
- i: is the operating point index
- e_{x_i}: is the emission of the pollutant x in the operating point i
- w_i: is the weighting factor of the operating point i
- P_i: is the brake power in operating point i

Therefore, the blue and red bars of Figure 3.22 are the terms of summation of Equation 3.13. It results immediately clear that the most important points in terms of emissions are peak torque and peak power. For those points the most retarded timings have been adopted to reduce NOx and satisfy the regulation, due to low AFR, caused by insufficient boost pressure, resulting in poor efficiency (especially at peak power). They would extremely benefit of higher performance turbochargers, which would allow to increase simultaneously AFR and EGR, reducing Soot and NOx at the same time and adopting less retarded injection timing to improve fuel efficiency.

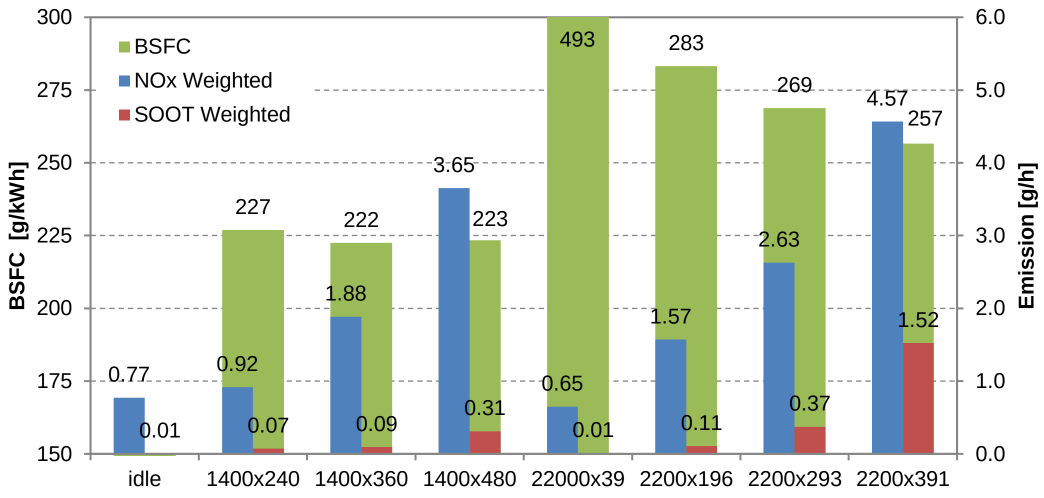

Figure 3.22 - NRSC breakdown

To evaluate the emissions over the NRTC, the first task to be addressed was the development of a transient calibration which allowed the engine to follow the extremely dynamic NRTC cycle (see Figure 1.4), as shown in Paragraph 3.4.2. The engine behaviour over the cycle can be observed in Figure 3.23 and in Figure 3.24 where the speed and torque traces, and the regression between target speed, target torque and target power versus actual values are reported respectively.

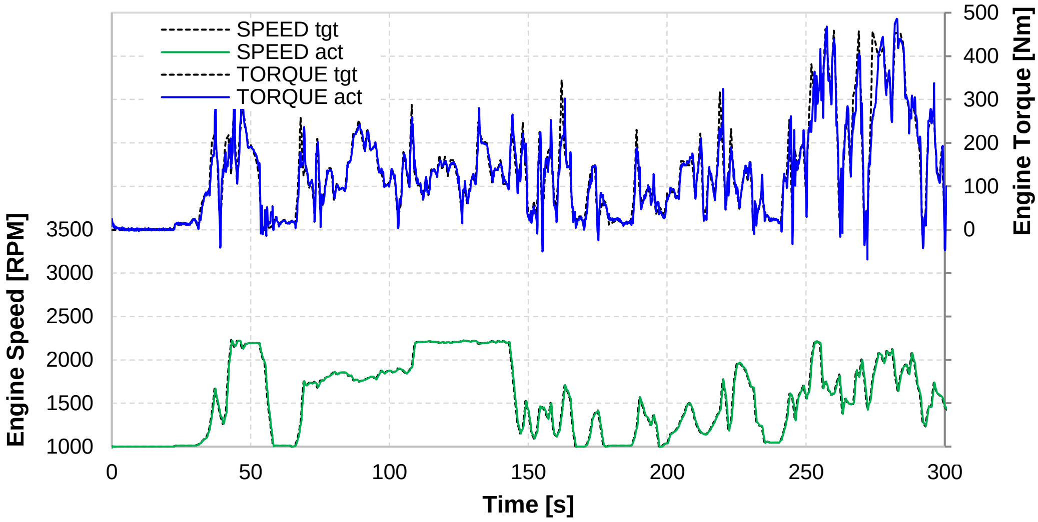

Figure 3.23 - NRTC Example

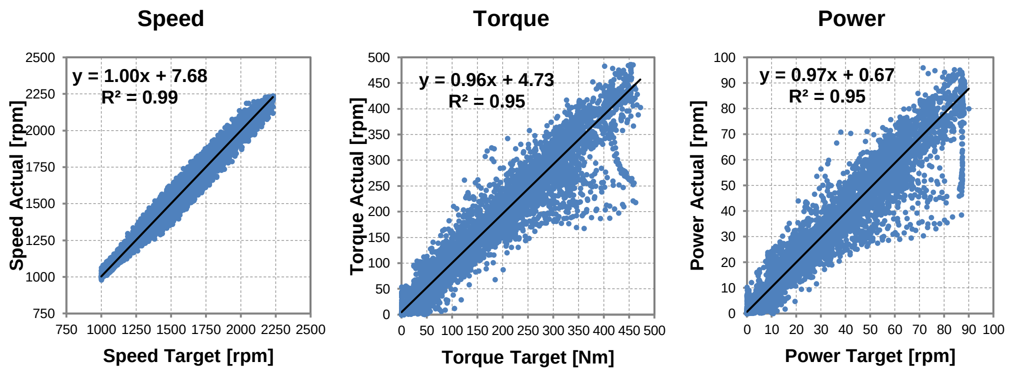

Figure 3.24 - NRTC compliance regressions

The compliancy of the test, which is based on the abovementioned regressions quality, is analysed Table 3.3, which confirms that all the criterions were met and the test was therefore valid.

Table 3.3 - NRTC compliance criterions

	SPEED		TORQUE		POWER	
	Meas	Limit	Meas	Limit	Meas	Limit
Slope	✔ 1.00	**0.95 ≤ X ≤ 1.030**	✔ 0.96	**0.83 ≤ X ≤ 1.030**	✔ 0.97	**0.83 ≤ X ≤ 1.030**
Intercept	✔ 7.68	**X ≤ 100**	✔ 4.73	**X ≤ 9.6**	✔ 0.67	**X ≤ 1.8**
R^2	✔ 0.99	**X ≥ 0.97**	✔ 0.95	**X ≥ 0.85**	✔ 0.95	**X ≥ 0.91**
SEE	✔ 31.3	**X ≤ 112**	✔ 25.3	**X ≤ 48**	✔ 5.01	**X ≤ 9.0**

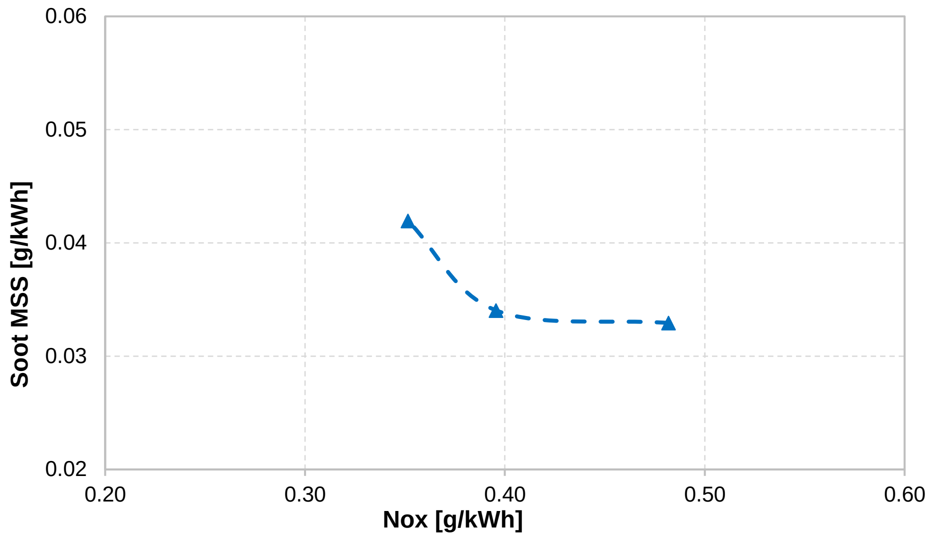

Figure 3.25 - NRTC NOx - Soot Tradeoff

In Figure 3.25 the results of three compliant NRTC runs, measured with different offset between transient and steady state control maps are reported. By reducing the offset between steady-state and transient-optimized maps, the modulation of EGR during transient is reduced, causing lower NOx and higher soot emissions, in a kind of Soot-Nox tradeoff. Those results were used to define the offset value to be used to meet the defined targets.

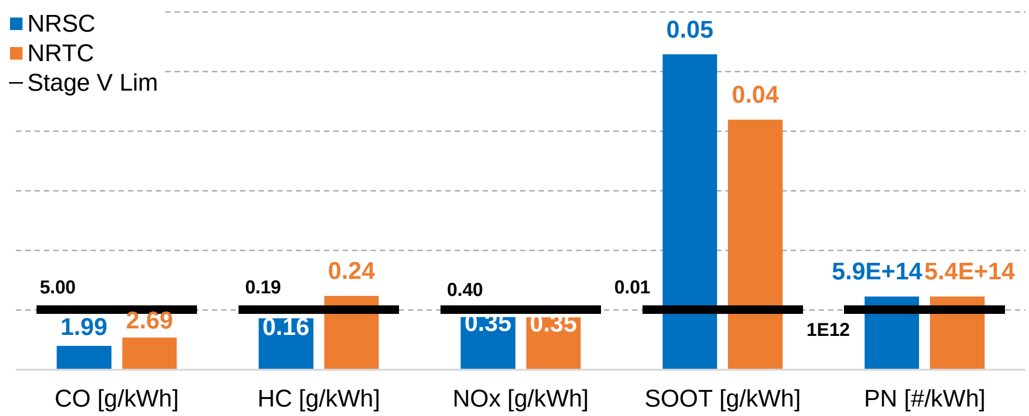

Figure 3.26 - NRSC and NRTC Engine Out Emission results

In Figure 3.26 the engine out emission results of the NRSC and of the lowest-NOx NRTC run of Figure 3.25, are compared with the regulated targets. For both tests it was possible to achieve more the 10% margin on NOx, with a level of Soot, HC and CO that can be easily handled by the DOC and DPF. Concerning the Soot, it must be pointed out that it was measured by the MSS, which is affected by various sources of losses as widely discussed in Appendix A, and the value reported here must be therefore increased by 30% to be compared with a SM-like measurement according to the correlation in Figure 3.3a. Moreover, the regulated value refers to particulate matter mass, while SM and MSS measure soot, which is only its solid fraction. Given the high load level of the cycles, soot can be estimated to be around 80% of the total particulate mass.

PN is the only regulated emission to exceed the provisional engineering targets of Table 1.4. To investigate if this level of engine out particles could result in excessive tailpipe emissions, NRTCs with tailpipe-configured APC were carried out. The total PN measured in those tests was several orders of magnitude lower than the regulated values.

The choice of reporting engine out instead of tailpipe emission, is related to the fact that tailpipe soot and particulate number measurements were found to show poor repeatability due to the very low concentrations. More in details, tailpipe particle number was found to a value of 10^9 #/kWh over an NRTC with the same calibration of the cycle reported above, in which 10^{14} #/kWh was measured at engine out. These two values correspond to a DPF filtration efficiency of 99.999% which could seem to be unrealistic, even though some comparable values can be found in literature [39][40].

Chapter 4

Conclusion and Outlook

As shown in the previous Chapter, the predefined emission targets have been accomplished and the engine was able to run a compliant EU Stage V certification procedure. However, the provisional engine build and some not optimized components have caused poor efficiency in some operating conditions.

This Chapter is focused on the analysis of the improvement potentialities of this engine architecture by means of a 1D-CFD model, used to identify the key aspects of the provisional engine layout to be re-engineered in order to improve engine performance and efficiency.

Afterwards the conclusions and the outlook of the study will be discussed.

4.1 Engine improvement potentials

As shown in the previous Chapter the main challenge of this engine architecture is the ability to recirculate high amount of EGR to control NOx and to keep at the same time acceptable AFR to control soot emissions. Therefore, the more the turbocharging system is able to pump fresh air and EGR into the engine (means low oxygen concentration but high AFR), the less NOx and Soot will be emitted. When the EGR rate effectively routed with acceptable AFR is not enough to reach the target NOx, because the turbocharger is producing the maximum boost pressure or is limited by an operating limit (i.e. exhaust manifold pressure), the only way to proceed is retarding the combustion to reduce NOx, at the expenses of high fuel consumption. This is the reason why the engine showed a progressive worsening of BSFC by increasing load and speed as shown in Figure 3.15: in fact, in the peak power operating point the maximum allowed turbine inlet pressure (5.2 bar) is reached, defining the wastegate preload and the maximum boost pressure over the entire engine map. To reach the target of 0.35 g/kWh of NOx in the peak power operating points an extremely retarded timing had to be adopted resulting in the in cylinder pressure trace of Figure 4.1, in which the pressure during combustion is much lower than the pressure at the end of the compression stroke. It results clear how, the possibility of exploiting a combustion closer to TDC would drastically improve efficiency.

In the following paragraphs solutions to improve the boosting performance will be analysed using the 1D-CFD model presented in Appendix B and validated on the Full Load curve as reported in the following Paragraph.

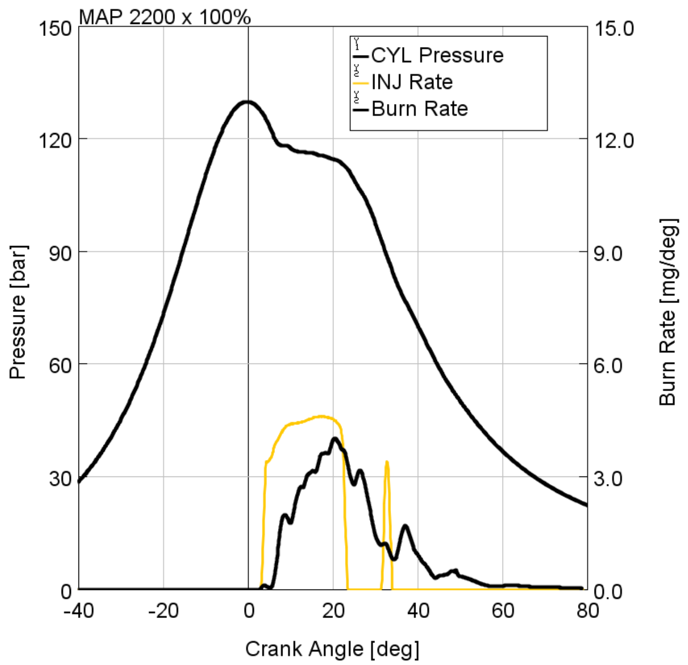

Figure 4.1 – Exp. in Cyl. pressure and burn rate of peak power operating point

4.1.1 Full – Load Model Validation

As already mentioned, a GT-Suite model of this engine featuring a predictive combustion model and emission models, was build and widely validated, as reported in Appendix B.

To empower the results of the study discussed in this Chapter, a careful validation of the model predictivity on the Full-Load operating conditions is presented in this Paragraph.

The results of two different model configurations are presented hereafter in Figure 4.2, Figure 4.3, Figure 4.4 and Figure 4.5 and compared to the experimental results.

The model named "VALIDATION" and reported in blue, uses two PID controllers acting independently on the high pressure and low pressure wastegate targeting the experimental low pressure compressor and high pressure compressor outlet pressure. This may appear nor fair since the real engine features only a mechanical wastegate on the high pressure stage. However, the turbochargers maps provided by the manufacturers, which are normally measured on a steady flow bench at constant temperature, can differ consistently to the real turbocharger operation when coupled to an internal combustion engine. Therefore, respecting the controller architecture in the model may lead to consistent errors in the mass flow rate or lead to unrealistic overcalibration of the pressure drop of the intake and exhaust lines.

Nevertheless, given the model validation on the "overcontrolled" configuration, the results with the real architecture of the boost controller referred as "REFERENCE" and depicted in green are also reported. In this configuration, only the high pressure WG is controlled targeting the single value of the maximum boost pressure of 3.2 bar over all the operating points. This model, which should be more representative of the real engine behaviour, will be used as reference for the studies presented in the next Paragraph.

Except for the abovementioned difference the two models are identical and the main features are the following:

- Predictive combustion and emission models presented in Appendix B, Paragraph 4.2B.1.
- Intercooler and aftercooler gas outlet temperature imposed to 60°C.
- Load controller acting on the main injection quantity to target the experimental Brake Mean Effective Pressure (BMEP).
- EGR controller acting on the diameters of two orifices representing the exhaust flap and the EGR valve, using the optimized positioning laws of Paragraph 3.4.1, to target the experimental EGR rate.
- Chenn-Flynn model for FMEP [41].

Referring to Figure 4.2, the "Validation" model well represents the flow characteristic of the engine as shown by the volumetric efficiencies plots and the BSFC is calculated with an error lower than 2 g/kWh. The "Reference" model has a higher volumetric efficiency in the middle-range speed due to slight overestimation of the high pressure stage performances. The higher boost pressure of course affects the AFR and slightly the PFP.

In Figure 4.3 the good agreement on the combustion parameters of MFB50 and DUR1075 confirms the effectiveness of the predictive combustion model. As far as the pressures are concerned a special focus must be taken on the HP turbine inlet pressure and on the DPF outlet pressure. The first is the limit on which the WG preload was set on the actual engine and the second is a combined result of the pressure drop across exhaust line and EGR line and of the EGR control logic. This pressure is object of the studies of Paragraph 4.1.2 and is very well calculated by the model.

Concerning the temperatures reported Figure 4.4, the model shows a very high level of correlation especially for the two compressor outlet temperatures and high pressure turbine inlet which are very important performance limiter of a turbocharged engine. In Figure 4.4 the results of the emission models are also reported. As far as the NOx are concerned, a very good correlation with experimental measurements is observed (results presented in this Paragraph were obtained with the same set of calibration parameters of Paragraph 4.2B.1.3 and no ad-hoc calibration were carried out for the full load points, nor for the combustion model, nor for the emissions model). The soot model, instead, fairly confirms to be able to catch the trends only.

In Figure 4.5 the comparison of the simulated and experimental in cylinder pressure and burn rate is reported for four operating points (2200, 1800, 1400 and 1600 rpm). Given the excellent correlation, the combustion model confirms to be able to successfully reproduce the Diesel combustion with very high accuracy.

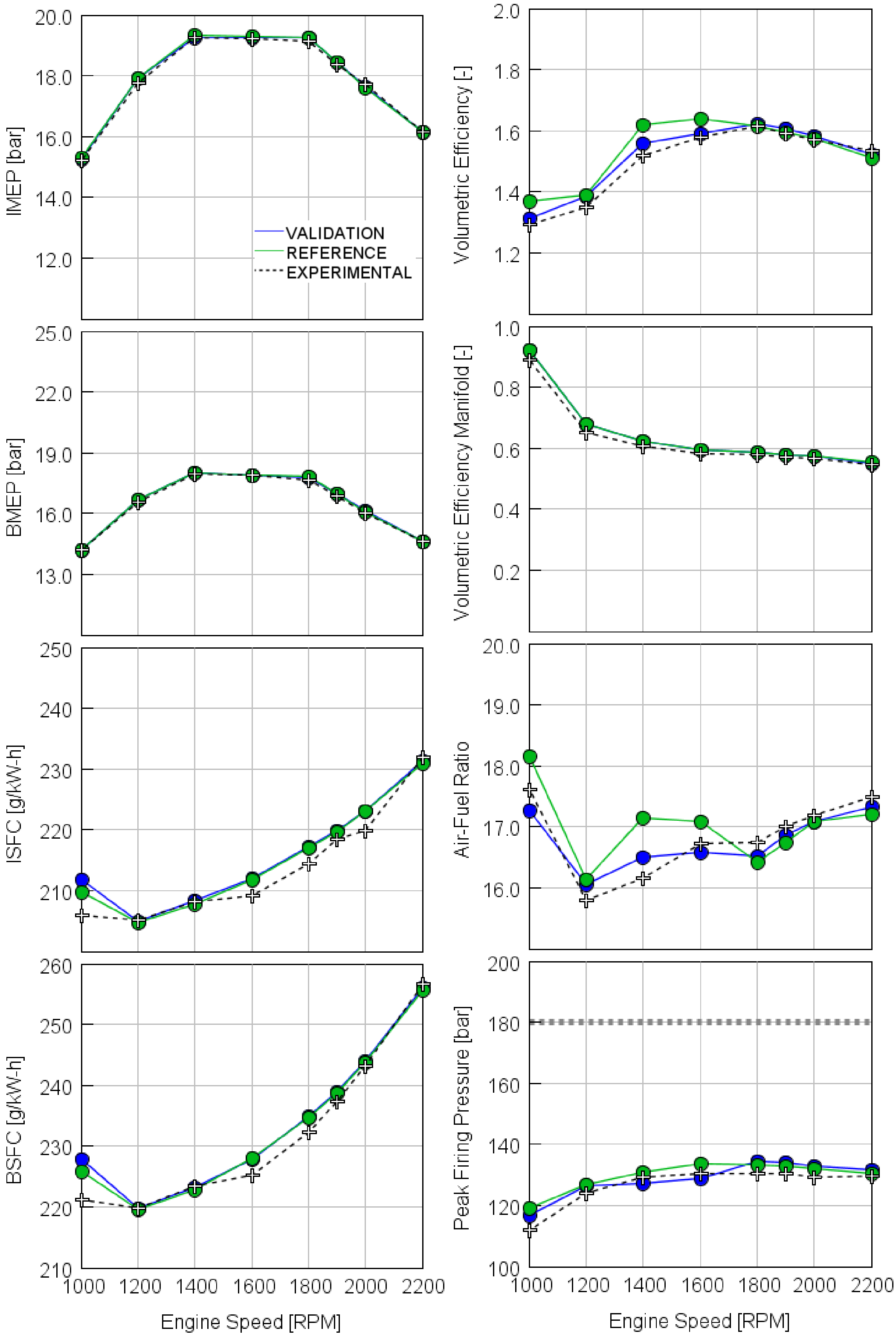

Figure 4.2 - FL Model Validation 1/4

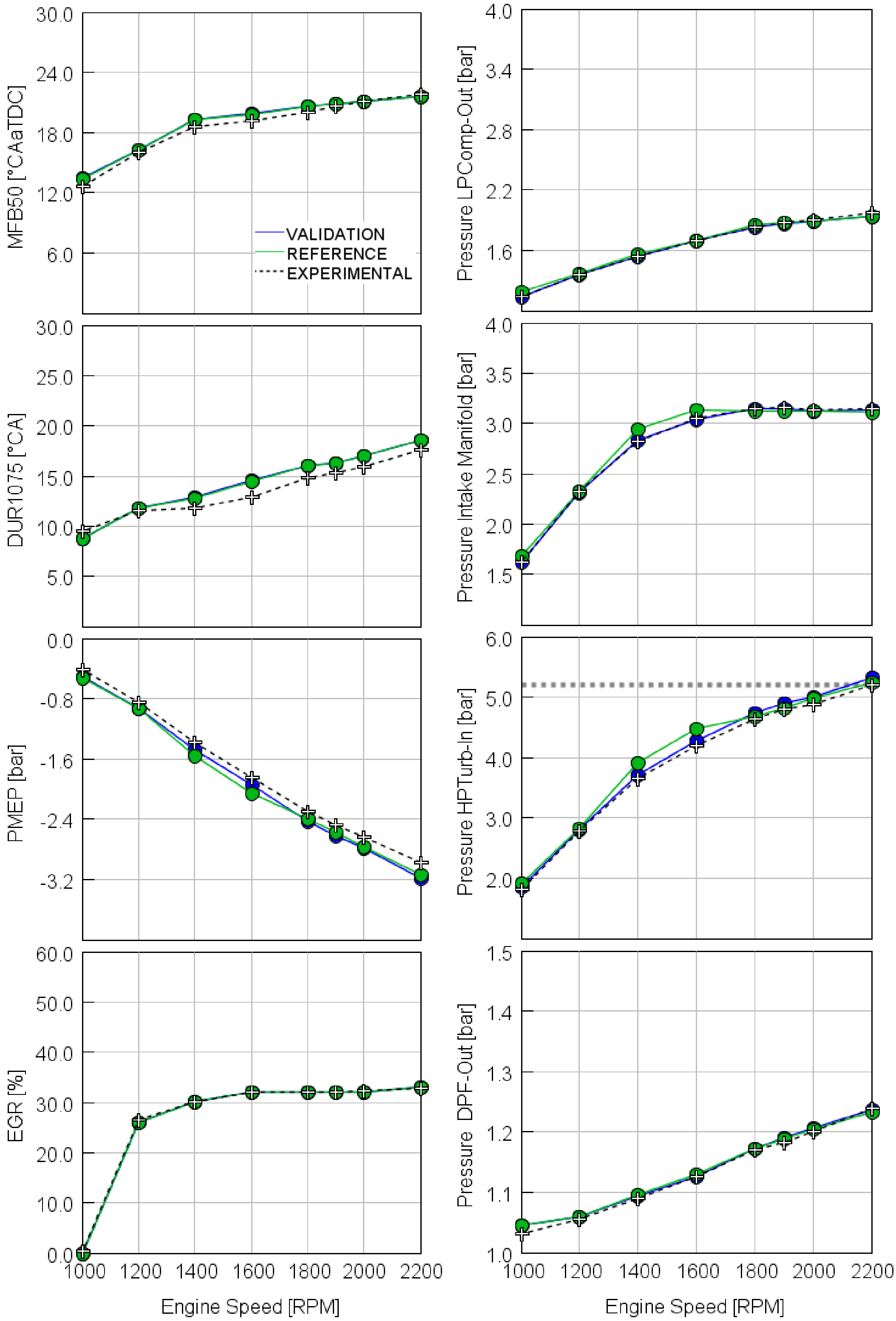

Figure 4.3 - FL Model Validation 2/4

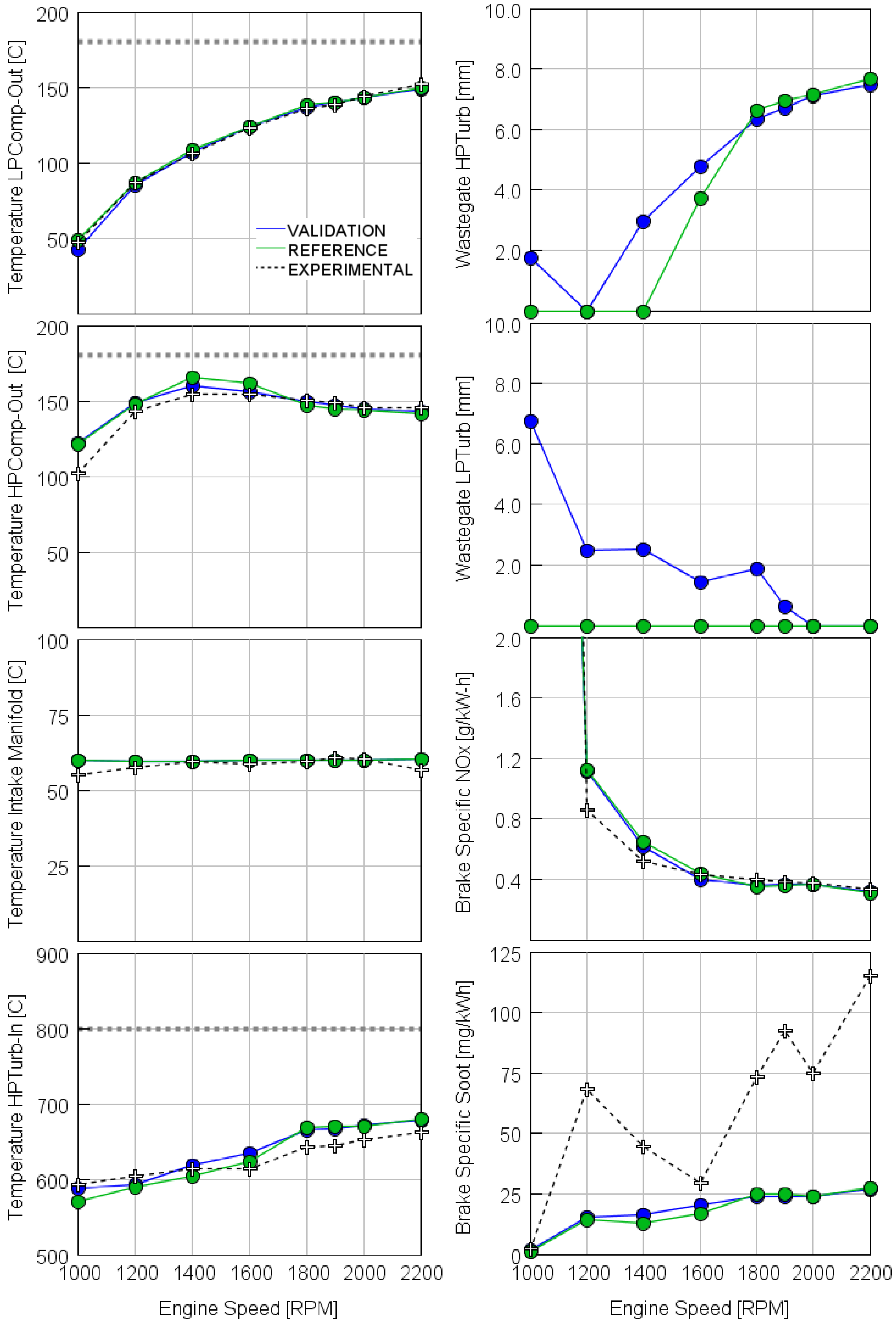

Figure 4.4 - FL Model Validation 3/4

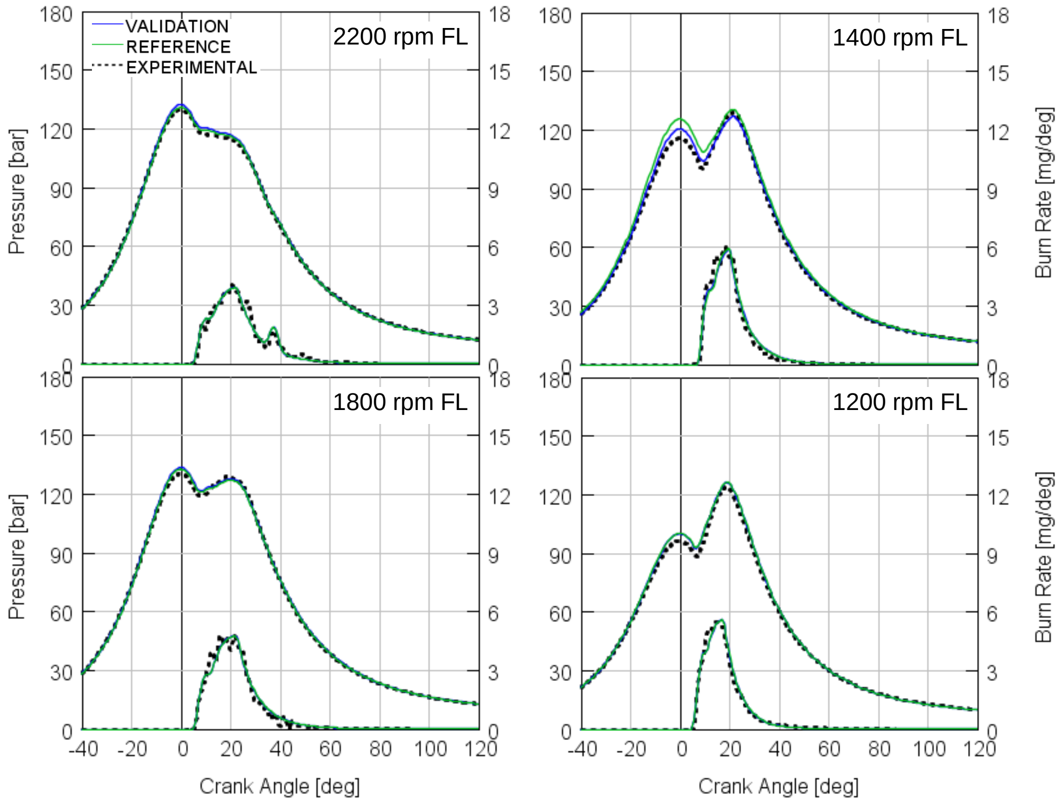

Figure 4.5 - FL Model Validation 4/4

4.1.2 Exhaust and EGR Line pressure drop improvements

As already mentioned, at peak power the maximum turbine inlet pressure was reached limiting the boost pressure, therefore any improvement that would decrease the backpressure would allow a boost pressure increase.

One of the possible options is to reduce the DPF outlet pressure upstream of the exhaust flap, which at peak power point reached 1.23 bar. This level of pressure is necessary to route the desired EGR in the EGR pathway. A well-designed EGR line is expected to require only the pressure drop generated by the exhaust line and muffler and no additional backpressure should be generated by the exhaust flap to route the EGR. The exhaust flap, in fact, should be used only in part load condition when the flow rate is too low to generate enough backpressure to route the EGR.

The first investigation was therefore carried out to evaluate how much an EGR line with higher permeability would have improved the engine performances. In order to do that, since all the sources of pressure drop of the exhaust and EGR line were grouped into the equivalent areas of the two valves (refer to Paragraph 3.4.1), the equivalent areas of the positioning laws of the EGR control were upscaled by 15% in order to obtain a pressure drop across the exhaust line (upstream exhaust flap and ambient) representative of a well sized muffler estimated around 130 mbar at peak power. Thanks to this modification (which can be translated in practice with higher sizing of the valves, pipes and EGR cooler) the model immediately predicted a reduction of the turbine inlet pressure over the complete speed range that could be translated in higher boost pressure and higher EGR rate.

To fully exploit the possibilities offered by the higher boost, the engine model was modified with a “electronic-like” wastegate controller in the high pressure stage. It means that the boost pressure could be adjusted freely in each operating point and it is not limited to the single value defined for the mechanical WG at peak power. An optimization on the engine calibration (Timing and EGR) was run to minimize the BSFC with the following constrains:

- Lower or Equal NOx emission of the “REFERENCE” model
- Higher or equal AFR of the “REFERENCE” model
- Engine operating limit:
    - PFP limit: 180 bar
    - HP turbine inlet temperature: 800 °C

The boost pressure was set to the maximum achievable in each operating point respecting the following limits:

- HP and LP compressors outlet temperature:180°C
- HP turbine inlet pressure: 5.2 bar

The choice of setting a constrain on the lowest AFR is somehow like to constrain the smoke emission to a value lower or equal to the “Reference” model. In fact the soot model was not good enough to be directly used with calibration purposes as the NOx one is, and therefore the constrain was set to the parameter which has the higher impact on soot. It is worth to point out that soot has an high dependency also with the injection timing as shown in Figure 2.7, however this effect cannot be taken into account in this evaluation.

The results are reported in red bullets and referred to as “RED_EP” in the legends of Figure 4.8 and in Figure 4.9. They are compared with the results of the “Reference” model presented in the previous Paragraph and with the results of the study presented in the following Paragraph.

It results immediately clear how, the increased boost pressure at peak power, allowed to increase the EGR rate of about 5% with the same AFR. The reduced NOx emission permitted to anticipate the combustion of about 4°CA to obtain the same NOx and improving the efficiency of around 10 g/kWh, as shown by the MFB50 plot and in the indicating diagrams. The lower speed operating points benefit as well of the higher permeability EGR line and of the possibility to increase the boost up to the maximum turbine inlet pressure thanks to the flexible controller. Thanks to the above explained mechanism the BSFC could be greatly improved up to 1400 rpm where the difference in boost pressure with the “Reference” model is negligible.

4.1.3 Improved Turbochargers Efficiency

Another improvement potential that has been investigated, was a better matching of the turbochargers. This investigation was carried out by means of the Advanced Optimizer of GT-Suite, trying to minimize BSFC on the peak power and peak torque operating point, varying the dimension of the turbochargers using similarities laws [42], and keeping the constrains listed in the previous Paragraph. The optimizer, however, could not find a solution that improved consistently one operating point without big drawbacks on the other.

The two stages, in fact, are quite well matched as showed in Figure 4.6 in which the operating point of the model with the reduced backpressure are plotted on the compressors and turbines maps.

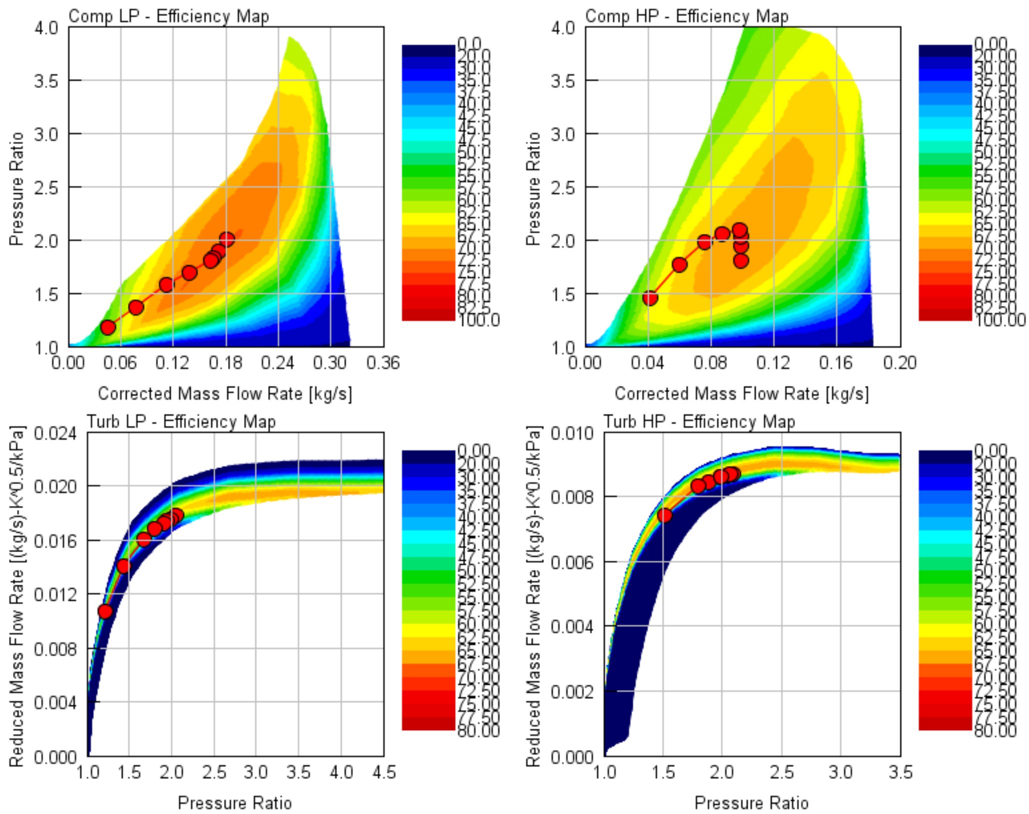

Figure 4.6 – FL operating points on the turbocharger maps for the "LOW_EP" model

Nevertheless, both compressors and turbines seemed to have quite low maximum efficiency. The global efficiency of the turbocharging system strongly influences the turbine inlet pressure, which has been shown to be the most limiting parameter for this engine. The higher is the efficiency, the higher is the pressure ratio realized by the compressors at the same total pressure ratio in the exhaust line thus improving engine efficiency for the mechanism explained before.

Therefore, the impact of a higher turbocharger efficiency was investigated as follows: it was assumed that a well matched compressor and turbine should operate with 75% and 65% efficiency respectively in the peak power point. Efficiency multipliers on the turbines and compressors maps were applied with this goal. The results of this operation are reported in Figure 4.7 where the turbocharger efficiencies of the RED_EP model and of the new “TC_OPT” model are compared. For all the components the efficiency was increased by 4 to 7% depending on the operating point except for the High Pressure Turbine in which the efficiency was slightly reduced

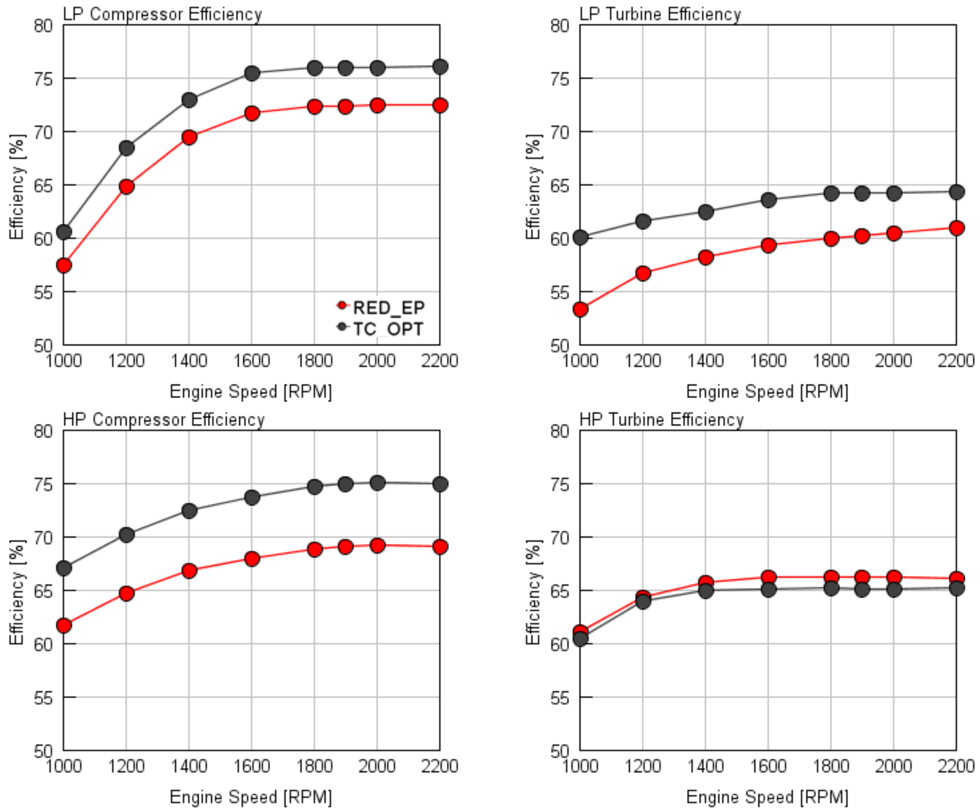

Figure 4.7 - Turbocharger s efficiency comparison of "RED_EP" and "TC_OPT" Models

The effect of the efficiency scaling is reported in Figure 4.8 and in Figure 4.9 in which the results of this model (“TC_OPT” – grey bullets) are plotted together with the “RED_LP” and “REFERENCE” model. The engine calibration was optimized in the same way of “RED_LP” model. It results immediately clear that in most of the operating point it was possible to reach the same level of NOx of the “REFERENCE” model with higher AFR and therefore possibly lower smoke, and the SOI was limited by the peak firing pressure. The BSFC in this configuration was greatly improved reaching 214 g/kWh at peak torque and 240 g/kWh at peak power. Moreover, the EGR was increased between 5 and 10% if compared to the reference model, increasing the backpressure again, therefore another loop of optimization of the EGR line permeability may bring some other benefits.

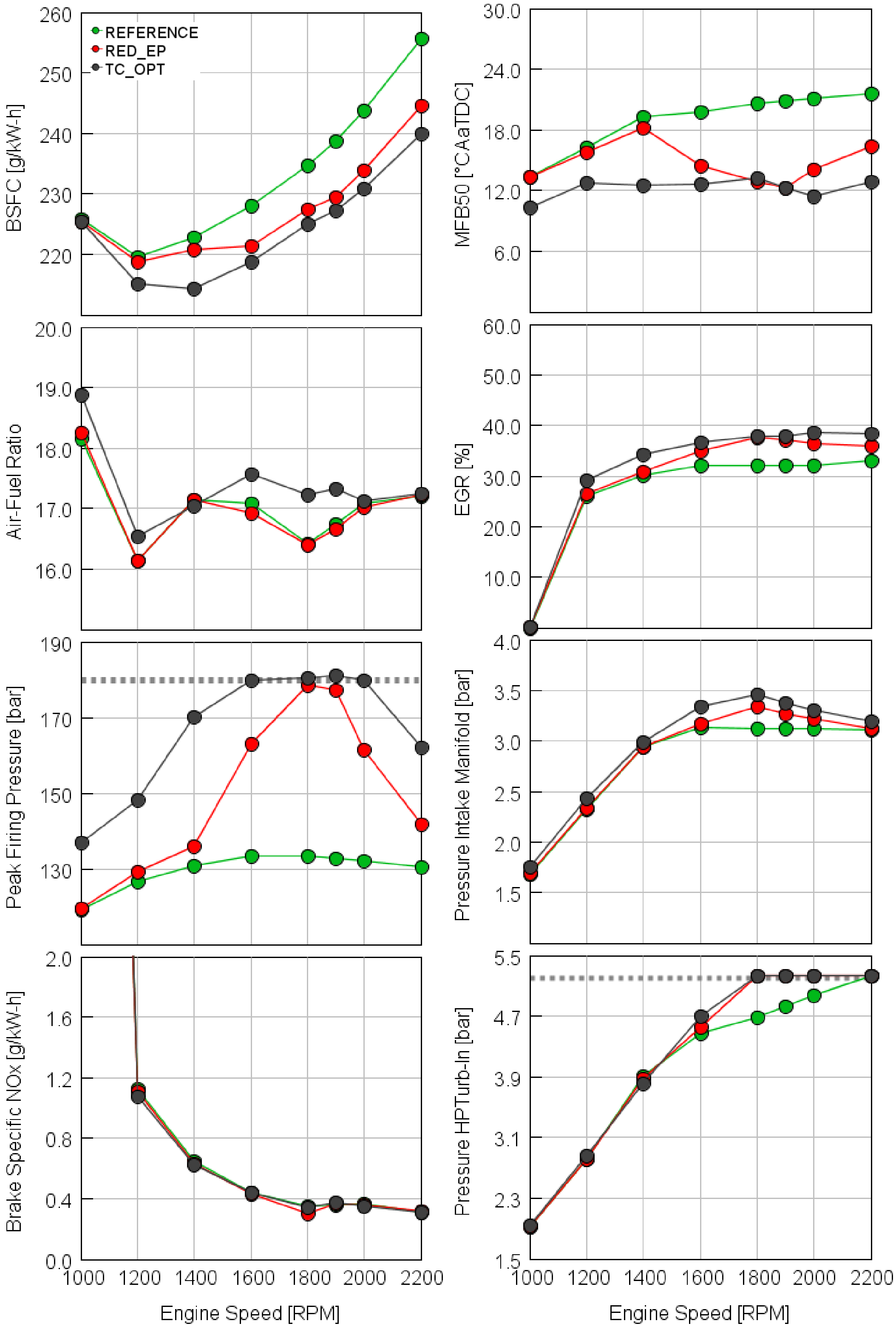

Figure 4.8 - Engine Improvement Potentials 1/2

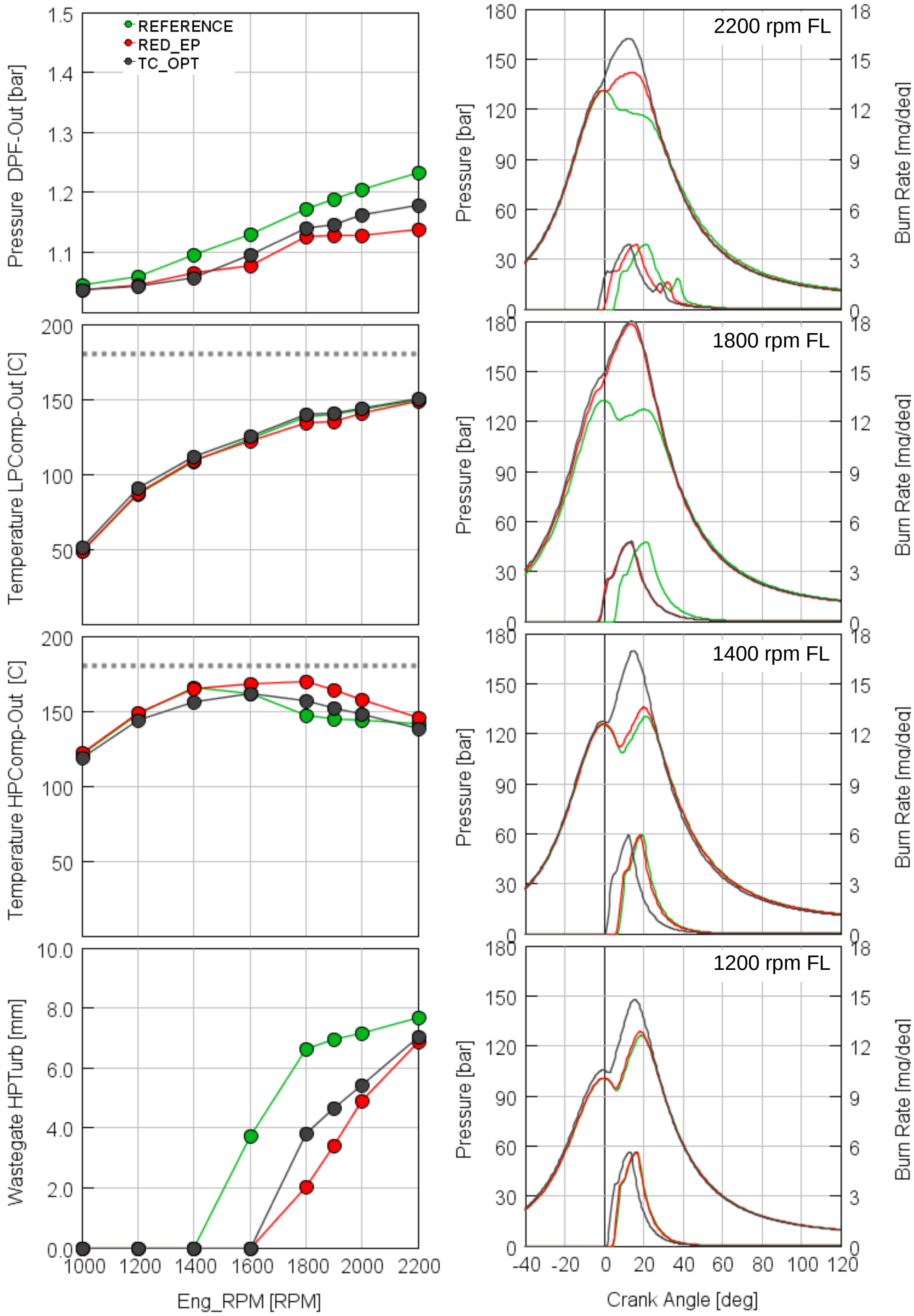

Figure 4.9 - Engine Improvement Potentials 2/2

4.2 Conclusions

In this work a feasibility study to meet the EU Stage V emission regulations on a 90 kW NRMM Diesel Engine without specific aftertreatment for NOx was carried out.

The project, carried out in collaboration with Politecnico di Torino, Kohler, Ricardo and Denso, evaluated an engine layout based on the Kohler KDI3404 featuring a twin stage turbocharging system, a long route EGR and an extremely high pressure FIS.

This engine architecture was found to be very effective in reducing engine out NOx with a level of particle matter and particle number which could be easily managed by the closed coupled DOC + DPF. The key technology was the high pressure common rail fuel injection system provided by Denso, capable of 3000 bar injection pressure which allowed to drastically improve Soot-NOx, BSFC-NOx and PN-Nox trade off. The effect of the high injection pressure was also investigated in terms of particle size distribution, proving that it is not consistently affected by increasing the injection pressure from 2000 to 3000 bar. Moreover, the use of a close after injection was found to be extremely effective in reducing soot.

A steady state and transient calibration was developed, making the engine able to run a compliant Stage V certification procedure (NRSC and NRTC) with more than 10% engineering margin on NOx.

Issues were found in the provisional engine architecture which did not allowed to exploit the complete potential of the concept, causing poor engine efficiency in the high power area. For this reason, a 1D-CFD model, featuring predictive combustion and emissions model, was built in order to evaluate the impact of some hardware modifications. It was found that with a higher permeability EGR line and a slightly higher performances turbocharging system BSFC can be improved by 10 g/kWh at peak power, at the same engine-out NOx and potentially lower smoke.

In parallel to this project, Kohler developed a Stage V compliant version of the KDI3404 with same power output exploiting a more conventional engine layout with HP EGR + DOC + DPF + SCR as emission control devices which is now on the market [43]. A comparison of the brake efficiency at full load operating conditions between the experimental data of the SCR-free layout object of this thesis, the optimized results obtained via simulation and the published data of the SCR version is reported in Figure 4.10. The gap between the experimental values of the SCR-free architecture and the SCR version is consistent, ranging between 20 g/kwh at peak Torque to 25 g/kWh at peak power, making the SCR free version to consume on average 8% more fuel at full load.

However, if some basic hardware optimizations are carried out on the SCR-free version, the gap is almost halved, becoming 10g/kWh at peak torque and at peak power.

Moreover, other two aspects should be taken in to account. First, the combustion system of the SCR version is expected to be a quite mature technology, since, thanks to the adoption of DPF, no further engine out emissions reduction is required, and the Stage IV/Tier IVf version could be adopted. The SCR-free version, instead, is a completely new concept and thanks to the lessons learned and to the experimental data gathered in this project, a new loop of optimization of the combustion system is expected to give another improvement step in the engine efficiency, further reducing the gap. Second, even though urea is much cheaper than Diesel fuel, urea consumption must be taken into account when comparing Total Cost of Ownership of those architectures.

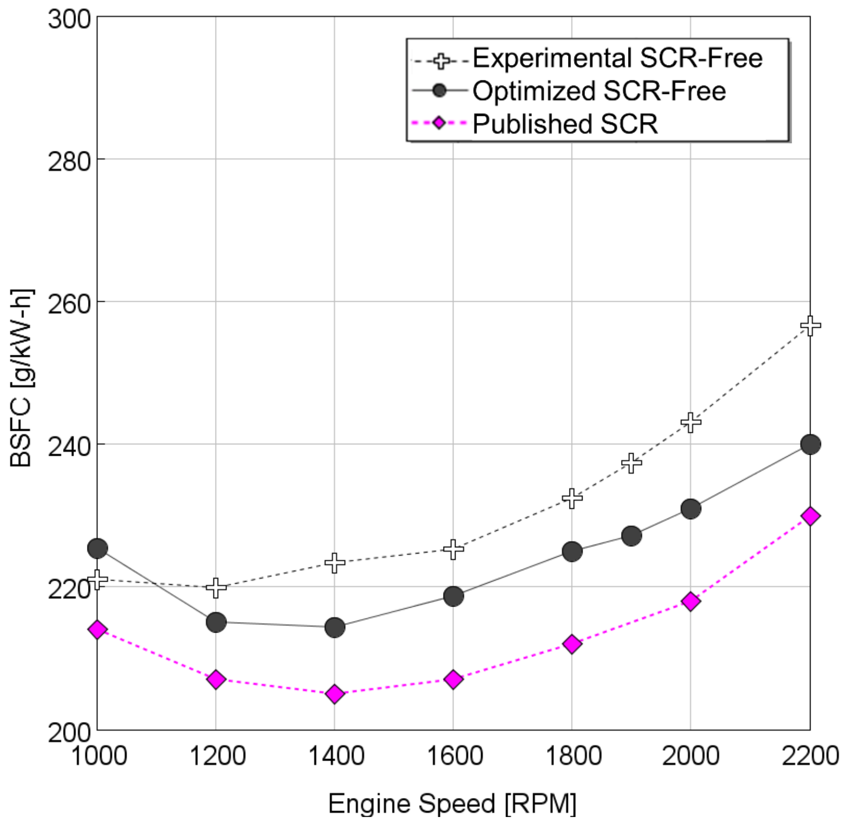

Figure 4.10 - KDI3404 architectures efficiency comparison.

Other options to further improve the engine efficiency may be found in more advanced turbocharging system, for example by swap the high pressure wastegate controlled turbocharger with a Variable Geometry Turbine (VGT) unit, which may reduce the pumping work and improve the transient performances [44]. Some application are already on the market [45], however this technology is not common for the NRMM engines due to cost and reliability.

To conclude, SCR-free architecture is a viable option to meet the Stage V emissions regulation and, with some further engine optimization, could potentially give the same performance of a more complex SCR architecture. The choice between the two solutions is not trivial, it may be application dependent and must carefully consider, cost, reliability, packaging and engineering effort.

Appendix A

Particulate measurements correlations

As shown in Paragraph 3.2, several particulate related measurement devices were used in this project to measure steady and transient particulate mass, number and diameter distribution.

As a side activity, correlations between these measurements were assessed in order to check the consistency of the results. The results of this study is presented hereafter and it is based on the data measured for the hardware assessment (Paragraph 3.2) and for the final Steady State calibration assessment (Paragraph 3.3).

A.1 Microsoot – Smokemeter correlation

The AVL Microsoot Sensor (MSS) measures only the solid fraction of the particulate matter, namely soot. The working principle is based on the photoacoustic measurement method, in which the exhaust gases loaded with strongly absorbing soot particulates, are exposed to a modulated light. The periodical warming and cooling, and the resulting expansion and contraction of the carrier gas, can be regarded as a sound wave and detected by means of microphones: the signal rises proportionally to the concentration of soot in the measurement volume [46].

Smokemeter (SM), instead, measures by means of a reflectometer the blackening of a filter paper through which the exhaust gases are flowed. It outputs a non-dimensional parameter, the Filter Smoke Number (FSN), which indicates the soot content in the exhaust gas [47]. The AVL Smokemeter outputs directly the soot concentration in (mg/m^3) using the empirical correlation reported in Figure A.1.

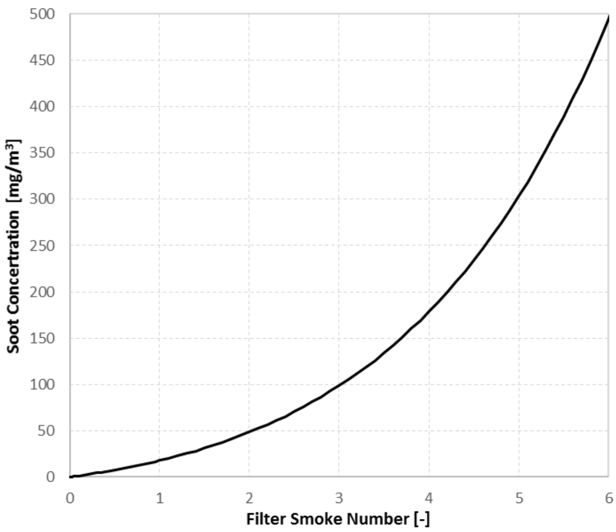

Figure A.1 - FSN - Soot Concentration correlation

This correlation allows to compare directly the measurements of the MSS and of the SM.

However, soot measurement from raw exhaust gas suffers from various sources of losses such as turbulent deposition, diffusional losses and thermophoresis losses. Thermophoresis losses can be compensated knowing the difference between the temperature of the gas at the inlet and at the outlet of the sampling line (which can be assumed equal to the temperature of the heated dilution cell of 120°C) using the empirical function proposed by Kittleson [48] in Equation (A.1):

$$c_{exh} = \frac{c_{measured}}{\left(\frac{T_{in}\,[K]}{T_{exh}[K]}\right)^{0.38}} = \frac{c_{measured}}{\left(\frac{393}{T_{exh}[K]}\right)^{0.38}} \tag{A.1}$$

The subscript exh refers to the sampling point, and in to the dilution point. No compensation should be applied for $T_{exh} < 120°$ since for low exhaust temperatures the uncertainty of the loss compensation becomes high because the amount of thermophoretic losses gets low compared to other loss mechanisms, which do not show good reproducibility and vary a lot between different applications (turbulences, diffusion and sampling artifacts).

For US HDIUT, AVL proposed another correction formula for the MSS measurement which is reported in Equation (A.2):

$$c_{exh} = c_{measured} \cdot (1 + L) \tag{A.2}$$

Where:

$$\begin{cases} L = 0.25 \cdot \dfrac{T_{exh}[°C] - 150}{300} & if\ T_{exh} > 150\ °C \\ L = 0 & if\ T_{exh} > 150\ °C \end{cases}$$

In Figure A.2 the correlations between SM and raw and corrected measurement of the MSS are reported. Uncorrected comparison (Figure A.2b) shows a linear regression between the two instruments but the MSS shows a 25% lower soot value.

Implementing the MSS corrections of Equation A.1 and A.2, the difference between the two measurement becomes lower than 10% (Figure A.2b and c).

Since the uncorrected correlation between MSS and SM measurements is anyway linear, the results of MSS are reported in this thesis without any correction.

A.2 Particle Number - Mass correlation

The AVL Particle Counter (APC) measures the number concentration for the particle with an aerodynamic diameter higher than 23 nm. The particle number concentration decreases along the engine exhaust pathway due to agglomeration phenomena. Agglomeration depends highly on the initial concentration and on the residence time that is linear with the exhaust mass flow rate. Therefore correlation with mass-related particle measurement could only be investigated at the same operating point with similar calibration (similar particle distribution and similar mass flow). For this reason, in Figure A.3 the regression of particle number versus FSN and MSS soot concentration are reported for the EGR sweep in the 4 operating points described in Paragraph 3.2. Surprisingly the particle number seems linear with the FSN other than soot concentration.

A.3 Particle Counter – SMPS

Finally, the correlation between APC and the total count of the Scanning Mobility Particle Sizer (SMPS) was checked. The two particle counters have different counting efficiencies: TSI SMPS features a 3020A ultrafine particle counter with a counting efficiency of 50% at 3 nm and 90% at 5 nm. For the APC, instead, the minimum diameter is not declared however it is compliant with UN-ECE Regulation 83, Revision 4 and Regulation 49 Revision 5, which requires a minimum counting efficiency of 50% at 23nm and 90% at 41 nm. Due to the different counting efficiency and sensitivity a not univocal correlation is expected between the two instruments depending on the particle distribution. Moreover, the different sampling and dilution systems are other sources of measurement discrepancy.

In Figure A.4 the comparison of the measurement of SMPS and APC in four operating points is reported. As expected a linear correlation is found but the regression coefficient is different per each operating point (different particle size distributions).

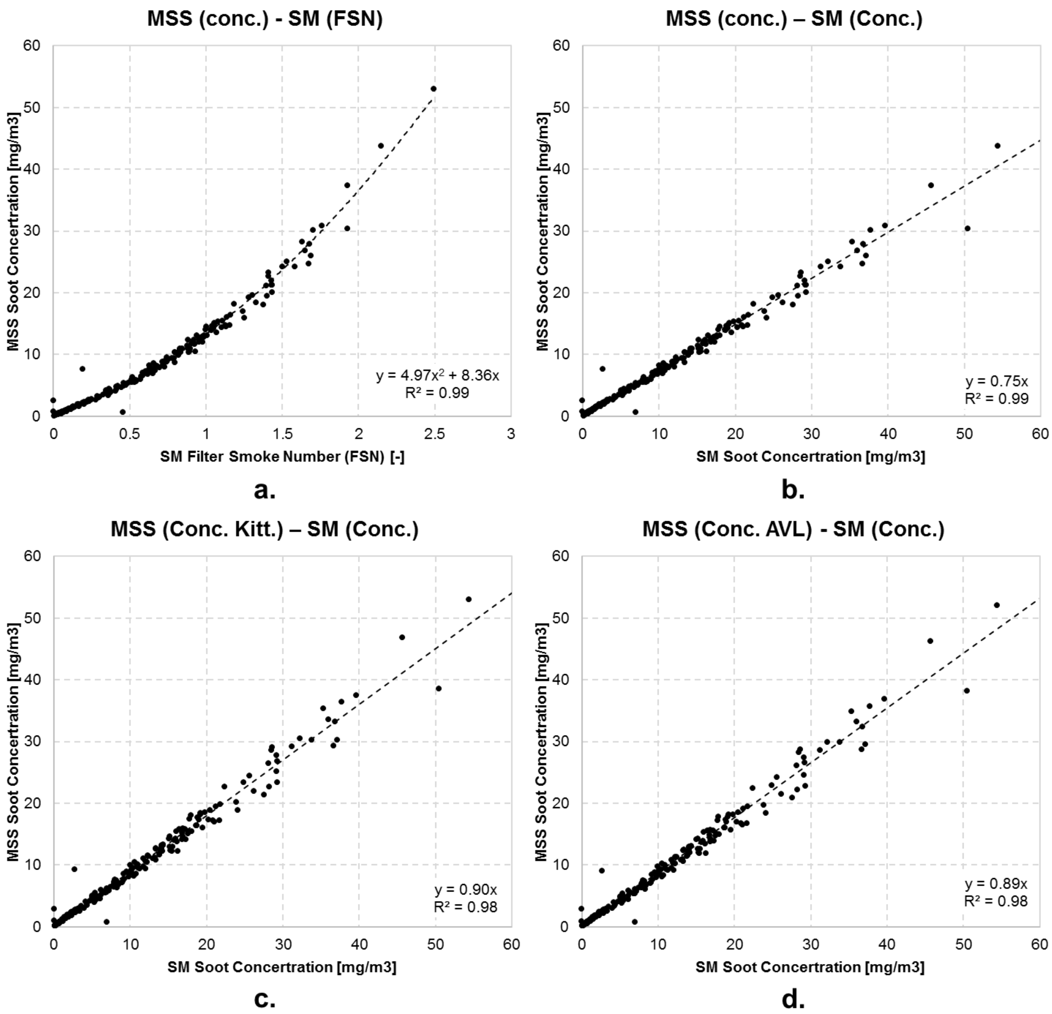

Figure A.2 - Particulate measurement correlations

a) SM FSN / MSS conc. uncorr.
b) SM soot conc. / MSS conc. uncorr.
c) SM soot conc. / MSS conc. Kittelson corr.
d) SM soot conc. / MSS conc. AVL corr.

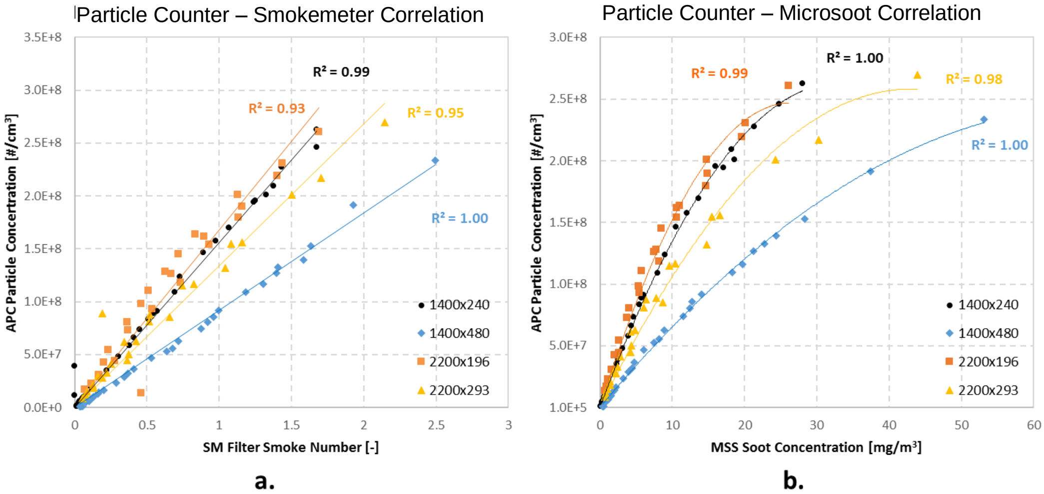

Figure A.3 - Particle Number - Mass Correlation

a) Particle Counter / Smoke Meter (linear fitting)
b) Particle Counter / Microsoot Sensor (quadratic fitting)

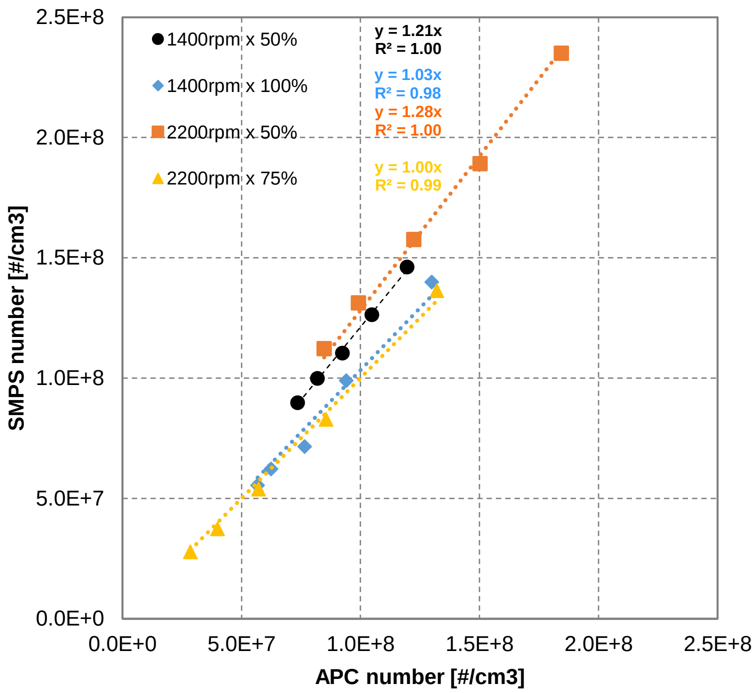

Figure A.4 - APC - SMPS Correlation

Appendix B

1D – CFD Model

Part of the work described in this chapter has been previously published in:

- Millo F, Boccardo G, Piano A, Arnone L, Manelli S, Tutore G, et al. *Numerical Simulation of the Combustion Process of a High EGR, High Injection Pressure, Heavy Duty Diesel Engine*. SAE Tech Pap 2017;2017-24–00. doi:10.4271/2017-24-0009.

As mentioned within the text, even though this engine achieved the predetermined target to comply with Stage V emission regulation with acceptable transient performance, the layout was not optimized and was not possible to exploit all the potentialities that this architecture may offer.

For this reason, a 1D-CFD model was built in GT-Suite to try to evaluate which are the real potentials of this engine layout, in terms of flow characteristics of exhaust and intake line, boosting system and calibration optimization. An engine model with this aim could not disregard predictive combustion and emissions models (at least NOx) which are of crucial importance for this architecture, and the DIPulse developed by Gamma Technologies and built-in GT-Suite, fit for the purpose.

In the following paragraphs the construction and the calibration of the engine model will be presented, together with an extensive validation over the wide experimental data portfolio available already discussed in Paragraph 3.2 and 3.3.

B.1 Predictive Combustion Model

B.1.1 Di-Pulse

As already extensively reported in [49] DIPulse is a predictive combustion model developed by Gamma Technologies. It is based on the discretization of the cylinder contents in three thermodynamic zones, each with its own temperature and composition, as shown in

Figure B.1. The Main Unburned Zone (MUZ) contains all cylinder mass at Intake Valve Closure (IVC), the Spray Unburned Zone (SUZ) includes injected fuel and entrained gas, and the Spray Burned Zone (SBZ) contains combustion products. The basis of this model is to track the fuel as it is injected, evaporates, mixes with surrounding gas, and burns [50]. This model can be applied to single or multiple injection events and each injection event is defined as an injection pulse which is then tracked separately from all other pulses.

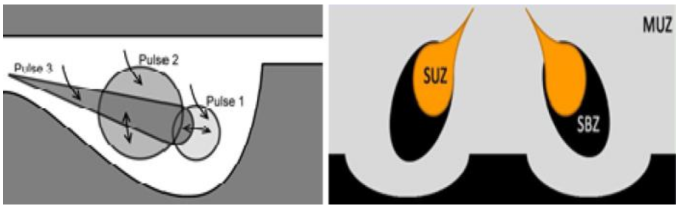

Figure B.1 - Multizone DIPulse Approach [49]

B.1.2 Calibration Approach

The calibration can be performed using a cylinder pressure only analysis (CPOA) approach, which is a stand-alone model that requires the measured in-cylinder pressure trace. This model starts with a preliminary calculation of the combustion burn rate by using Woschni model for heat transfer calculation. Then, the resulting burn rate is applied during the forward simulation cycle and the heat transfer rate is then calculated again [49]. The DIPulse model is then calibrated varying its calibration parameters to minimize the root mean squared error between its own generated burn rate and the burn rate output of the CPOA. The set of parameters which are used for the calibration of combustion model is the following:

- Entrainment Rate Multiplier
- Ignition Delay Multiplier
- Premixed Combustion Rate Multiplier
- Diffusion Combustion Rate Multiplier

Moreover, the user has the possibility to add 3 more parameters that control the shape of the Diffusion combustion rate, which is calculated by means of the following equation [50]:

$$\frac{dm}{dt} = C_{df} m \frac{\sqrt{k}}{\sqrt[3]{V_{cyl}}} f([O_2]) \tag{B.1}$$

Where:

$\frac{dm}{dt}$ is the rate of fuel mass burned
C_{df} is the Diffusion Combustion Rate Multiplier
m is the mass of fuel within the cylinder
k is the turbulent kinetic energy
V_{cyl} is the cylinder volume
$[O_2]$ is the oxygen concentration

DIPulse uses an empirical function (see Figure B.2) to reduce the Diffusion Combustion Rate Multiplier along the combustion process at high loads, accounting for spray-spray and spray-wall interactions [50]. The three additional parameters that control the shape of this correction function, are:

- Diffusion Multiplier Transition Timing
- Diffusion Multiplier Final Value
- Diffusion Multiplier Transition Rate

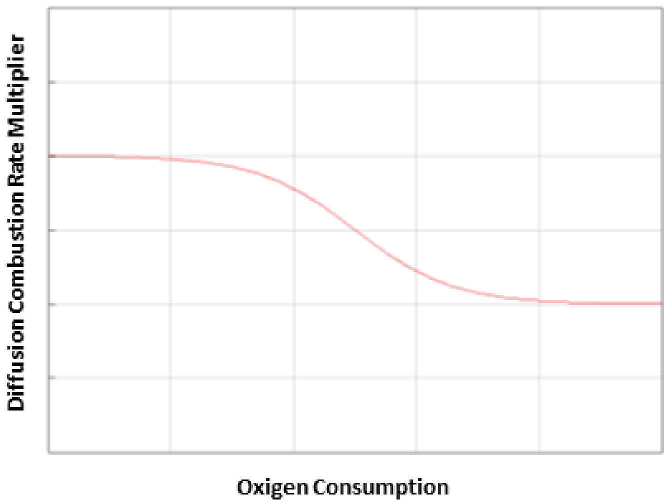

Figure B.2 - DIPulse Diffusion Combustion Rate Multiplier vs O_2 consumption parameter [51]**.**

The possibility to tune these additional three parameters was extremely useful in this work since the diffusion combustion has a different shape than the one expected from the standard settings of the combustion model: in particular the diffusion combustion intensity increases along the evolution of the combustion process, instead of decreasing.

An example of this behaviour is reported in Figure B.3, where a comparison between the calculated burn rates with the two different approaches (i.e. with and without the use of the 3 additional parameters to control the diffusion combustion rate) is shown. It is bright clear that, if the “standard” simulation approach, which employs only 4 parameters for the combustion process simulation, is used, the experimentally measured trend of the burn rate (shown as “CPOA” in Figure 4) cannot be matched. On the contrary, thanks to the additional 3 parameters which can be used to model the diffusion combustion phase, an improved matching between simulation and experimental results can be achieved. This particular pattern of the burn rate was systematically found in the experimental measurements for all the operating points, thus suggesting that this phenomenon is engine-related and it is probably connected to the particular design of the combustion chamber [14][26].

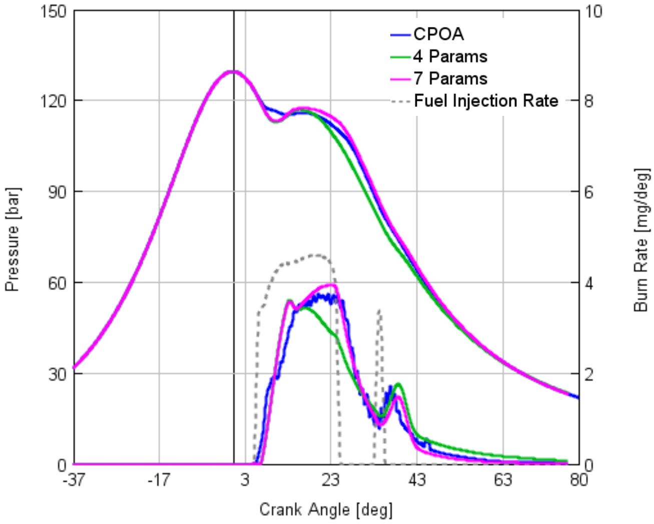

Figure B.3 - Diffusion combustion simulation. Effects of different simulation approaches using 4 or 7 parameters (2200 rpm, Full Load) [51]

Concerning the operating points used for the calibration, they were selected between the experimental measurement already presented in Paragraph 3.2 and 3.3 (EGR sweeps, after injection exploration, engine map). In total 53 of them representative of the whole engine operating conditions in terms of load, speed, EGR rate, injection pressure, and injection pattern, were chosen.

Using 7 parameters instead of 4, a DoE approach (as in [49]) was not possible due to the extremely high computational time required. A Genetic Algorithm optimization was then performed using the Advanced Direct Optimizer built in GT-Suite, that can push down the computational time to a level comparable to the DoE approach. The Advanced Direct Optimizer was set to work with a population size of 30 and the number of generation was set equal to 20 after checking for the stability of the solution. With this setting the optimizer runs 601 iterations per case, that required around 2 hours with 20 cores (Intel i7-6700 3.4Ghz).

Once the calibration was completed the combustion model was implemented in the full engine model to assess its prediction capabilities.

B.1.3 Emissions Models

NOx and Soot Emissions Model Calibration

After the predictive combustion model has been properly calibrated, and a satisfactory agreement between predicted an experimental burn rates has been achieved, the NOx and soot emission models could be calibrated.

The formation of NOx during combustion is predicted based on the extended Zeldovich mechanism [52] which includes the N2 oxidation, N oxidation and OH reduction reactions described by Equations B.2, B.3 and B.4, respectively.

$$O_2 + N_2 \leftrightarrow NO + N \tag{B.2}$$
$$N + O_2 \leftrightarrow NO + O \tag{B.3}$$
$$N + OH \leftrightarrow NO + H \tag{B.4}$$

The NOx emission model uses 6 calibration multipliers: the NOx Calibration Multiplier multiplies the NOx concentration output of the model, while the other 5 are the Arrhenius constants of the abovementioned equations.

A Genetic Algorithm optimization was again used to minimize the error between the experimental and simulated values of NOx concentration.

A first run of the optimizer was performed with all the parameters, setting the exploration range for each parameter between 0.1 and 10 (default value = 1). After the first run, the parameters that showed the highest sensitivity have been selected to run a second optimization loop with a restricted range.

As far as soot concentration prediction is concerned, the Modified Hiroyasu model [53][54] was applied. “Soot Formation Multiplier” and “Soot Burnup Multiplier” give the opportunity to control the soot evolution and oxidation, respectively. The same procedure adopted for NOx calibration was followed, in this case with the aim to minimize the error between experimental and predicted exhaust soot concentration.

B.1.4 Injection Rates Map

Since Diesel combustion is very sensitive to the injection rate profile, an extensive experimental campaign should be carried out to build up a meaningful injection rates profiles library (which will be hereafter referred to as Injection Rates Map).

In this case only three injection rates were available, measured at 3000 bar injection pressure with different Energizing Time (ET) (Figure B.4). To generate the injection rates map the following assumptions were made at constant rail pressure:

1. The hydraulic delay is constant (depends only on rail pressure).
2. The rising slope of the mass flow rate is constant (depends only on rail pressure).
3. Once the injector is at full lift (maximum mass flow rate), the mass flow rate is constant since the controlling part is the nozzle.
4. The descent phase of the mass flow rate is constant (depends only on rail pressure).

To some extent this is equal to assume that the dependency of the dynamic of the injector on the ET is negligible as suggested by the three experimental injection rate available shown in Figure B.4.

Given those hypotheses, it was possible to extrapolate the profiles at 3000 bar extending the experimental profiles until the maximum injected quantity used in the dataset was obtained and cutting it backwards with the descent slope, to generate all the intermediate profiles. The results of this process are shown in Figure B.6.

The next step was the generation of the profiles for lower rail pressures by making the following assumption: at constant ET the shape of the injection rate is constant and it is only scaled by a factor that does not depend on the nozzle. The factor was calculated according to the EMI curve (injector-characteristic relation between injected quantity and energizing time) published in [55], by calculating the ratio of the injected quantity at constant ET between different rail pressures, and extrapolating the trend up to 3000 bar (the EMI curves published in [55] reach 2500 bar). The calculated factors are then applied at the generated injection rates at 3000 bar. The results of this second step are reported in Figure B.6 for a given ET.

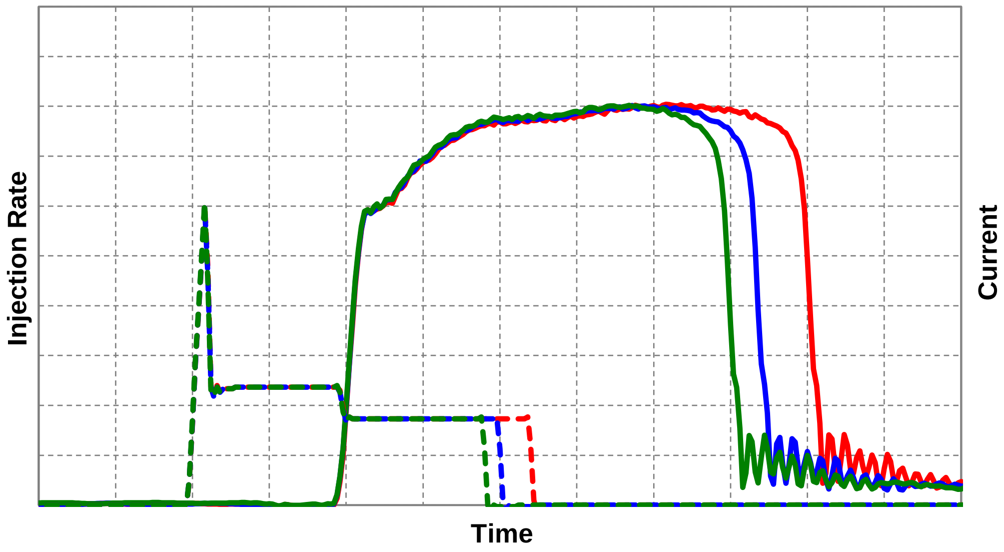

Figure B.4 - Available experimental injection rates [51]

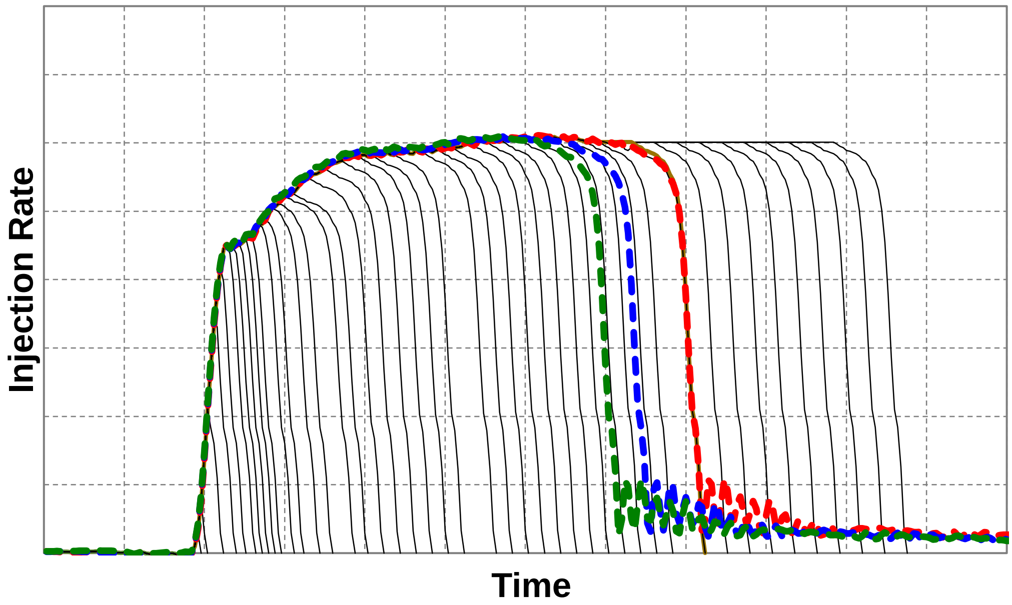

Figure B.5 - Injection profiles generation at constant rail pressure [51]

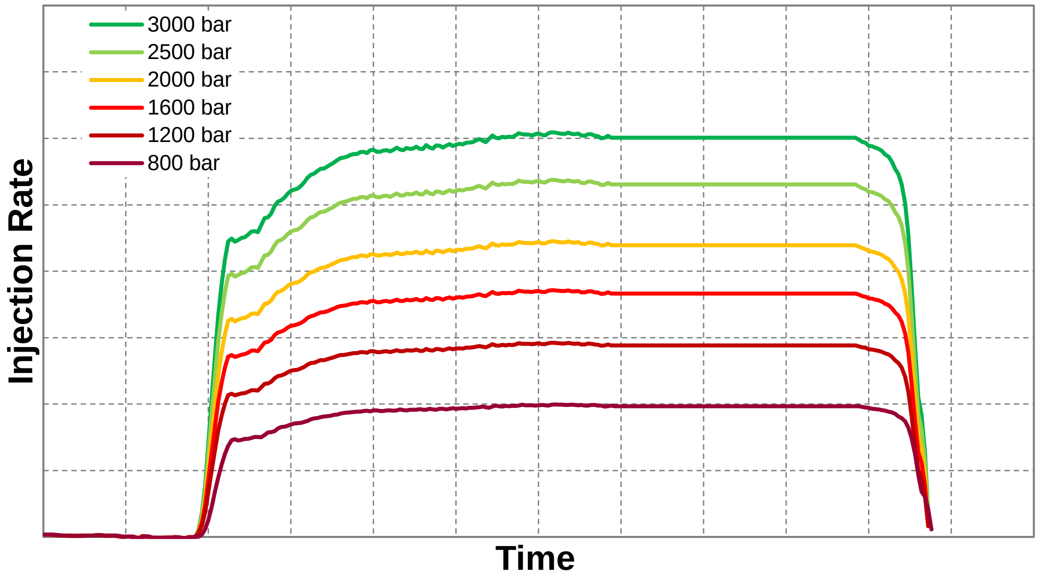

Figure B.6 - Injection profiles generation at constant energizing time [51]

B.1.5 Results

The results in terms of main performance parameters will be presented as the output of the detailed engine model, while the comparison of the burn rates and of the in cylinder pressure are the results of the cylinder pressure only analysis.

As reported in Figure B.7, the predictive combustion model can satisfactory reproduce the combustion process, with errors which are on average, for the 95% of the tested operating conditions, lower than 5 bar of maximum cylinder pressure and 2 degrees on MFB50, with a very good regression quality. The combustion duration 10-75% is a little more dispersed, however this could be related to the combustion ending phase which is extremely sensitive to measurement uncertainty.

Also the engine performance parameters, reported in Figure B.8 show good results, with an error on IMEP, BMEP and BSFC generally lower than 5%. However, it must be pointed out that the model was set to work at fixed injected quantity and a Chenn-Flynn model was used to estimate FMEP. Therefore, as confirmed by comparing the results for IMEP and BMEP, the loss of accuracy should be attributed to the friction model rather than to the predictive combustion model.

Concerning the indicating results output by the single cylinder model (CPOA), in Figure B.9 four different operating points are reported, with different load, rail pressure, and injection pattern, proving that the model is able to catch very well the variations of those parameters.

As far as the after injection sweep is concerned, four points with different dwell time between main and after, reported in Figure B.10, show that the variations of the burn rate of the after is well captured. In Figure B.11 a sweep of rail pressure at constant EGR rate at 1400 rpm x 100% load is presented, while in Figure B.12 a sweep of EGR rates is shown,. All these sets of data were measured keeping the SOI of the main injection pulse constant. The results shown in the abovementioned figures prove that the model is able to properly capture the variations in the combustion process caused by the main engine calibration parameters.

B.1.6 Emissions

As far as the NOx emissions are concerned, the Extended Zeldovich Mechanism is able to reproduce the experimental data with an average confidence interval of ±20%, as shown in Figure B.13a, where simulated vs measured NO_X emissions for all the available engine operating points (corresponding to an EGR variation range from 14 to 57%) are shown.

As far as soot emissions are concerned, although the model is not capable to reproduce the experimental data, as reported in Figure B.13b, it is generally able to catch the trends as shown in Figure B.14, and could therefore be used at least for qualitative analysis. On the other hand, these results could be expected, since soot formation mechanisms are extremely sensitive to local fuel concentration and thermodynamic conditions and are therefore almost impossible to be fully captured by means of a zone approach.

A possible alternative for soot emissions estimation could be the neural network approach. This method though would require a huge experimental campaign for the training of the neural network and moreover it is not predictive. It could therefore give unexpected results when applied outside of the training domain, thus significantly limiting its possible use to support engine calibration and hardware selection activities. Another option could be the exploitation of 3D CFD combustion modelling, which could, thanks to its higher spatial resolution, better address the issue of the sensitivity of soot formation to local fuel concentration and thermodynamic conditions. However, the extremely high computational time requirements would in this case represent a significant obstacle for exploring a wide range of engine operating parameters.

For the abovementioned reasons the approach based on the exploitation of the DIPulse combustion model was preferred: in this way a kind of “virtual test rig” was obtained, on which the effects of different engine calibration and hardware set-up could be analysed, on a quantitative basis as far as engine performance and NOx emissions are concerned, and at least on a qualitative basis as far as soot emissions are concerned.

COMBUSTION PARAMETERS **PERFORMANCE PARAMETERS**

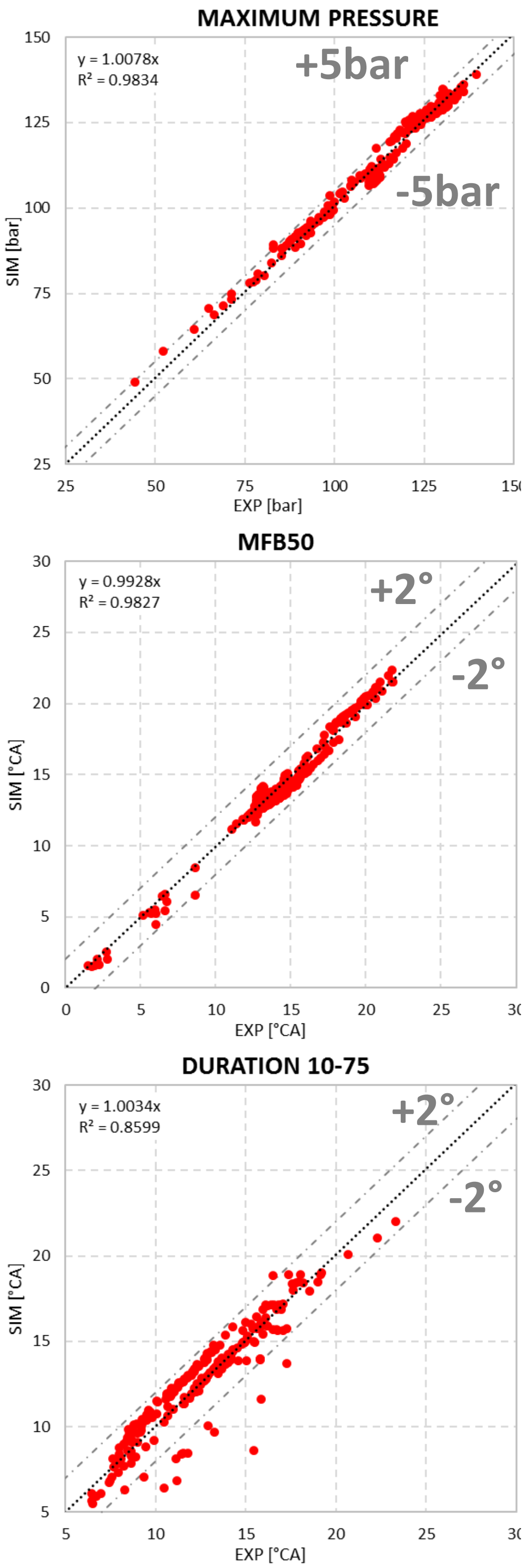

Figure B.7 - Combustion parameters comparison (detailed Engine Model) [51]

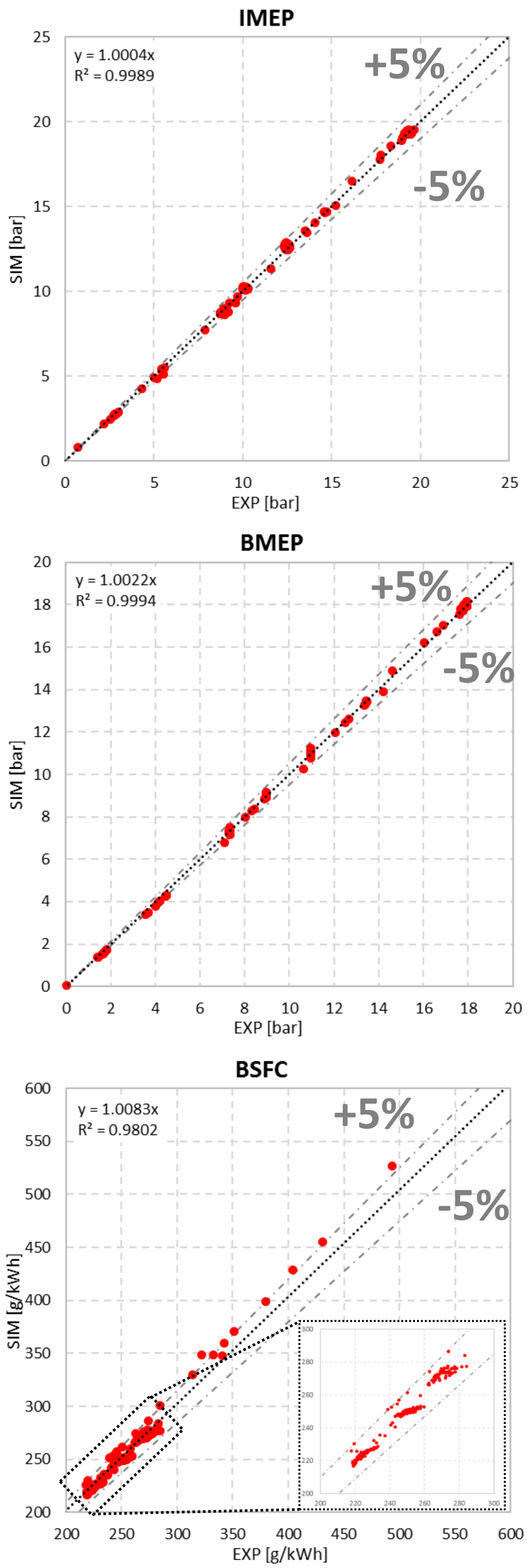

Figure B.8 - Engine Performance parameters comparison (detailed Engine Model) [51]

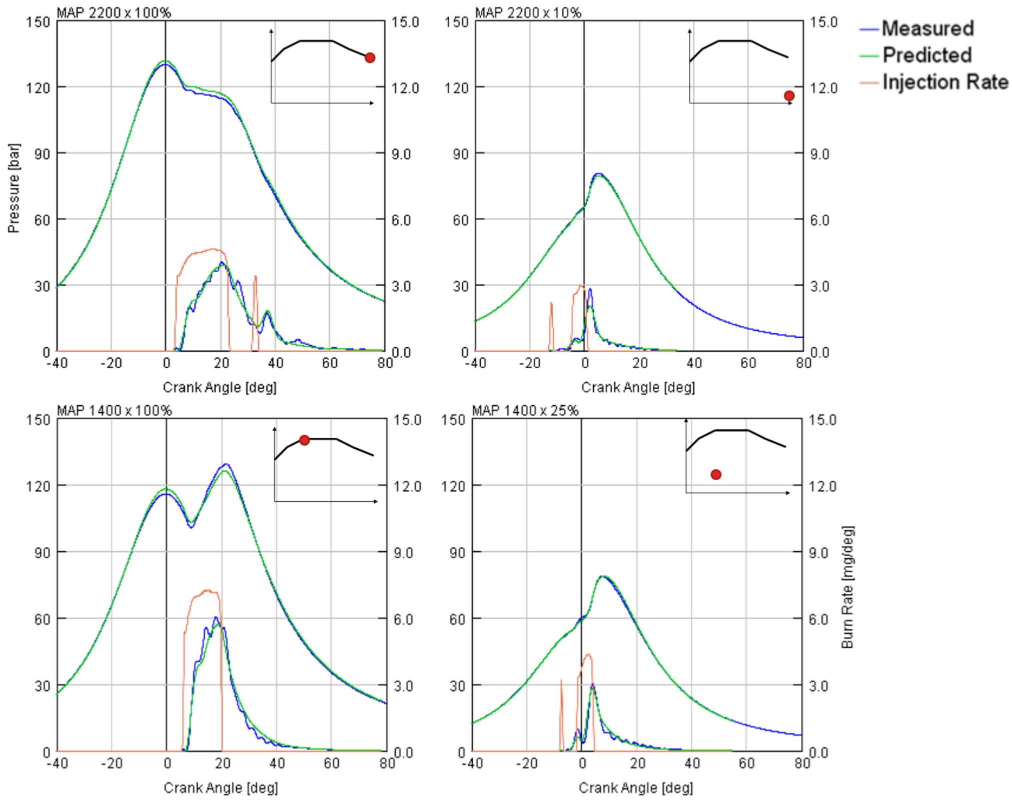

Figure B.9 - Predicted vs Measured indicating results on Engine Map. [51]

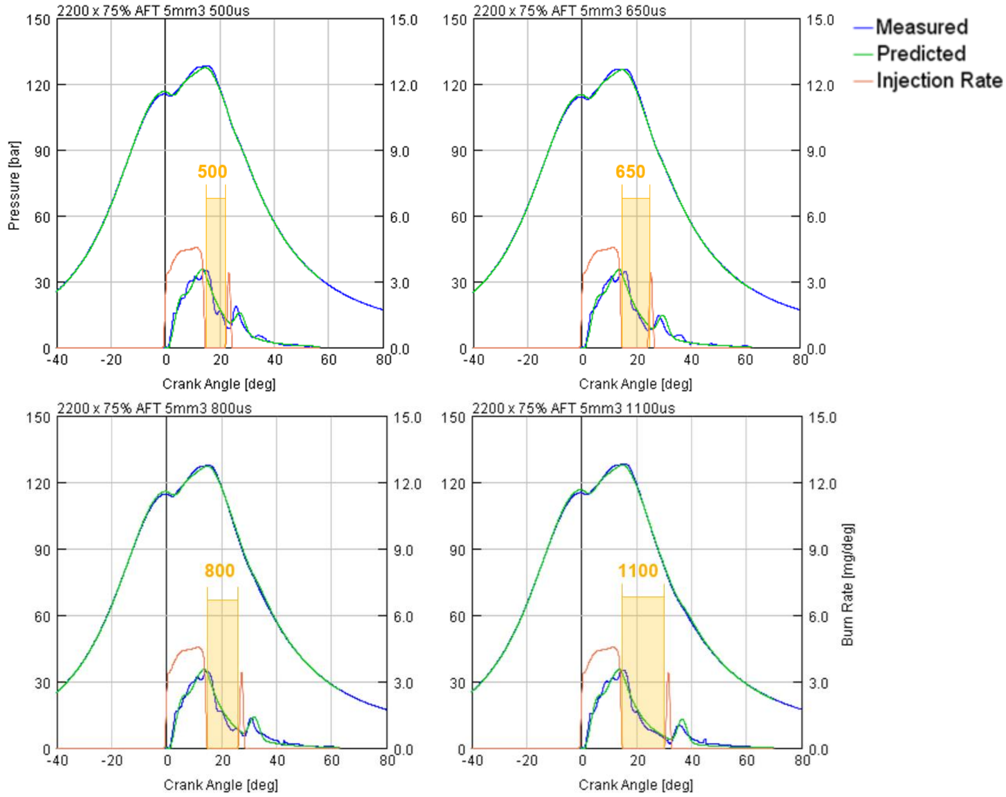

Figure B.10 - Predicted vs Measured indicating results on After Injection [51]
Exploration @ 2200 rpm x 75% load. Dwell time 500→1100 μs.

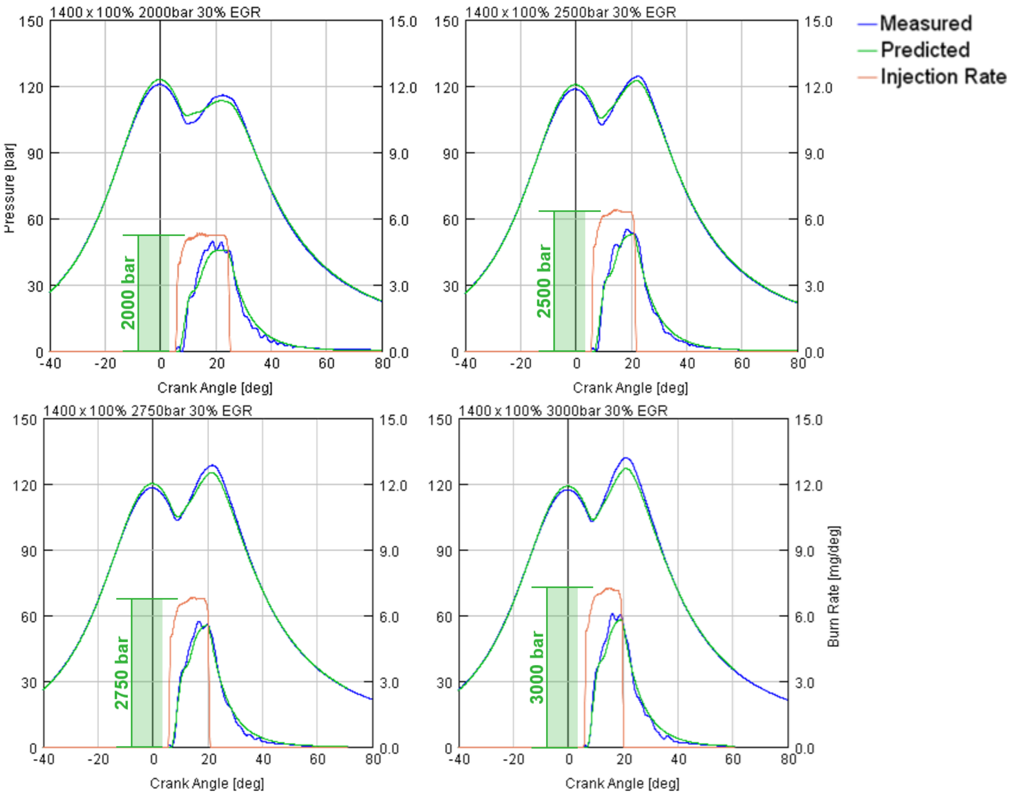

Figure B.11 - Predicted vs Measured indi. results @1400 rpm x 100% load. Rail pressure Sweep 2000 → 3000 bar [51]

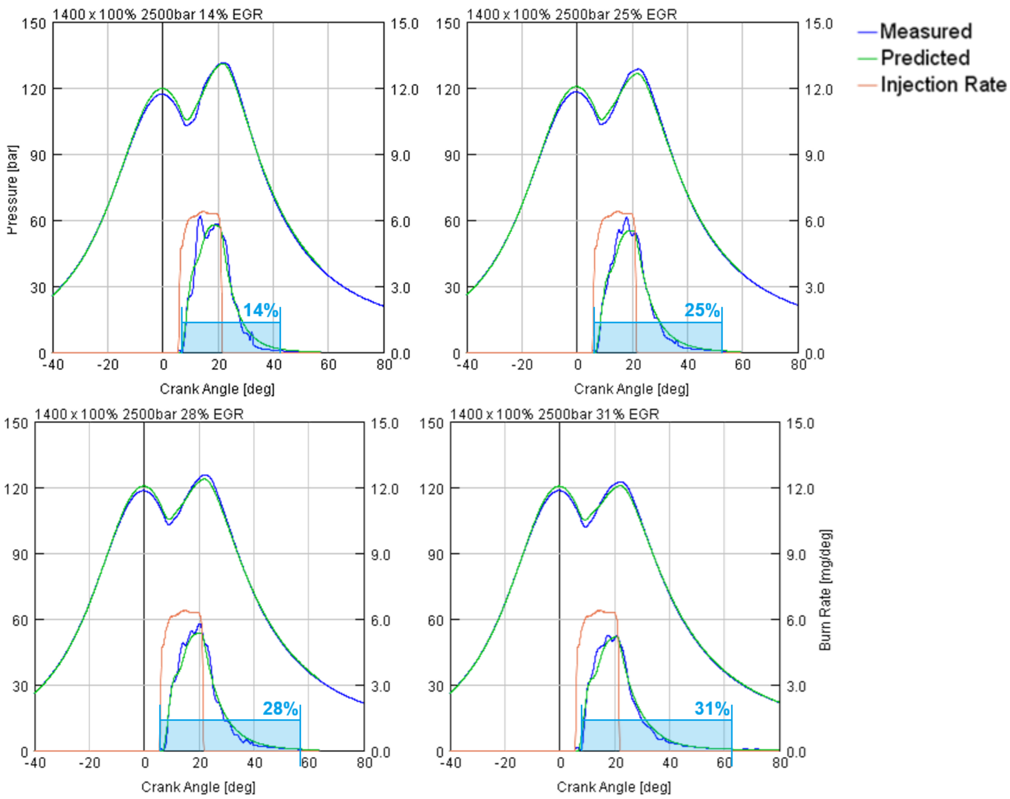

Figure B.12 - Predicted vs Measured indi. Results @1400 rpm x 100% load. EGR Sweep 14 → 31% [51]

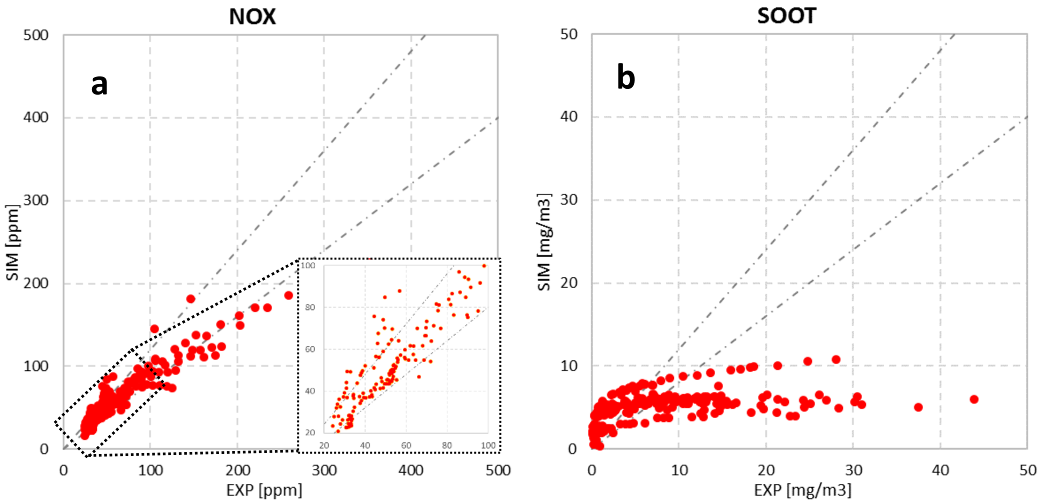

Figure B.13 - NOx and Soot emissions comparison [51]

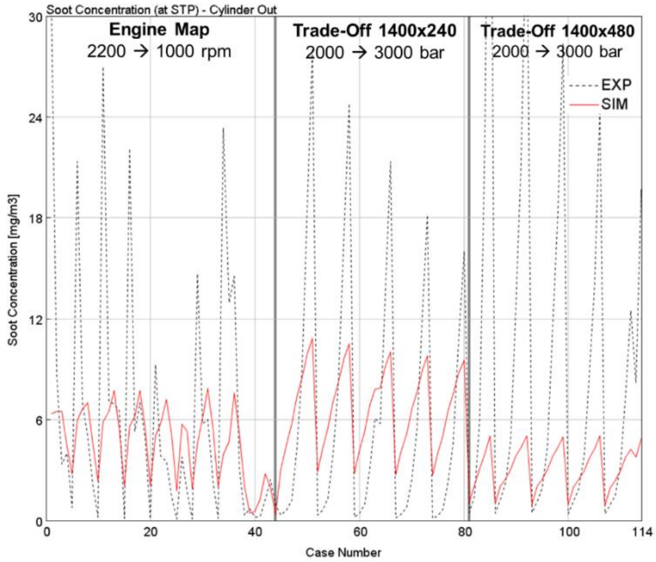

Figure B.14 - Case Resolved Soot Emissions Comparison (each point on the X axis represent a specific engine operating condition) [51]

B.1.7 Calibration Points Number Sensitivity

A sensitivity analisys on the number of calibration points was carried out in order to evaluate if the combustion model guarantees a good predictive capability using less calibration points, improving the computational time. Four cases were studied:

1. 53 Points: it is the reference case (detailed results presented in the previous pages).
2. 35 Points: chosen between the 53 of case 1
3. 23 Points: as for case 2
4. 16 Points: as for case 2

It is important to point out that no analisys was carried out on the relative weight of each operating point, and the points were chosen “randomly” between the 53 of case 1 in order to cover as much as possible homogeneusly the whole engine operation range. The Genetic Algorithm was set to operate in the same way for all the cases, starting from the default values of the calibration parameters and running with a population size of 30 and 20 generations, resulting in 601 iterations per case. It is worth to point out that the computational time is linear with the number of calibration points. The results are reported in Figure B.15a as the output of the single cylinder model (CPOA) as an error distribution of IMEP during combusiton (IVC – EVO), in order to quantify the effect only of the combustion model.

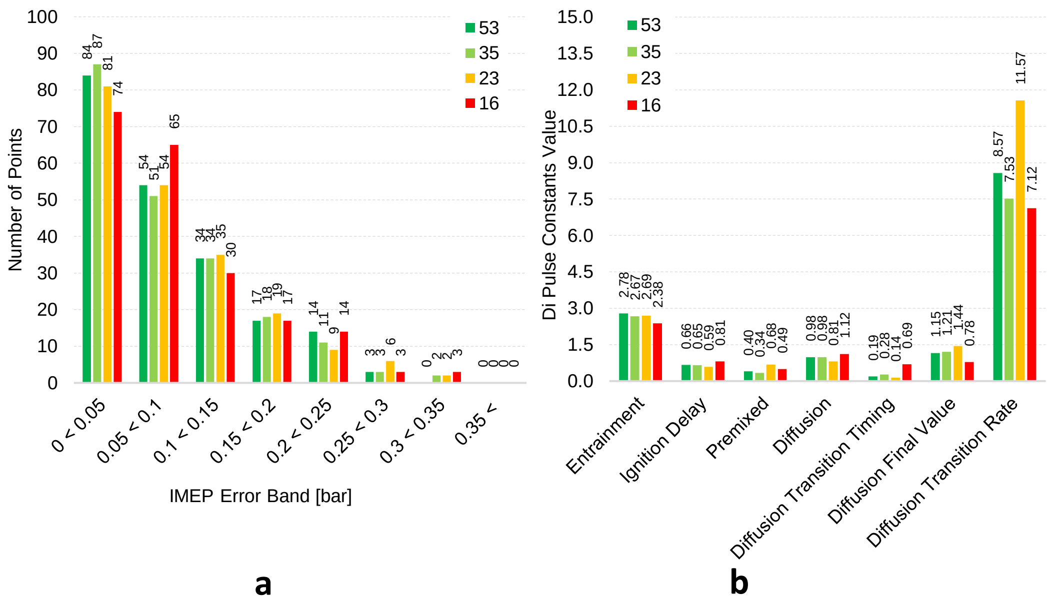

Figure B.15 - Calibration Points Number Sensitivity [51]
a. IMEP IVC-EVO Error Distribution
b. Variation of the calibration parameters

The analisys showed that moving from 53 to 23 calibration points does not seems to worsen sensibly the quality of the results, while further decreasing the calibration points to 16 results in a sensible increase in the error band between 0.05 bar and 0.1 bar.

The calibration parameters value found by the optimizer (in Figure B.15b) confirms the results shown in Figure B.15a: in fact the variation in the constants for the 53, 35, 23 cases is very limited, while for the 16 points case a larger deviation is observed.

References

[1] European Environment Agency, *Air quality in Europe - 2017 Report*. 2017.

[2] E. E. A.-A. I. R. S. (AIRS), “Air pollutant emissions,” 2017.

[3] European Commission, “Regulation (EU) 2016/1628 Of The European Parliament And Of The Council Of 14 September 2016,” *Euratom*, vol. 2016, no. 167, 2016.

[4] N. | © M. of L. 2017, “What is Non Road Mobile Machinery?” [Online]. Available: http://nrmm.london/content/what-non-road-mobile-machinery.

[5] S. Charlton, “Developing Diesel Engines to Meet Ultra-Low Emission Standards,” *Tech. Pap.*, no. 2005-11–1, p. 42, 2005.

[6] The International Council on Clean Transportation (ICCT), “European Stage V non-road emission standards,” no. November, 2016.

[7] T. Dallmann and A. Menon, “Technology pathways for diesel engines used in non-road vehicles and equipment,” *White Paper*, 2016. [Online]. Available: http://www.theicct.org/sites/default/files/publications/Non-Road-Tech-Pathways_white- paper_vF_ICCT_20160915.pdf.

[8] DieselNet, “EU: Nonroad Engines.” [Online]. Available: https://www.dieselnet.com/standards/eu/nonroad.php. [Accessed: 25-Jan-2018].

[9] DieselNet, “US: Nonroad Engines.” [Online]. Available: https://www.dieselnet.com/standards/us/nonroad.php.

[10] DieselNet, “ISO 8178.” [Online]. Available: https://www.dieselnet.com/standards/cycles/iso8178.php.

[11] DieselNet, “Nonroad Transient Cycle (NRTC).” [Online]. Available: https://www.dieselnet.com/standards/cycles/nrtc.php.

[12] DieselNet, “Emission Test Cycles: NTE (Not-To-Exceed) Testing.” [Online]. Available: https://www.dieselnet.com/standards/cycles/nte.php. [Accessed: 20-Apr-2018].

[13] DieselNet, “Emission Test Cycles: ESC.” [Online]. Available: https://www.dieselnet.com/standards/cycles/esc.php. [Accessed: 20-Apr-2018].

[14] P. Gatti *et al.*, “Investigation of a ‘SCR-free’ system to meet the Stage IV and beyond emissions limits,” in *Heavy-Duty, On- and Off-Highway Engines 2016 11th International MTZ Conference*, Ulm, Germany: MTZ, 2017, pp. 274–291.

[15] D. Queck and O. E. Herrmann, “Next steps towards EGR-only concept for medium-duty industrial engine,” in *Internationaler Motorenkongress 2017: Mit Konferenzen Nfz-Motorentechnologie und Neue Kraftstoffe*, J. Liebl and C. Beidl, Eds. Wiesbaden: Springer Fachmedien Wiesbaden, 2017, pp. 555–572.

[16] Y. Shinohara, K. Takeuchi, O. E. Herrmann, and H. J. Laumen, “3000 bar Common Rail System,” *MTZ Worldw. eMagazine*, vol. 72, no. 1, pp. 4–9, 2011.

[17] E. (VIF) Schalk *et al.*, “Limits for NOx reduction by EGR in a Heavy Duty Diesel Engine at stationary and transient conditions,” in *ASME Internal Combustion Engine Division’s 2012 Fall Technical Conference*, 2012, pp. 1–7.

[18] K. Natti *et al.*, “Studies on the Impact of 300 MPa Injection Pressure on Engine Performance, Gaseous and Particulate Emissions,” *SAE Int. J. Engines*, vol. 6, no. 1, pp. 2013-01–0897, 2013.

[19] S. Reifarth, “Efficiency and Mixing Analysis of EGR-Systems for Diesel Engines,” KTH, Internal Combustion Engines, 2014.

[20] A. Banks, M. Niven, and P. Andersson, “Boosting technology for Euro VI and Tier 4 final heavy duty diesel engines without NOx aftertreatment,” in *9th International Conference on Turbochargers and Turbocharging - Institution of Mechanical Engineers, Combustion Engines and Fuels Group*, 2010, pp. 35–47.

[21] F. Millo, P. F. Giacominetto, and M. G. Bernardi, “Analysis of different exhaust gas recirculation architectures for passenger car Diesel engines,” *Appl. Energy*, vol. 98, pp. 79–91, Oct. 2012.

[22] G. Boccardo, F. Millo, A. Piano, L. Arnone, S. Manelli, and C. Capiluppi, “A Fully Physical Correlation for Low Pressure EGR Control Linearization,” *SAE Tech. Pap.*, vol. 2017–Septe, 2017.

[23] M. Palanisamy, J. Lorch, R. J. Truemner, and B. Baldwin, “Combustion Characteristics of a 3000 Bar Diesel Fuel System on a Single Cylinder Research Engine,” *SAE Int. J. Commer. Veh.*, vol. 8, no. 2, pp. 2015-01–2798, 2015.

[24] O. Herrmann *et al.*, “Ultra high pressure and enhanced multiple injection – potentials for the diesel engine and challenge for the fuel injection system,” in *Fuel Systems for IC Engines*, 2012, pp. 103–114.

[25] J. A. Wloka, S. Pflaum, and G. Wachtmeister, “Potential and Challenges of a 3000 Bar Common-Rail Injection System Considering Engine Behavior and Emission Level,” *SAE Int. J. Engines*, vol. 3, no. 1, pp. 801–813, 2010.

[26] R. Cornwell and F. Conicella, “Direct injection diesel engines,” Patent US8770168(B2) 8 Aug 2014, JP5826189(B2) 2 Dec 2015, WO2011092459 (A1) 4 Aug 2011, 2011.

[27] F. Conicella, R. Cornwell, S. Fagg, and J. Mullineux, “Investigation of Fuel Injection Strategies on a Low Particulate Combustion Development Programme for Tier 4 Legislation,” in *Institution of Mechanical Engineers Conference May*, 2009.

[28] A. Tolley and F. Conicella, “Low particulate combustion development of the JCB Dieselmax mid-range off highway engine,” in *Conference, Internal Combustion Engines; performance, fuel economy and emissions*, 2009, pp. 117–132.

[29] F. Conicella, “Low Particulate Combustion Development of a Medium Duty Engine for Off-Highway Applications,” in *MTZ Conference on On/Off Highway Engines, Friedrichshafen*, 2009.

[30] C. Such, P. Gatti, M. Bonanni, and L. Arnone, “Advanced Combustion System for a New Engine Family Below 56 kW,” in *ATZ Live Conference*,

Kiel, 2011.

[31] L. Arnone, S. Manelli, M. Bonanni, C. Such, S. Fagg, and P. Gatti, “Performance Development of a New Tier 4 Final Engine Family below 56 kW,” 2013.

[32] F. Millo *et al.*, “Particle Number and Size Emissions from a Small Displacement Automotive Diesel Engine: Bioderived vs Conventional Fossil Fuels,” *Ind. Eng. Chem. Res.*, vol. 51, no. 22, pp. 7565–7572, 2012.

[33] J. O’Connor and M. Musculus, “Post Injections for Soot Reduction in Diesel Engines: A Review of Current Understanding,” *SAE Int. J. Engines*, vol. 6, no. 1, pp. 2013-01–0917, 2013.

[34] D. B. Kittelson, “Engines and nanoparticles: A review,” *J. Aerosol Sci.*, vol. 29, no. 5–6, pp. 575–588, 1998.

[35] T. Lind, G. Roberts, W. Eagle, C. Rousselle, Ö. Andersson, and M. P. Musculus, “Mechanisms of post-injection soot-reduction revealed by visible and diffuse-background-illumination soot extinction imaging,” *SAE Tech. Pap.*, vol. 01–0232, pp. 1–20, 2018.

[36] T. Minami, K. Takeuchi, and N. Shimazaki, “Reduction of Diesel Engine NOx Using Pilot Injection,” no. 412, 1995.

[37] S. Tullis and G. Greeves, “Improving NOx Versus BSFC with EUI 200 Using EGR and Pilot Injection for Heavy-Duty Diesel Engines,” no. 412, 1996.

[38] F. Mallamo, M. Badami, and F. Millo, “Analysis of Multiple Injection Strategies for the Reduction of Emissions, Noise and BSFC of a DI CR Small Displacement Non-Road Diesel Engine,” no. 724, 2002.

[39] M. P. Orihuela, A. Gómez-Martín, P. Miceli, J. A. Becerra, R. Chacartegui, and D. Fino, “Experimental measurement of the filtration efficiency and pressure drop of wall-flow diesel particulate filters (DPF) made of biomorphic Silicon Carbide using laboratory generated particles,” *Appl. Therm. Eng.*, vol. 131, pp. 41–53, 2018.

[40] D. Imhof and M. Kasper, “Particle number emissions of offroad engines in NRSC and NRTC using the EC standardised PMP measuring method,” pp. 1–4, 2009.

[41] S. K. Chen and P. F. Flynn, “Development of a Single Cylinder Compression Ignition Research Engine,” *SAE Tech. Pap.*, Feb. 1965.

[42] B. Ernst, J. Kammeyer, and J. R. Seume, “Improved Map Scaling Methods for Small Turbocharger Compressors,” *Proc. ASME Turbo Expo 2011, GT2011, June 6-10, 2011, Vancouver, Br. Columbia, Canada*, pp. 1–12, 2011.

[43] Kohler, “Kohler Diesel KDI ® 55 – 105,” *Prod. Broch.*, vol. Rev.03 11/.

[44] Q. Xin, *Diesel Engine System Design*. 2011.

[45] John Deere, “Final Tier 4/Stage IV | Industrial Engines | John Deere US.” [Online]. Available: https://www.deere.com/en/engines-and-drivetrain/final-tier-4-stage-iv/. [Accessed: 19-Apr-2018].

[46] AVL, “Avl Micro Soot Sensor Avl Exhaust Conditioning Unit Operating

Manual Product Guide," no. May, 2008.

[47] AVL, "Smoke Value Measuement with the Filter-Paper-Method. Application Notes.," no. June, 2005.

[48] "International Standard ISO 8178-1." p. Annex C1, 2006.

[49] A. Piano, F. Millo, G. Boccardo, M. Rafigh, A. Gallone, and M. Rimondi, "Assessment of the Predictive Capabilities of a Combustion Model for a Modern Common Rail Automotive Diesel Engine," in *SAE Technical Paper*, 2016, vol. 2016–April.

[50] G. Technologies, "GT-SUITE Engine Performance Application Manual." 2016.

[51] F. Millo *et al.*, "Numerical Simulation of the Combustion Process of a High EGR, High Injection Pressure, Heavy Duty Diesel Engine," *SAE Tech. Pap.*, vol. 2017-24–0, 2017.

[52] J. B. Heywood, *Internal Combustion Engine Fundementals*, vol. 21. 1988.

[53] T. Morel and R. Keribar, "Heat Radiation in D.I. Diesel Engines," *SAE Tech. Pap. 860445,* 1986.

[54] T. Morel and S. Wahiduzzaman, "Modeling of Diesel Combustion and Emissions," in *Proceedings of XXVI FISITA Congress*, 1996.

[55] S. Matsumoto, K. Date, T. Taguchi, and D. Olaf Erik Herrmann, *The New Denso Common Rail Diesel Solenoid Injector*, vol. 74. 2013.

List of Abbreviations

AFR	Air-to-Fuel Ratio
APC	AVL Particle Counter
ASC	Ammonia Slip Catalyst
BMEP	Brake Mean Effective Pressure
BSFC	Brake Specific Fuel Consumption
CFD	Computational Fluid Dynamics
CLRTAP	Convention on Long-Range Transboundary Air Pollution
CPOA	Cylinder Pressure Only Analysis
CR	Common Rail
DENERG	Energy Department of Politecnico di Torino
DOC	Diesel Oxidation Catalyst
DoE	Design of Experiment
DPF	Diesel Particulate Filter
DR	Dilution Ratio
DT	Dwell Time
DUR1075	10 to 75% fuel mass burnt combustion duration
DUR1090	10 to 90% fuel mass burnt combustion duration
ECU	Engine Control Unit
EGR	Exhaust Gas Recirculation
EO	Engine Out
EPA	Environment Protection Agency
ET	Energizing Time
EU	European Union
EVO	angle at Exhaust Valves Closure
FIS	Fuel Injection System
FMEP	Friction Mean Effective Pressure
FSN	Filter Smoke Number
HP	High Pressure
HRR	Heat Release Rate
IMEP	Indicating Mean Effective Pressure
ISFC	Indicated Specific Fuel consumption
IVC	crank angle at Intake Valves Closure

LP	Low Pressure
MFB50	crank angle at 50% Mass of Fuel Burnt
MSS	MictoSoot Sensor
MUZ	Main Unburned Zone
NRMM	Non-Road Mobile Machinery
NRSC	Non-Road Steady Cycle
NRTC	Non-Road Transient Cycle
NTE	Not To Exceed zone
OEM	Original Equipment Manufacturer
PEMS	Portable Emissions Measurement System
PFP	Peak Firing Pressure
PM	Particulate Matter
PN	Particle Number
RH	Relative Humidity
SBZ	Spray Burned Zone
SCR	Selective Catalytic Reduction
SM	Smoke Meter
SMPS	Scanning Mobility Particle Sizer
SOI	angle of Start of Injection
SUZ	Spray Unburned Zone
TCO	Total Cost of Ownership
TP	Tailpipe
TTT	Time To Torque
TVCS	Twin Vortex Combustion System
UNECE	United Nations Economic Commission for Europe
US	United States of America
VGT	Variable Geometry Turbine
WG	WasteGate valve
WHO	World Health Organization
WLTC	Worldwide Harmonized Light Vehicles Test Cycle